

**EXPLORING URANYL-OXO ACTIVATION VIA IMIDO SUBSTITUENTS  
AND EXPANDING THE LIBRARY OF URANIUM MULTIPLE IMIDO  
COMPLEXES**

by

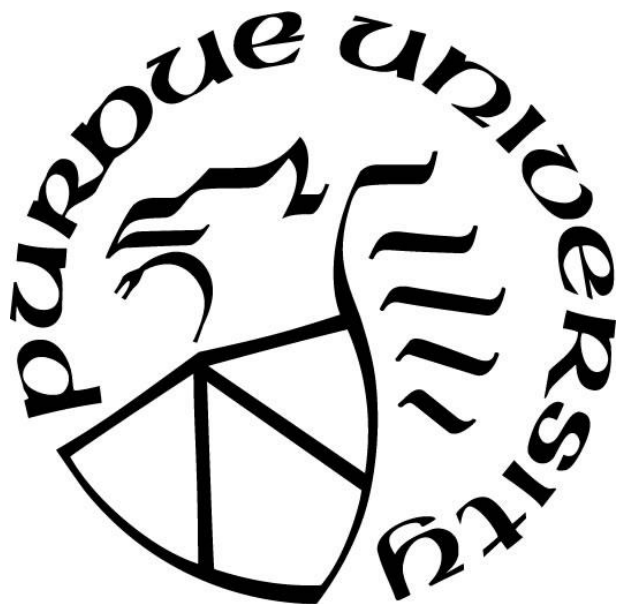
**Tyler S. Collins**

**A Dissertation**

*Submitted to the Faculty of Purdue University*

*In Partial Fulfillment of the Requirements for the degree of*

**Doctor of Philosophy**



Department of Chemistry

West Lafayette, Indiana

May 2022

**THE PURDUE UNIVERSITY GRADUATE SCHOOL**  
**STATEMENT OF COMMITTEE APPROVAL**

**Dr. Suzanne C. Bart, Chair**

Department of Chemistry

**Dr. Tong Ren**

Department of Chemistry

**Dr. Corey M. Thompson**

Department of Chemistry

**Dr. Christopher Uyeda**

Department of Chemistry

**Approved by:**

Dr. Christine Hrycyna

*Dedicated to William DeMeester*

## ACKNOWLEDGMENTS

I would like to thank all the friends that I have made while at Purdue, they have helped me get through classes we thought were moving way too fast, we've commiserated about cumulative exam scores, figured out what and how we are supposed to write an OP—and proof read our ramblings so no one important saw them—and just had fun sharing all the random things that happened to our labs as things broke down, as new instruments arrived and old ones had to be removed. I know that I wouldn't have had as much fun as I did without them. To the Bart Lab, I have enjoyed my time in the facility for the enrichment of *f*-block advancement. I know I wouldn't have become the scientist I am today without Caleb and Shane showing me what I can do, and what it means to be a researcher. I would like to thank Ezra for his help with the pentakis(imido) chemistry, and for the great crystal structure. Colby, you have been a great undergrad, I have enjoyed all the conversations I have had with you, and I hope I have taught you a few useful things too. For the current members, I hope I have been helpful, I know I have been sarcastic, but I hope that you know I do it because you already know the answer. You all can, and will, do great chemistry. I will miss all the conversations about literally anything that I can have with everyone. To Matthias I just want to say, thank you. Thank you for dealing with all of my almost crystals and helping me with my actual crystals and with all the details that completing a CIF and refining disorder on all the solvents you don't think we should be using to grow crystals. I would like to thank the U.S. Department of Energy (DOE) Center for Actinide Science and Technology an Energy Frontier Research Center (EFRC) (Award number DE-SC0016568) for funding my work these last five years, without the support that I received through this grant none of this chemistry would have been possible. This support has also given me the ability to experience great collaborations with the Schelter group at UPenn, and Albrecht-Schönzart group at Florida State University. I want to thank my family and friends for their support during my time at Purdue as well. I want to thank my parents for always believing in me and encouraging me to do whatever I put my mind to. Rachel, I can't thank you enough for your support and empathy as we both went through grad school. And finally, Tara, I can't ever thank you enough for staying with me through it all. All the drama, all the stress, both in my life and in yours. Thank you for living here, with me, thank you for putting up with all my idiosyncrasies and habits. There is absolutely no way I would have made it without you.

## TABLE OF CONTENTS

LIST OF TABLES .....	7
LIST OF FIGURES .....	8
LIST OF SCHEMES .....	10
LIST OF ABBREVIATIONS .....	11
ABSTRACT .....	13
CHAPTER 1. ELUCIDATION OF BOND ELONGATION IN A URANIUM(IV)- <i>CIS</i> - BIS(IMIDO) COMPLEX.....	14
1.1 Introduction.....	14
1.2 Results and Discussion .....	15
1.2.1 Synthesis and Characterization.....	15
1.2.2 Theoretical models.....	20
1.2.3 Preliminary Reactivity .....	26
1.2.4 Investigation of analogous synthesis with uranyl complexes.....	28
1.3 Conclusions.....	30
1.4 Experimental Methods .....	31
1.4.1 General Considerations.....	31
1.4.2 Synthesis .....	32
1.4.3 Computational details. ....	33
1.5 References.....	35
CHAPTER 2. INVESTIGATING THE STABILITY OF URANYL IMIDO COMPLEXES..	41
2.1 Introduction.....	41
2.2 Results and Discussion .....	42
2.2.1 NMR and Infrared spectroscopy.....	45
2.2.2 Literature Comparisons .....	48
2.2.3 Discussion of uranyl imido complex stability .....	49
2.2.4 Triphenylphosphine oxide supported uranyl compounds.....	50
2.3 Conclusions.....	51
2.4 Experimental Methods .....	52
2.4.1 General Considerations.....	52

2.4.2	Synthesis .....	52
2.5	References .....	55
CHAPTER 3. SYNTHESIS OF URANIUM(VI) PENTAKIS(IMIDO) COMPLEXES .....		57
3.1	Introduction.....	57
3.2	Synthesis and discussion of uranium 2,6-diisopropylphenyl pentakis(imido) .....	58
3.2.1	NMR and IR spectroscopy of uranium 2,6-diisopropylphenyl-pentakis(imido).....	61
3.2.2	Crystallographic data from a uranium 2,6-diisopropylphenyl-pentakis(imido) .....	64
3.2.3	2,6-diisopropyl imido donation reactivity .....	67
3.2.4	Investigations toward a uranium hexakis(imido) complex.....	68
3.3	Progress towards uranium multiple imido complexes with non-DIPP ligands .....	69
3.4	Investigations of analogous tungsten multiple imido complexes .....	70
3.4.1	Experiments towards tungsten multiple imido complexes .....	71
3.5	Conclusions.....	73
3.6	Experimental Methods .....	74
3.6.1	General Considerations.....	74
3.6.2	Synthesis .....	75
3.7	References.....	78
APPENDIX A: ADDITIONAL MATERIALS FOR ELUCIDATION OF BOND ELONGATION IN A URANIUM(IV)- <i>CIS</i> -BIS(IMIDO) COMPLEX.....		80
APPENDIX B: ADDITIONAL MATERIALS FOR INVESTIGATING THE STABILITY OF URANYL IMIDO COMPLEXES .....		93
APPENDIX C: ADDITIONAL MATERIALS FOR SYNTHESIS OF URANIUM(VI) PENTAKIS(IMIDO) COMPLEXES.....		102
VITA .....		109
PUBLICATION .....		110

## LIST OF TABLES

Table 1.1 Comparison of Structural Parameters. ....	18
Table 1.2. Structural parameters for [U(NDIPP) <sub>2</sub> (NPh <sub>2</sub> ) <sub>3</sub> ]K <sub>2</sub> .....	28
Table 3.1 Structural parameters for [U(NDIPP) <sub>5</sub> ]K <sub>4</sub> (Et <sub>2</sub> O) <sub>4</sub> .....	66
Table 3.2 Selected Bond Lengths of [W <sub>2</sub> ( <sup>t</sup> BuN) <sub>4</sub> (μ- <sup>t</sup> BuN) <sub>2</sub> ]K <sub>2</sub> .....	73

## LIST OF FIGURES

Figure 1.1 Molecular structure of $[U(NDIPP)_2(NTSA)_2]K_2(Et_2O)$ shown at 30% probability ellipsoids. Selected hydrogen atoms and co-crystallized solvent molecules have been omitted for clarity. ....	17
Figure 1.2 Electronic absorption spectra for $[U(NDIPP)_2(NTSA)_2]K_2(Et_2O)$ , UV-vis recorded from 275 to 800, NIR (inset) recorded from 800 to 1650 nm in toluene at 25 °C. ....	19
Figure 1.3 These models have been studied to understand the role of the potassium (pink sphere in M1) counterion, and steric factors of the ligands in the coordination arrangement around the U(IV) metal center. U(IV), nitrogen (N), carbon (C), and silicon (Si) atoms are depicted in magenta, blue, grey, and yellow balls, respectively. Geometries depicted correspond to optimizations performed at ZORA/PBE0/STO-TZP level of theory .....	21
Figure 1.4 Natural localized molecular orbitals (NLMOs) of M2. Bonding interactions between U(IV) and NDIPP ligands are shown. NLMO1a,b displays the $\sigma$ -type interactions, NLMO2a,b the in-plane $\pi$ -bond, and NLMO3a,b the $\pi$ -bond aligned with the $\pi$ -system of the phenyl rings. Letters a and b are used to distinguish between the two imido ligands. U(IV) contribution to the NLMO and its composition are given. NLMO-based bond orders (BO), and their corresponding hybrid overlap are also given. NLMOs marked with a star correspond to partially occupied antibonding NLMOs counterparts to NLMO3b. ....	23
Figure 1.5 NLMOs of $U(VI)(NPh)_2Cl_2THF_2$ . Main interactions between U(VI) and one imido ligand describing the $\sigma$ - (NLMO1) and $\pi$ - (NLMO2 and NLMO3) interactions. The other imido shows the same interactions with the same bond order (BO) and hybrid overlap. The semi-core 6p orbitals have been included to show the polarization of the core towards the 5f shell induced by the imido ligands. This effect supports the inverse-trans-influence in this system similar to that seen in $UO_2^{2+}$ . <sup>10</sup> .....	25
Figure 1.6 Molecular structure of $[U(NDIPP)_2(NPh)_3]K_2$ shown with 30% probability ellipsoids. Hydrogen atoms and co-crystallized solvent molecules have been omitted for clarity.....	27
Figure 1.7 $^1H$ NMR spectra of proposed $[UO_2(NTSA)_2]Li_2$ complex.....	30
Figure 2.1 $^1H$ NMR spectra of $UO_2(^tBubpy)(NArF_5)$ (pyridine- $d_5$ ) .....	46
Figure 2.2 $^{19}F$ NMR Spectra for $UO_2(^tBubpy)(NArF_5)$ (pyridine- $d_5$ ) .....	46
Figure 2.3 Infrared Spectra of $UO_2(^tBubpy)(NArF_5)$ , KBr pellet.....	47
Figure 2.4 Infrared spectra of $UO_2(^tBubpy)(N3,5-CF_3)$ , KBr pellet .....	48
Figure 3.1 $^1H$ NMR spectra of $[U(NDIPP)_5]K_4(Et_2O)_4$ .....	62
Figure 3.2 NMR trends for uranium multiple imido complexes. ....	63
Figure 3.3 $^1H$ NMR spectra of cesium supported pentakis(imido), $[U(NDIPP)_5]Cs_4$ .....	64



Figure 3.4 Molecular Structure of $[\text{U}(\text{NDIPP})_5]\text{K}_4(\text{Et}_2\text{O})_4$ shown with 30% probability ellipsoids. Hydrogen atoms, potassium counter ions, and coordinated solvent molecules have been removed for clarity.....	65
Figure 3.5 $^1\text{H}$ NMR spectra of $[\text{U}(\text{NDIPP})_5]\text{K}_4(\text{Et}_2\text{O})_4$ imido donation reaction.....	68
Figure 3.6 Molecular structure of $[\text{W}_2(\text{}^t\text{BuN})_4(\mu\text{}^t\text{BuN})_2]\text{K}_2$ , shown at 30% probability ellipsoids. Hydrogen atoms and co-crystallized solvent molecules have been omitted for clarity.....	72

## LIST OF SCHEMES

Scheme 1.1 Initial reaction pathway for $[\text{U}(\text{NDIPP})_2(\text{NTSA})_2]\text{K}_2(\text{Et}_2\text{O})$ .....	16
Scheme 1.2 Rational synthetic route for $[\text{U}(\text{NDIPP})_2(\text{NTSA})_2]\text{K}_2(\text{Et}_2\text{O})$ .....	19
Scheme 1.3 Reactivity of 1 with $\text{NPh}_2$ , forming $[\text{U}(\text{NDIPP})_2(\text{NPh}_2)_3]\text{K}_2$ .....	26
Scheme 1.4 Proposed pathways to a <i>cis</i> -uranyl complex .....	29
Scheme 2.1 Reaction pathways to uranyl imido products .....	43
Scheme 2.2 Pathway to triphenylphosphine oxide supported uranyl imido products .....	50
Scheme 3.1 Synthetic pathways for the formation of $[\text{U}(\text{NDIPP})_5]\text{K}_4(\text{Et}_2\text{O})_4$ .....	59
Scheme 3.2 Synthetic routes to $[\text{U}(\text{NDIPP})_5]\text{Cs}_4$ .....	61
Scheme 3.3 Imido donation observed with DIPP pentakis(imido) complexes .....	67
Scheme 3.4 Proposed synthetic route for tungsten tetrakis(imido) complex .....	71
Scheme 3.5 Synthetic route to $[\text{W}_2(\text{}^t\text{BuN})_4(\mu\text{}^t\text{BuN})_2]\text{K}_2$ .....	71

## LIST OF ABBREVIATIONS

<b>3,5-CF<sub>3</sub></b>	3,5-bis(trifluoromethyl)phenylimido
<b>bpy</b>	2,2'-bipyridine
<b>C<sub>6</sub>D<sub>6</sub></b>	Benzene- <i>d</i> 6
<b>C<sub>6</sub>H<sub>6</sub></b>	Benzene
<b>CsC<sub>8</sub></b>	cesium graphite
<b>DIPP</b>	2,6-diisopropylphenylimido
<b>Et<sub>2</sub>O</b>	Diethyl ether
<b>IR</b>	Infrared spectroscopy
<b>KBn</b>	benzyl potassium
<b>KC<sub>8</sub></b>	potassium graphite
<b>KNTSA</b>	potassium <i>tert</i> -butyl-(dimethyl)silyl-amide
<b>LiNTSA</b>	lithium <i>tert</i> -butyl-(dimethyl)silyl-amide
<b>Mes</b>	2,4,6-trimethylphenylimido
<b>NArF<sub>5</sub></b>	2,3,4,5,6-pentafluorophenylimido
<b><i>n</i>Bu-Li</b>	<i>n</i> -butyl-lithium
<b>NH<sub>2</sub>3,5-CF<sub>3</sub></b>	3,5-bis(trifluoromethyl)phenylaniline
<b>NH<sub>2</sub>ArF<sub>5</sub></b>	2,3,4,5,6-pentafluorophenylaniline
<b>NH<sub>2</sub>DIPP</b>	2,6-diisopropylaniline
<b>NH<sub>2</sub>Mes</b>	2,4,6-trimethylphenylaniline
<b>NH<sub>2</sub><i>p</i>-CF<sub>3</sub></b>	<i>para</i> -trifluoromethylaniline
<b>NH<sub>2</sub><i>p</i>-F</b>	<i>para</i> -fluorophenylaniline
<b>NH<sub>2</sub><i>p</i>-tol</b>	<i>para</i> -methylaniline
<b>NHPh<sub>2</sub></b>	bisphenylamine
<b>NHTSA</b>	<i>tert</i> -butyl-(dimethyl)silyl-amine
<b>NIR</b>	Near infrared region of electronic absorption spectroscopy
<b>NMR</b>	Nuclear magnetic resonance spectroscopy
<b>N<i>para</i>-CF<sub>3</sub></b>	<i>para</i> -trifluoromethylphenylimido
<b>N<i>para</i>-F</b>	<i>para</i> -fluorophenylimido

<b>NTSA</b>	<i>tert</i> -butyl-(dimethyl)silyl-amide
<b>OPPh<sub>3</sub></b>	triphenylphosphine oxide
<b><i>p</i>-tol</b>	<i>para</i> -methylphenyl
<b>Py-d<sub>5</sub></b>	pyridine- <i>d</i> 5
<b>RbC<sub>8</sub></b>	rubidium graphite
<b>SO-CASSCF</b>	Spin-orbit complete active-space self-consistent-field calculation
<b>SR-CASSCF</b>	Space-restricted complete active-space self-consistent-field calculation
<b>'Bubpy</b>	4,4'- <i>tert</i> -butyl-2,2'-bipyridine
<b>'BuNH<sub>2</sub></b>	<i>tert</i> -butylamine
<b>THF</b>	tetrahydrofuran
<b>Tol</b>	toluene
<b>UV-vis</b>	ultra-violet-visible region of electronic absorption spectroscopy
<b>XRD</b>	X-ray diffraction

## ABSTRACT

Uranium imido complexes are highly sought after for their analogous nature to the uranyl moiety. Because of the highly reactive characteristics of uranium imido bonds compared to uranyl oxygen bonds these complexes have been used to investigate chemistry that can be used to activate the uranyl moiety. The activation of the *trans*-oxo groups of the uranyl moiety would open the door for the recycling of spent nuclear waste, diverting these chemicals from long term storage to a second life beyond nuclear fission. A suitable analog to the uranyl moiety has been discovered with the uranium bis(imido) family of complexes, these complexes can participate in chemistry that is similar if not, exactly the same as uranyl complexes. Studies with the uranium bis(imido) complex have been used to probe uranyl reactivity because the analogous nature of the two moieties. With that a uranium(IV) *cis*-bis(imido) complex was synthesized demonstrating how electron donation to the metal center can disrupt the Inverse Trans Influence (ITI) can as a result activate the *trans*-ligands on uranium. This complex is the first reported U(IV) bis(imido) with *trans* imido groups and achieved this geometry without large steric ligands to facilitate the *cis*-geometry. Computational analysis of this complex shows the stable nature of the geometry and how the fundamental electronics of this complex are the leading factor in the resultant geometry. When reactivity of the *cis*-bis(imido) was explored via protonation experiments a unique U(V) complex was isolated.

Additional protonation reactivity was explored using  $\text{UO}_2(\text{}^t\text{Bubpy})(\text{NTSA})_2$  with a variety of anilines to synthesize uranyl imido complexes. These experiments showed that the electronic environment—not the steric profile—of the anilines has a much greater effect on the stability of the resulting uranyl imido. The resulting uranyl imido complexes demonstrate the analogous nature of uranyl and uranium imido chemistry.

Activation of the *trans*-imido groups on uranium bis(imido) complexes has also been shown with the synthesis of the uranium tris- and tetrakis(imido) complexes. These later complexes have shown that increased electron donation to the uranium metal center weakens and elongates the imido bonds, exposing these compounds to reactivity previously unavailable to uranium compounds with fewer multiply bound groups.

# CHAPTER 1. ELUCIDATION OF BOND ELONGATION IN A URANIUM(IV)-*CIS*-BIS(IMIDO) COMPLEX

## 1.1 Introduction

Efficient chemical processing of spent nuclear fuels represents a major hurdle in the nuclear fuel cycle, preventing its widespread use and contributing to the overall cost of this fuel source.<sup>1-3</sup> Understanding how to close this fuel loop with an eye towards recycling has been a strong driver within the actinide community for the elucidation of the electronic structures of actinide derivatives with metal-element multiple bonds.<sup>4</sup> Of particular interest is gaining new insight into fundamental bonding trends and harnessing redox properties of *f*-block elements for transformation to more value added materials.

The ubiquitous uranyl ion, which features the *trans*- arrangement of  $[\text{O}=\text{U}=\text{O}]^{2+}$  multiple bonds and a hexavalent uranium ion, has been studied for decades. This moiety is postulated to be enforced by the Inverse Trans Influence (ITI).<sup>5,6</sup> This thermodynamic effect has been well studied for the actinides,<sup>7-10</sup> and originates from the mixing of core *p* orbitals with valence axial *f* orbitals, de-emphasizing the toroid and increasing the radial extent of the lobes in the *z* (axial) direction.<sup>5</sup> The result is a preference for a strongly bound ligand positioned *trans*- to another strongly bound ligand.

In recent years, this effect has been observed for uranium imido species, which mimic the electronic structure of uranyl ions, but are easier to work with due to their tunability and monomeric nature.<sup>11-13</sup> Such is the case for the uranyl analogues synthesized by Boncella and coworkers. This family of uranium *trans*-bis-(imido) compounds,  $\text{U}(\text{NR})_2\text{I}_2$  (*R* = Ph, <sup>t</sup>Bu) was found to have a similar electronic structure to uranyl derivatives, but with increased covalency in its multiple bonds compared to its oxygen congener.<sup>11</sup> Prior to the discovery of this family of uranyl analogues, C. Burns and co-workers had synthesized  $\text{Cp}^*_2\text{U}(\text{NPh})_2$ , a *cis*-uranium(VI)-bis(imido) that features bulky Cp\* ligands to sterically constrain the imido groups.<sup>14</sup> In this case, the large ancillary ligands disrupt this commonly observed ITI.

This latter example has also been studied for its reduction chemistry. Simultaneous two-electron reduction of multiply bonded uranium has been observed for uranyl but is fairly uncommon for bis(imido) species. Specifically, Burns showed two electron reduction of  $\text{Cp}^*_2\text{U}(\text{NPh})_2$  by dihydrogen, forming the corresponding uranium(IV) amide,  $\text{Cp}^*_2\text{U}(\text{NHPh})_2$ .<sup>15</sup>

Reduction also results simply by heating this *cis*-bis(imido), forming the cyclometallated uranium(IV) derivative, where a C-H bond of the Cp\* methyl is added across the U=N multiple bond.<sup>16</sup> Similarly, a reductive cycloaddition results for the related uranium(VI) bis(imido), Cp\*<sub>2</sub>U(NSiMe<sub>3</sub>)N[P(SiMe<sub>3</sub>)(Mes)].<sup>17</sup> More recently, Cp\*Al was used to reduce a U(VI) bis(imido) complex to U(IV).<sup>18</sup>

Based on this interesting geometric dichotomy in the realm of imido chemistry, we proposed that it should be possible to generate other *cis* arranged species by making use of bulky ancillary ligands. It was reasoned that using the *tert*-butyl(dimethylsilyl)amide (NTSA),<sup>19-22</sup> which is both sterically bulky and synthetically straightforward, may make it possible to form a uranium *cis*-bis(imido) species in a lower oxidation state than Burns' example. This electron-rich species should show activated uranium-nitrogen multiple bonds that may lend themselves to increased reactivity and functionalization. Using the bulky NTSA ligand a uranium(IV) bis(imido) species was successfully isolated, this complex was exceedingly exciting as the imido ligands are *cis* to one another, a unique and rare arrangement for a uranium bis(imido). Comparisons have also been made computationally to the hexavalent derivative. The control that appears to be afforded by the NTSA ligand on the geometry of uranium bis(imido) complexes has exciting implications for controlling the electronic nature of uranium multiply bound species.

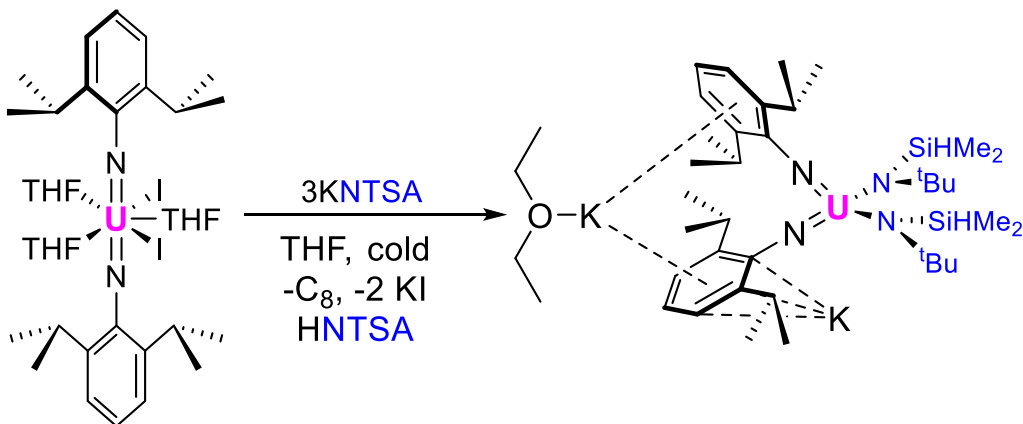
## 1.2 Results and Discussion

### 1.2.1 Synthesis and Characterization

Treating one equivalent of a thawing THF solution of uranium(VI) bis(2,6-diisopropylphenyl)imido, U<sub>2</sub>(NDIPP)<sub>2</sub>(THF)<sub>3</sub>,<sup>23</sup> with three equivalents of KNTSA in cold THF followed by stirring for one hour and workup furnished a dark brown powder (Scheme 1).<sup>24</sup> Purification was achieved by dissolution of this material in diethyl ether and layering with pentane, which resulted in the precipitation of blocks of dark red crystals. The <sup>1</sup>H NMR spectroscopic data clearly reveal several broadened and shifted peaks, consistent with a paramagnetic species. Also present is a resonance consistent with the free amine, HNTSA, indicating that some of the base likely served as a reductant. The multiplicity associated with the diamagnetic U(VI) starting material is noticeably absent, supporting reduction from uranium(VI) occurred during the course of the reaction. The presence of imido ligands is supported by the absence of N-H absorptions by

infrared spectroscopy. The bonding of the -NTSA moiety is also confirmed by a 70  $\text{cm}^{-1}$  shift in the SiH band as seen by IR spectroscopy, from 1929  $\text{cm}^{-1}$  in KNTSA to 2003  $\text{cm}^{-1}$  in this new product.<sup>24</sup>

Scheme 1.1 Initial reaction pathway for  $[\text{U}(\text{NDIPP})_2(\text{NTSA})_2]\text{K}_2(\text{Et}_2\text{O})$



Single crystals were grown in an analogous fashion to the purification procedure, and analysis by X-ray crystallography revealed a tetrahedral uranium compound,  $[\text{U}(\text{NDIPP})_2(\text{NTSA})_2]\text{K}_2(\text{Et}_2\text{O})$ , **1** (Figure 1.1; Table 1.1). The U-N<sub>imido</sub> bond distances in **1** are 2.069(17) and 2.149(11) Å, which are 0.2 to 0.3 Å shorter than the U-N<sub>TSA</sub> distances of 2.365 Å, supporting the presence of two imido and two amido bonds. The U-N bonds are consistent with those for other uranium(IV) imidos, including (MeC<sub>5</sub>H<sub>4</sub>)<sub>3</sub>UNPh<sub>2</sub> (2.019(6) Å),<sup>25</sup> Tp\*<sub>2</sub>UNMes (1.976(3)),<sup>26</sup> Tp\*<sub>2</sub>UNAd (1.953(3)),<sup>26</sup> Cp\*<sub>2</sub>UNMes\* (1.952(12) Å),<sup>27</sup> and Cp\*<sub>2</sub>UNDIPP (2.006(5) Å).<sup>27</sup> The potassium ions are outer sphere, with U-K1 and U-K2 distances of 3.7627(12) Å and 4.422(3) Å, respectively; K2 is also associated to a DIPP group in an adjacent molecule in the crystal lattice. Based on charge balance in **1**, the oxidation state of the uranium is best described as +4, making this the first example of a crystallographically characterized uranium(IV) *cis*-bis(imido) species. With this positive identification of **1**, the formation of HNTSA is likely attributed to the fact that some of the KNTSA served as a reductant, and that H-abstraction from solvent resulted during the reaction.



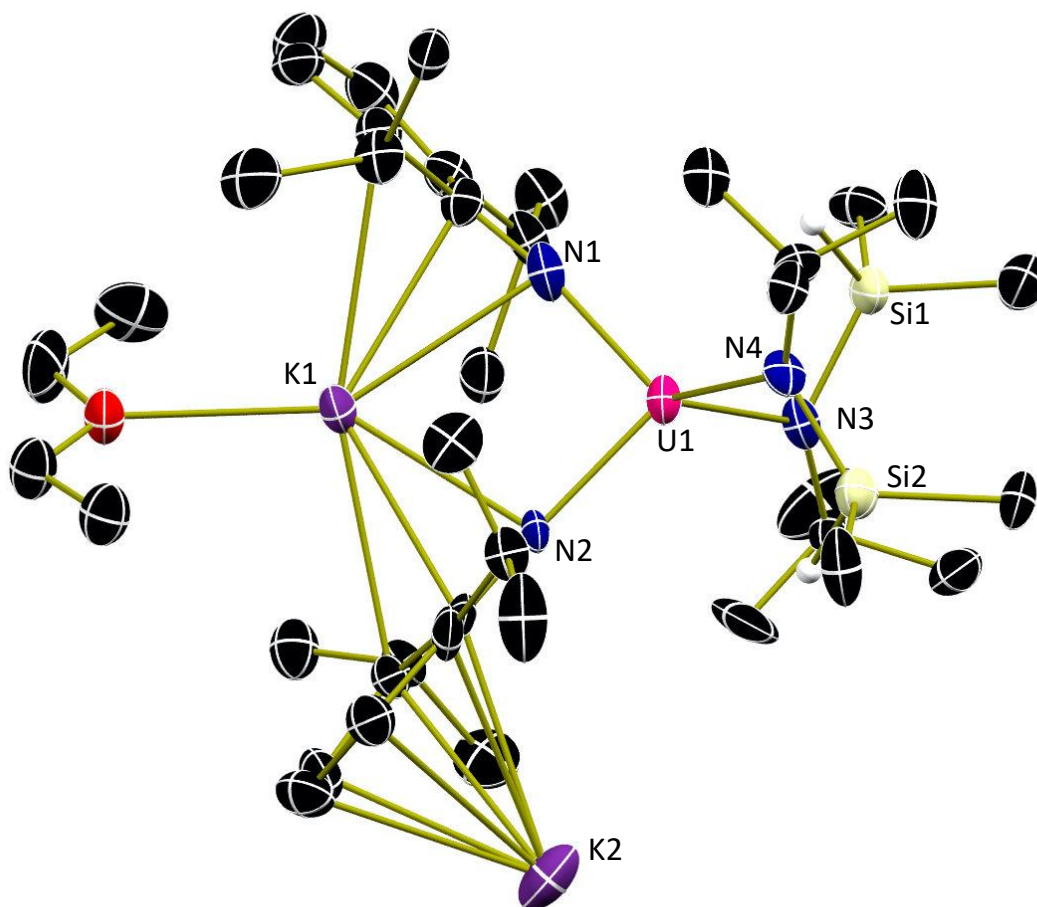


Figure 1.1 Molecular structure of  $[U(NDIPP)_2(NTSA)_2]K_2(Et_2O)$  shown at 30% probability ellipsoids. Selected hydrogen atoms and co-crystallized solvent molecules have been omitted for clarity.

In hexavalent  $Cp^*_2U(NPh)_2$ ,<sup>14</sup> the  $U-N_{imido}$  distance is 1.952(7) Å, which is 0.16 Å longer as compared to that in **1**. Similarly, that distance for **1** is approximately 0.22 Å longer than in *trans*- $UI_2(NDIPP)_2(THF)_3$ ,<sup>23</sup> which is the starting material for **1**. These differences in bond length trend well with the increased atomic radius of U(IV) compared to U(VI). The *cis* nature of the imido groups in **1** is supported by the  $N_{imido}-U-N_{imido}$  angle as well; with **1** having an angle of 95.2(3)° which is 3.5° shallower than that seen in the *cis*-bis(imido) complex,  $Cp^*_2U(NPh)_2$ , at 98.7(3)°,<sup>14</sup> and 74.1° more shallow than the starting *trans*-bis(imido) complex  $N_{imido}-U-N_{imido}$  angle of 169.3(1)°.<sup>19</sup>

Table 1.1 Comparison of Structural Parameters.

	$\text{I}_2\text{U}^{6+}\text{-N}_{\text{imido}}$	$\text{NTSA}_2\text{U}^{4+}\text{-N}_{\text{imido}}$	$\text{Cp}^*_2\text{U}^{4+}\text{-N}_{\text{imido}}^2$
$\text{U-N}_{\text{imido}}$ (Å)	1.887(2), 1.889(2)	2.069(17), 2.149(11)	1.952(7)
$\text{N}_{\text{imido}}\text{-U-N}_{\text{imido}}$ (°)	169.35(14)	95.2(3)	98.7(4)

Electronic absorption spectroscopy was used to assess the electronic structure of **1** (Figure 1.2). Data were acquired from 300-1650 nm as solutions in toluene. The UV-visible region of the spectrum shows extremely broad transitions in this range, with a noticeable transition around ~325 nm. The NIR spectrum also shows broad transitions from 800-1650 nm, which is unusual for uranium(IV),  $f^2$  ions; typically, these transitions are sharp and weakly absorbing.<sup>28</sup> However, the presence of these transitions support the reduction from uranium(VI),  $f^0$ , which would be expected to be flat in this region. Additionally, a pentavalent uranium ion would typically show sharp transitions around 1700 nm, which is not observed here, supporting the +4 oxidation state for **1**.<sup>29</sup>

Due to the unusual reaction stoichiometries for the synthesis of **1**, an independent, rational synthesis was designed. Reduction of  $\text{UI}_2(\text{NDIPP})_2(\text{THF})_3$  from uranium(VI) with one equivalent of potassium graphite for one hour, followed by addition of three equivalents of KNTSA furnished **1** in high yield (94%) after workup (Scheme 1.2.). Analysis by  $^1\text{H}$  NMR spectroscopy confirmed the formation of **1**, validating the need for reduction of the uranium(VI) center in the original synthesis, prior to salt metathesis. Given that this reaction proceeds in much higher yield than the original route, the efficiency of this reduction step seems to play a significant role in the formation of **1**. This supports the notion that at least one of the equivalents of KNTSA acts as a reductant in the original synthesis and is the source of the HNTSA.

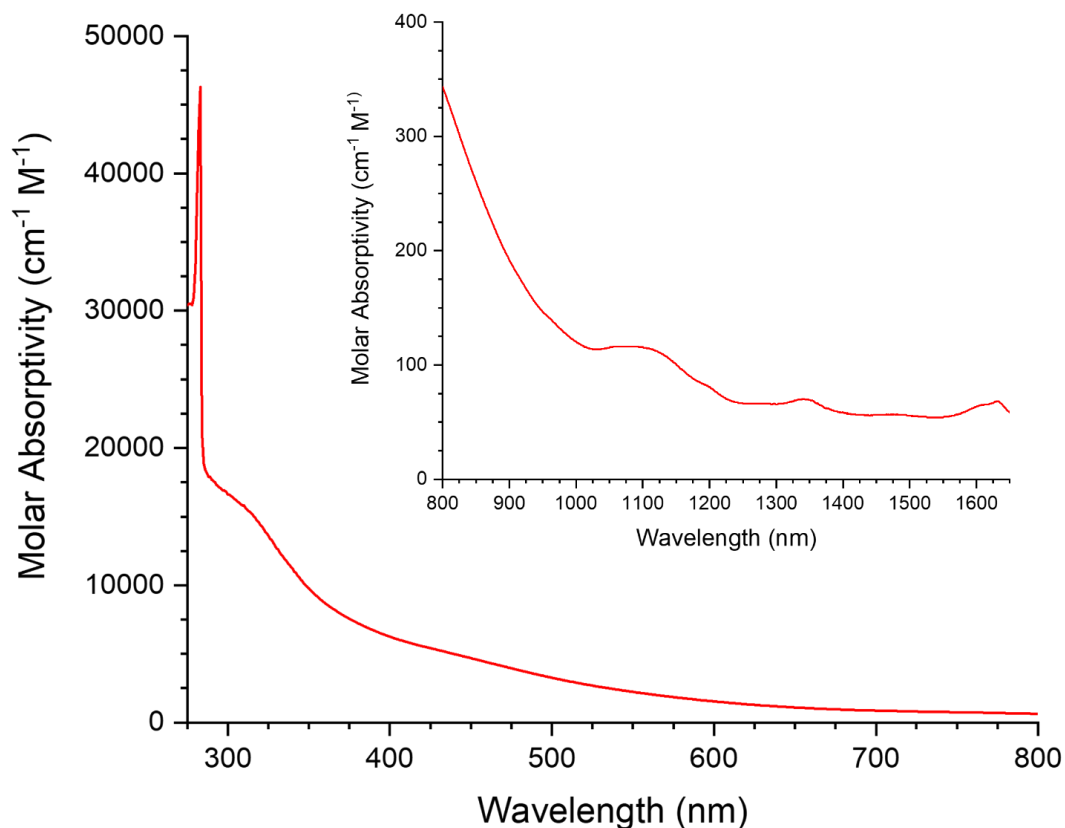
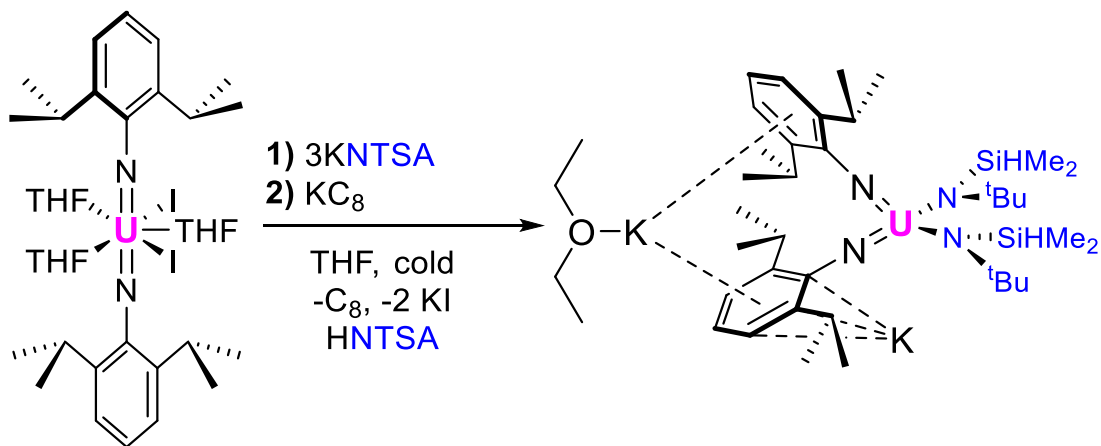


Figure 1.2 Electronic absorption spectra for  $[U(NDIPP)_2(NTSA)_2]K_2(Et_2O)$ , UV-vis recorded from 275 to 800, NIR (inset) recorded from 800 to 1650 nm in toluene at 25 °C.

Scheme 1.2 Rational synthetic route for  $[U(NDIPP)_2(NTSA)_2]K_2(Et_2O)$



Synthesis of **1** is significant as the *cis*-arrangement of the imido substituents marks disruption of the Inverse Trans Influence (ITI) in this uranium species. Based on the crystallographic data, the potassium ion appears to play a role in coordinating to the aryl groups,

helping to stabilize the *cis* arrangement of the imido groups. Interestingly, the arrangement in **1** is quite reminiscent of  $\text{Cp}^*_2\text{U}(\text{NPh})_2$ , where the  $\text{Cp}^*$  rings, although bulky, take on the typical bent metallocene geometry. Because of the analogous nature of U-N and U-O bonds in the respective bis-imido and uranyl derivatives, it will be interesting to see if these results can be generally applied to uranyl complexes, which would facilitate the activation and recycling of spent nuclear fuel to generate more useful materials.

This electron rich uranium(IV) bis(imido) dianion is reminiscent of a recent thorium example reported by P. Arnold and co-workers,  $[\text{K}_2(\text{S})_x][\text{Th}(=\text{NDipp})_2\text{N}''_2]$ .<sup>30</sup> This thorium example is also dianionic, and the authors attribute the long Th-N<sub>imido</sub> bonds of 2.165(3) Å to the fact that this molecule is electron-rich, despite its thorium(IV) oxidation state. Thus, it is reasonable to expect that some of the elongation in this uranium system is also due to its anion nature.

### 1.2.2 Theoretical models.

To understand the role of the counterion, steric effects, and NTSA coordination in the bis(imido) structure, four theoretical models have been considered (Figure 1.2). The first model, **M1**, consists of the optimized crystal structure including the counterion stacked in between the two phenyl rings of the imido ligands. Model 2 (**M2**) corresponds to **M1** without the inclusion of the counterion. Model 3 (**M3**) derives from **M2**, in which the substituents were simplified. Finally, model 4 (**M4**) represents the simplest model, including only two phenylimido (NPh) ligands coordinated to U(IV). Geometrical parameters for these models, including the experimental values for comparison are summarized in Table 4A (Appendix A). From these data, clear trends emerge: U-N<sub>imido</sub> bond lengths are shortened, and the angle defined by N<sub>imido</sub>-U(IV)-N<sub>imido</sub> increases when moving from **M1** to **M4**. These findings are consistent with the counterion preventing the opening of the angle of the N-phenyl rings in **1**. This occurs as steric constraints are removed, and even further when NTSA ligands are not considered. The optimized (calculated) structure of **M4** provides insight into the interactions between U(IV) and the NPh ligands, where evidence of neither the trans influence (TI) nor ITI is observed (Figure 1A; Table 1A, Appendix A). As shown by the geometrical parameters of **M3**, the N<sub>imido</sub>-U(IV)-N<sub>imido</sub> angle is ~ 6° larger than the 109.5° expected for a perfect tetrahedron due to the multiple bond character of the U(IV)-NPh bonds. As a consequence, the NTSA-U(IV)-NTSA angle is decreased to ~106° (Table 1A, Appendix A). It

is very likely that if it were not for the counterions and hydrocarbon-substituents, the structure of **1** would be best described by valence-shell electron-pair repulsion theory (VSEPR).<sup>31</sup>

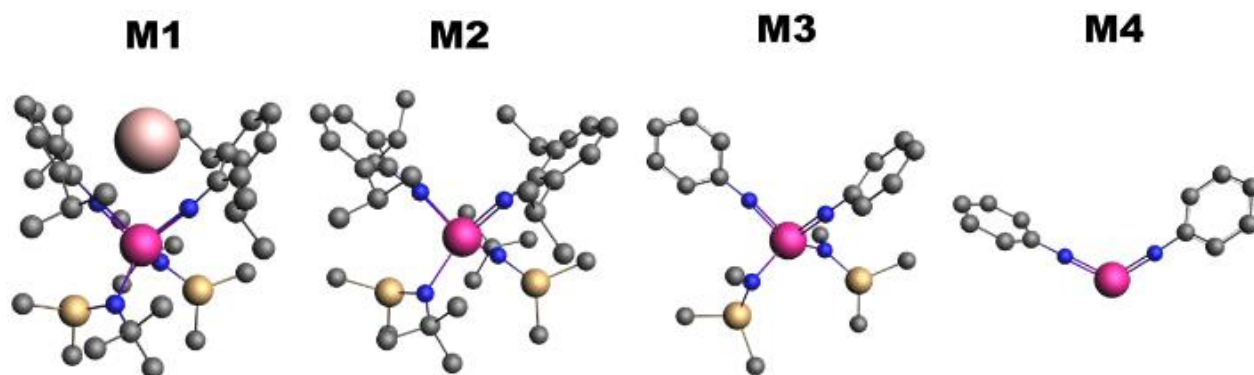


Figure 1.3 These models have been studied to understand the role of the potassium (pink sphere in M1) counterion, and steric factors of the ligands in the coordination arrangement around the U(IV) metal center. U(IV), nitrogen (N), carbon (C), and silicon (Si) atoms are depicted in magenta, blue, grey, and yellow balls, respectively. Geometries depicted correspond to optimizations performed at ZORA/PBE0/STO-TZP level of theory

### ***Electronic structure***

To understand the nature of the ground (GS) and excited states (ES) of **1**, spin-orbit complete active space self-consistent field (SO-CASSCF) calculations were performed. According to the SO-CASSCF calculations, the GS of **M2** corresponds to a  $J=4$  that is composed by 96% triplet, where 66% is assigned to the expected spectroscopic term  $^3H_4$ , with 4% of singlet contributions. Interestingly, the Hartree-Fock (HF) determinant only represents 56% of the GS, while another 21% corresponds to single excitations from a bonding  $\pi f$  orbital to its antibonding  $f\pi^*$  counterpart. The remaining contributions arise from single and double excitations from  $\pi f$  to non-bonding  $5f$  orbitals (Figure 2A, Appendix A). The unusual occurrence of  $\pi f \rightarrow f\pi^*$  excitations in the GS highlights the importance of electron correlation in the correct description of the chemical bond in **1**. In simpler words, correlation allows the population of antibonding orbitals that reduces the strength of one of the U(IV)–N<sub>imido</sub> bonds, which is observed experimentally.

### ***Bonding***

The nature of the chemical bond was investigated using the natural localized molecular orbitals (NLMOs) based on scalar relativistic (SR)-CASSCF densities. Three different types of NLMOs were identified for the interaction between U(IV)–NDIPP (Figure 1.4), whereas only two for the

U(IV)–NTSA bonds (Figure 3A, Appendix A). The NLMOs found for U(IV)–N<sub>imido</sub> (Figure 1.4) are very similar to the natural bond orbitals (NBOs) reported previously by Liddle and co-workers for [U(Tren<sup>TIPS</sup>)(NH)]<sup>1-</sup>,<sup>32</sup> i.e. one  $\sigma$ -type (NLMOs 1 in Figure 1.4) and two  $\pi$ -type (NLMOs 2-3 in Figure 1.4) are present. According to King *et al.*,<sup>32</sup> these NBOs suggest a triple bond associated with the U(IV)–N<sub>imido</sub> interaction; however, despite the similar bond pattern found in our system, in the case of **1** a formal triple bond description for this interaction is not supported. From Figure 1.3 it can be seen that the  $\sigma$ -NLMOs, NLMO1a and NLMO1b, are almost identical in polarization and composition. The same is true for  $\pi$ -NLMOs, NLMO2a and NLMO2b, which are mainly composed of the N<sub>imido</sub>-lone pair lying on the phenyl plane with 10% of U 5f-6d(40/60) hybrid orbital contribution. The second set of  $\pi$ -NLMOs, NLMO3a and NLMO3b, originates from the interaction between the N<sub>imido</sub>-lone pair aligned with the  $\pi$ -system and the uranium ion. These  $\pi$ -type NLMOs differ from each other because they depend on the orientation of the of the U(IV) ion hybridization, resulting in significant differences in both polarization and composition. For instance, NLMO3 (Figure 1.4) has substantial U(IV) contribution with a strong 5f character that is indicative of a less polar bond. Furthermore, this is the only NLMO having an antibonding counterpart, NLMO3b<sub>1</sub>\* and NLMO3b<sub>2</sub>\* (Figure 1.4), indicating that the strength of the bond is affected by the population of these NLMOs. The importance of electron correlation in this bond is reflected in the occupation numbers of 1.8, 0.95, and 1.65 for NLMO3b, NLMO3b<sub>1</sub>\*, and NLMO3b<sub>2</sub>\*, respectively.

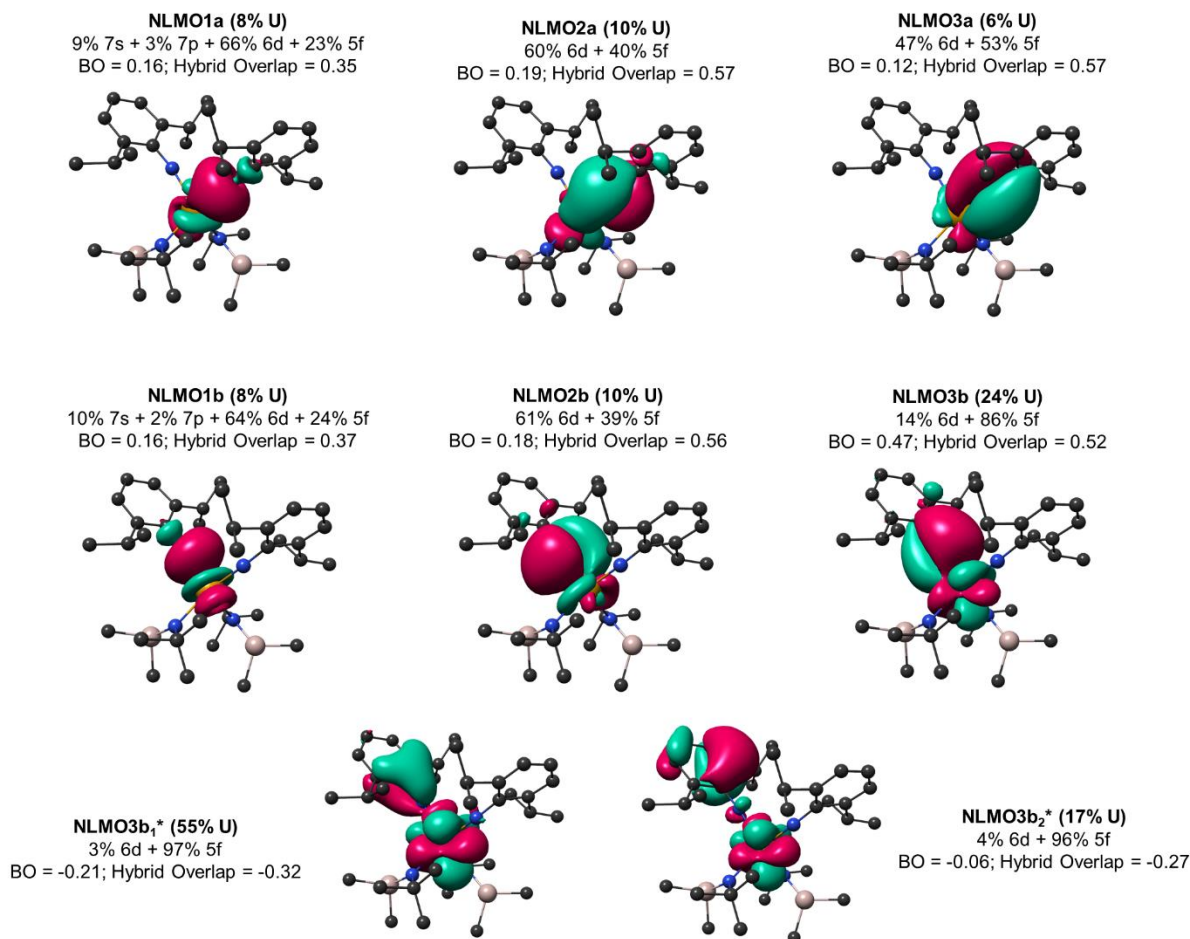


Figure 1.4 Natural localized molecular orbitals (NLMOs) of M2. Bonding interactions between U(IV) and NDIPP ligands are shown. NLMO1a,b displays the  $\sigma$ -type interactions, NLMO2a,b the in-plane  $\pi$ -bond, and NLMO3a,b the  $\pi$ -bond aligned with the  $\pi$ -system of the phenyl rings. Letters a and b are used to distinguish between the two imido ligands. U(IV) contribution to the NLMO and its composition are given. NLMO-based bond orders (BO), and their corresponding hybrid overlap are also given. NLMOs marked with a star correspond to partially occupied antibonding NLMOs counterparts to NLMO3b.

Covalency, from the orbital perspective, is discussed in terms of two main factors, the orbital overlap between ligand and metal orbitals and the energy gap between them. The only way for a covalent bond to become stronger is to increase orbital overlap. Energy match enhances orbital mixing and consequently the bond order, but it does not lead to bond stabilization.<sup>33, 34</sup> An overall qualitative picture of bond strength can be obtained by NLMO decomposition into individual contributions to the total bond order (BO) in addition to the individual hybrid overlap.

If we compare the interaction between each imido ligand with U(IV), it appears that they differ significantly. However, the seemingly ‘most covalent’ bond (NLMO3b Figure 1.4) is counterbalanced by the antibonding contribution to this bond. This can be seen in the total BO contribution coming from  $\sigma$ - and  $\pi$ -interactions, where U(IV)–N<sub>imido(a)</sub> and U(IV)–N<sub>imido(b)</sub> bonds are described with 0.47 and 0.54 bond indices, respectively, in agreement with the difference experimentally observed bond lengths 2.069(17) and 2.149(11) Å (Table 3A, Appendix A), respectively. On the other hand, the hybrid overlap shows that the strength of these bonds is dominated by the  $\pi$ -interactions with similar values between the two imido (Figure. 1.4) and the two NTSA ligands (Supplementary Figure 3, Appendix A).

Another approach to assess covalency is mapping the electron density of **1** using the quantum theory of atoms in molecules (QTAIM) approach based on SR-CASSCF densities. It is important to note the electron correlation between U(IV) and one of the imido ligands; the expansion of the active space was crucial to recover the true nature of the chemical bonds (Table 4A and Computational Details, Appendix A). As expected, U(IV)–N<sub>imido</sub> bonds are more covalent than U(IV)–NTSA bonds, mainly based on the increased accumulation of electron density at the bond critical point (BCP), as well as from increased delocalization indices and more negative energy densities. For partially covalent bonds such as actinide – ligand bonds, the ratio between potential (V) and kinetic (G) energy densities provides an estimation of the degree of polarization of the bond, or how covalent the bond is. U(IV)–N<sub>imido(a)</sub> displays more electron density at the BCP with 33% degree of covalency versus a value of 25% observed in U(IV)–N<sub>imido(b)</sub>. This reduction is attributed to Coulomb correlation that allows polarization of the U(IV)–N<sub>imido(b)</sub> electron density towards the fractionally-occupied 5*f* orbitals, which agrees well with the NLMO analysis.



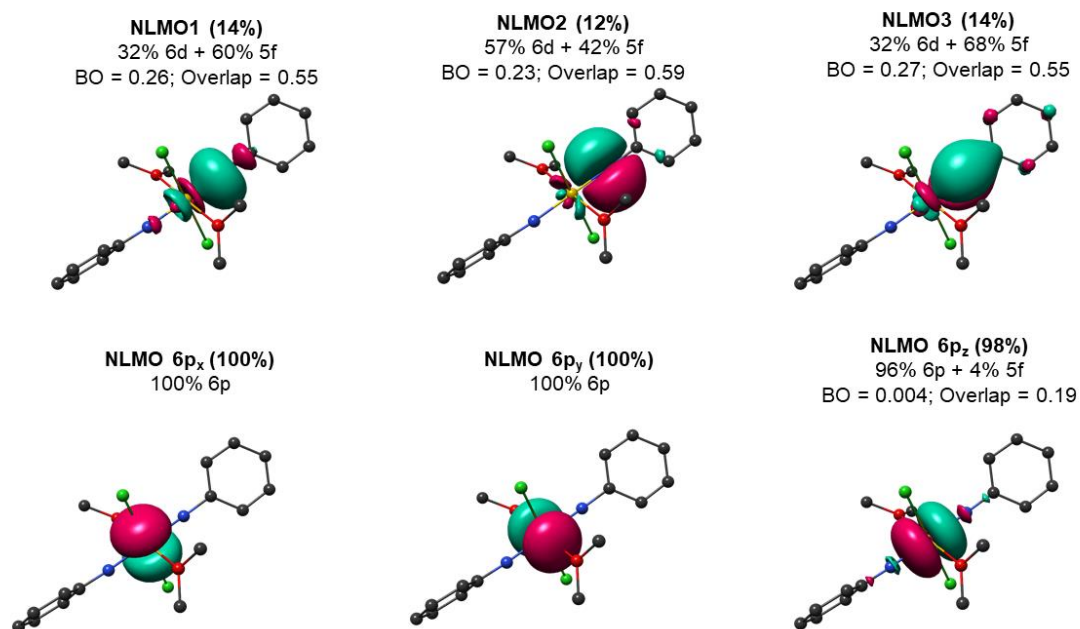


Figure 1.5 NLMOs of  $\text{U(VI)(NPh)}_2\text{Cl}_2\text{THF}_2$ . Main interactions between  $\text{U(VI)}$  and one imido ligand describing the  $\sigma$ - (NLMO1) and  $\pi$ - (NLMO2 and NLMO3) interactions. The other imido shows the same interactions with the same bond order (BO) and hybrid overlap. The semi-core  $6p$  orbitals have been included to show the polarization of the core towards the  $5f$  shell induced by the imido ligands. This effect supports the inverse-trans-influence in this system similar to that seen in  $\text{UO}_2^{2+}$ .<sup>10</sup>

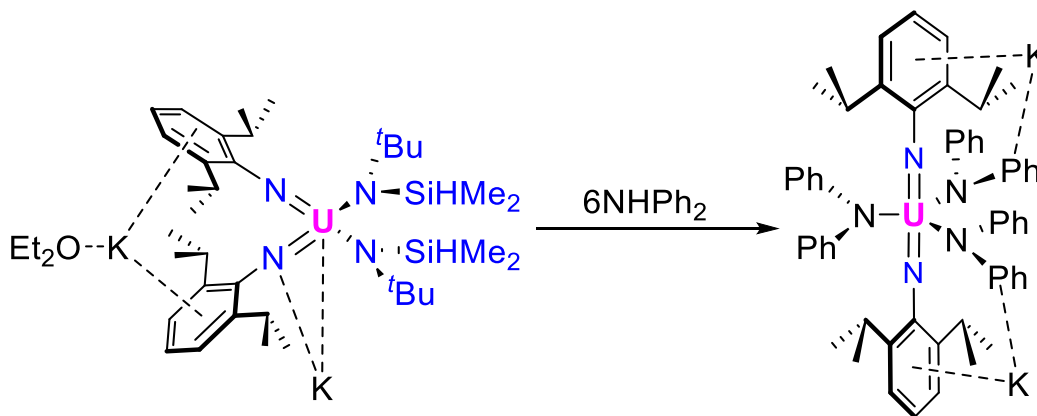
To elucidate differences in the  $\text{U(VI,IV)-N}_{\text{imido}}$  bonds, the  $\text{U(VI)(NPh)}_2\text{Cl}_2\text{DME}_2$  model was considered based on the crystal structure of  $\text{U(VI)(NDIPP)}_2\text{Cl}_2\text{THF}_2$ .<sup>35</sup> This model was developed to simplify the molecule as much as possible without influencing the electronic structure. Since the equatorial coordination - especially solvent coordination - does not bind covalently, the electronic structure is not affected by changing from THF to DME. The NLMO analysis revealed that  $\text{U(VI)-N}_{\text{imido}}$  bonds are more covalent than the  $\text{U(IV)-N}_{\text{imido}}$  ones. The most striking difference is that the  $\sigma$ -bond (NLMO1 in Figure 1.5) is composed of 14%  $\text{U(VI)}$ , displaying an increase of 6% with respect to the  $\text{U(IV)}$  bis(imido) complex, **M2**. Furthermore, the  $5f$  involvement in the formation of this bond is significantly higher (60%  $5f$ ). The strength of the  $\text{U-N}$  bond is also greater in the hexavalent complex, which is seen in the individual bond orders of the  $\sigma$  and  $\pi$  NLMOs. Also of note is the involvement of the semi-core  $6p$  orbitals in bonding. As shown in Figure 1.5, NLMO  $6p_z$  shows polarization towards the  $5f$  orbitals, although with a very low contribution to the actual bond ( $\text{BO} = 0.004$ ), supporting the ITI mechanism operating in this

hexavalent system. This polarization has been reported for other actinide systems, including the uranyl unit, where the NLMO composition for the  $6p$  orbital in the axis where the ITI occurs is very similar to that of Boncella's hexavalent uranium *trans*-bis(imido) complexes.<sup>10</sup> Further discussion about bonding in  $\text{U(VI)(NPh)}_2\text{Cl}_2\text{THF}_2$  can be found in the Supporting Information (Additional Discussion, Appendix A). From the combination of natural localization, deformation densities, and electron density topology mapping, we can conclude that despite the triple bond reported for the  $\text{U(IV)}\text{--bis(imido)}$  interaction,<sup>11</sup> our results support that the strength of the bond matches more closely to that of a formal single bond. Furthermore, the bond is clearly weakened by lowering the oxidation state of uranium, whereas the involvement of semi-core orbitals, and therefore observation of ITI, is only observed in the hexavalent oxidation state (Figure 1.5).

### 1.2.3 Preliminary Reactivity

To experimentally probe how activated the uranium imido nitrogen bonds are in **1** reactivity with primary amines was carried out. The chosen amine was diphenylamine ( $\text{NHPh}_2$ ) (Scheme 1.3) as this molecule only has one proton that will participate in protonation chemistry; moreover, having only the single proton available makes incomplete deprotonation of the amine

Scheme 1.3 Reactivity of **1** with  $\text{NHPh}_2$ , forming  $[\text{U(NDIPP)}_2(\text{NPh}_2)_3]\text{K}_2$



by **1** unlikely to occur. Using an excess of amine (six equivalents)—this will allow for full protonation of all ligands surrounding the uranium center—**1** was allowed to react overnight, upon work up and crystallization a uranium(V) complex was isolated and determined to be  $[\text{U(NDIPP)}_2(\text{NPh}_2)_3]\text{K}_2$ , **2**, (Figure 1.6). This complex provides experimental insight into the

stability that is provided by the NTSA ligands to the uranium center and to the imido ligands. Computations show that the steric effects of the NTSA ligands do not play a significant role in maintaining the *cis*- geometry of **1**, but this reactivity demonstrates there is a potential electronic stabilization effect that is removed once the NTSA ligands are protonated from **1**. The NPh<sub>2</sub> ligands are not much smaller sterically than the NTSA ligands but do lack the same electronic donation ability that is present with the NTSA ligand. This change in electronic effects appears to cause a reemergence of the ITI and with that an opening in the coordination sphere of the complex allowing a third ligand to bind the equatorial plane effectively reducing the oxidation state from U(IV) to U(V).

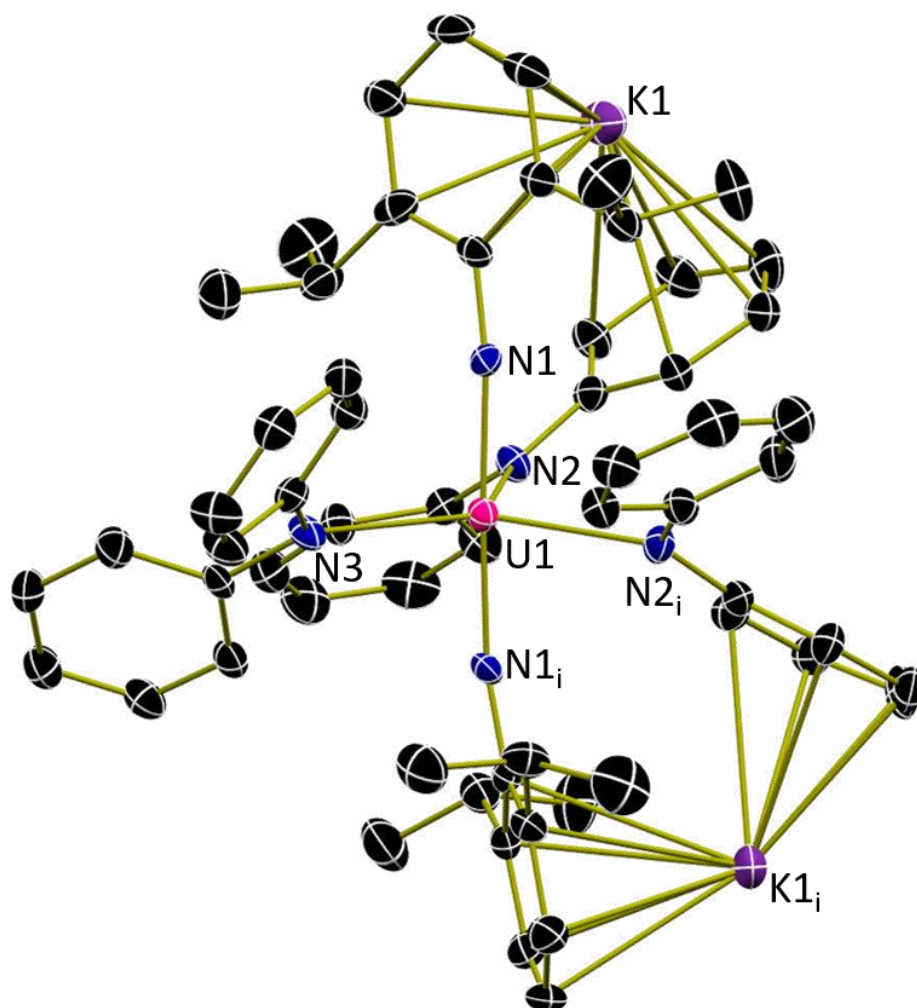


Figure 1.6 Molecular structure of [U(NDIPP)<sub>2</sub>(NPh<sub>2</sub>)<sub>3</sub>]K<sub>2</sub> shown with 30% probability ellipsoids. Hydrogen atoms and co-crystallized solvent molecules have been omitted for clarity.

Complex **2** has a reappearance of the ITI was disrupted by the NTSA ligands in **1**. It is not too surprising that the NTSA ligands were the first to be protonated by free NPh<sub>2</sub>, it is surprising that the exchange of NTSA ligands for NPh<sub>2</sub> eliminates the ability of the complex to hold the imido ligands *cis*- to one another. The addition of a third NPh<sub>2</sub> ligand makes sense, in order to fill the now open coordination environment. When looking at the bond distances found in **2** (Table 1.2) it is clear to see that the oxidation state has increased from uranium(IV) to uranium(V). This change in oxidation state is supported by the U-N1 distance as uranium imido bonds increase by approximately 0.1 Å, corresponding to an increase in the ionic radius of the uranium metal center as the oxidation state decreases. The distances of the NPh<sub>2</sub> ligands also support classification of these as amides, as the bond distance is approximately 0.5 Å longer than the now *trans*-imido ligands.

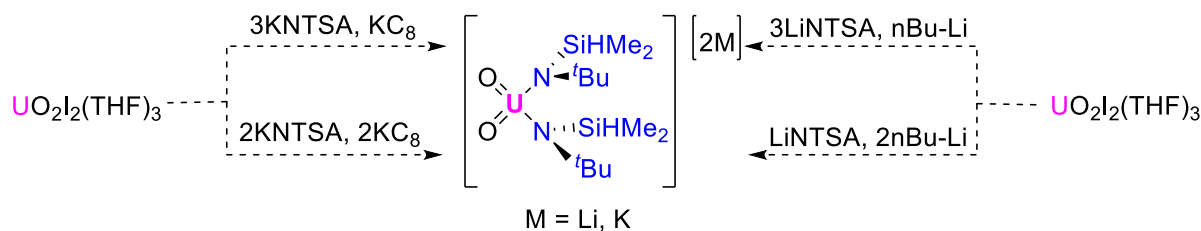
Table 1.2. Structural parameters for [U(NDIPP)<sub>2</sub>(NPh<sub>2</sub>)<sub>3</sub>]K<sub>2</sub>

Atoms	Bond Length, Å
U1-N1	1.983(6)
U1-N2	2.437(7)
U1-N3	2.535(9)

#### 1.2.4 Investigation of analogous synthesis with uranyl complexes

With the successful synthesis of **1** using KNTSA and KC<sub>8</sub>, synthetic routes using the same reagents and uranyl diiodide, UO<sub>2</sub>I<sub>2</sub>(THF)<sub>3</sub>, were investigated to determine whether the reactivity is transferrable from the uranium bis(imido) in order to synthesize a *cis*-uranyl complex (Scheme 1.4). Starting with the synthesis as described for **1**, the uranyl analog does not proceed in a similar fashion as that observed for the uranium imido complex. Unfortunately, the resulting reaction mixture does not have a clear uranium product. Spectroscopic data for this is analogous reaction appears to have little to no uranyl imido product as the free NTSA signals—that being unreacted KNTSA and protonated NHTSA—overpower any uranium or uranyl features that might be seen by <sup>1</sup>H NMR and IR spectroscopy. This result might come from the addition of KC<sub>8</sub> to the uranyl prior to KNTSA which could be reducing the uranyl starting material and creating a product that does not react with KNTSA as expected. To avoid this potential pitfall, the order of addition was reversed; however, this change did not improve the reaction, with similar handles seen by <sup>1</sup>H NMR spectroscopy as the original procedure.

Scheme 1.4 Proposed pathways to a *cis*-uranyl complex



These experiments show analogous reactions do not work for this uranyl starting material; therefore, variations were made to the quantity and order in which reductant and MNTSA (M=K or Li) were added. Prerduction with  $\text{KC}_8$  gave unidentifiable products, but also an insoluble dark powder that appears to be a uranium oxide species as  $^1\text{H}$  NMR spectroscopy showed the presence of the free amine, with no desired reaction products. When the order of addition was reversed a reaction appeared to occur as a brown solid was able to be separated *via* filtration, which upon work up of the filtrate leaves a dark red oil. However, attempts to characterize the oil by NMR spectroscopy showed free amine and solvent and no solids were recovered from crystallizations. Initial experiments to reduce with *n*-BuLi and LiNTSA did not work better as similar solids and oils were recovered, this is likely due to  $\text{Li}^+$  being a weaker reductant when compared to  $\text{K}^+$ . However, further experiments focused on stoichiometric amounts of LiNTSA and *n*-BuLi provided better results for the synthesis of a uranyl bis-NTSA complex. Looking at Figure 1.7, the three peaks for NTSA are shifted from the free amine, while they are broad this could be in part due to fluxional THF bonding to the molecule; there is a very broad resonance for THF when the spectra baseline is increased in intensity. This product does still have the issue of being an oily solid once worked up, which may also play into the broadness of the resonances seen by  $^1\text{H}$  NMR.

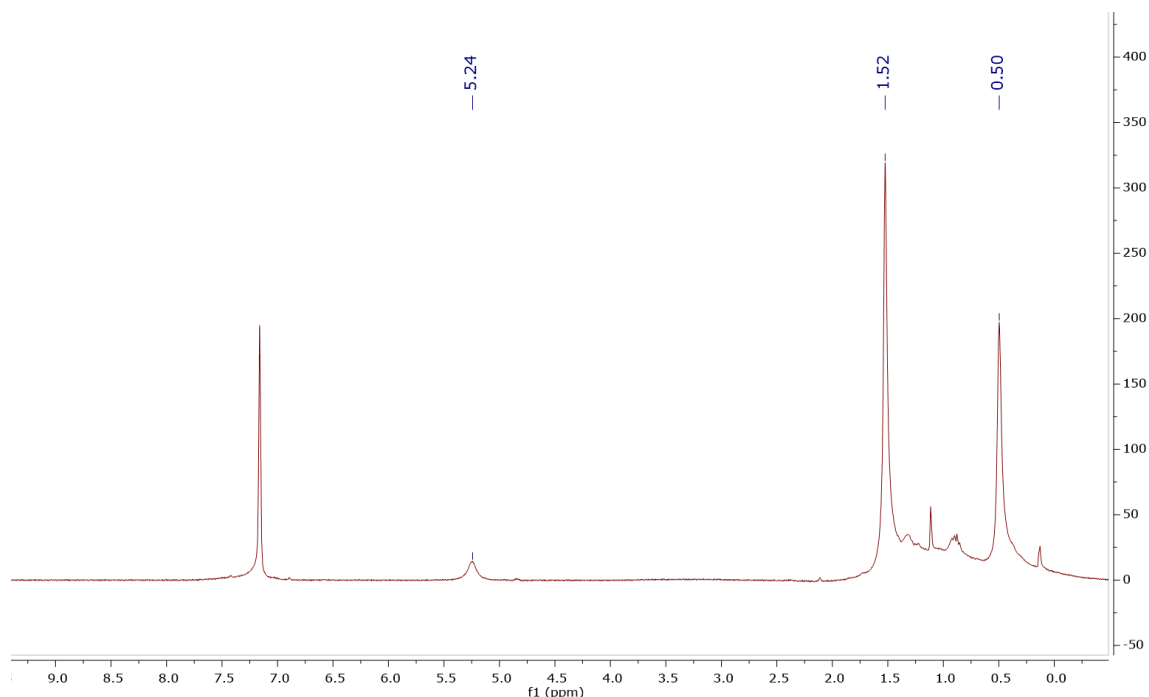


Figure 1.7  $^1\text{H}$  NMR spectra of proposed  $[\text{UO}_2(\text{NTSA})_2]\text{Li}_2$  complex.

These stoichiometric reactions with uranyl diiodide do show more promise for the synthesis of uranyl complexes analogous to **1** because of the shift in the NTSA ligand NMR resonances. Specifically, the resonance corresponding to the SiH proton. It has been shown from previous work with NTSA by our group that when bound to a uranium center the peak will shift downfield.<sup>19</sup> The resonance of the SiH in Figure 1.7 is at 5.25 ppm about 0.4 ppm from the free amine at 4.84 ppm, this supports bonding of the NTSA ligand to the uranium center, and the paramagnetic nature of the spectra also supports a uranium(IV) oxidation state.

### 1.3 Conclusions

In summary, the unusual bent uranium(IV) bis(imido) compound has been presented. Unlike its uranium(VI) counterparts, the U-N<sub>imido</sub> bonds are long due in part to the larger ionic radius of the uranium(IV) ion, but also in part to a unique electronic structure that was discovered by computational analyses. Full characterization using a variety of spectroscopic and crystallographic techniques supports this claim. From the theoretical viewpoint, the 5*f* orbitals play a crucial role in the bond formation of the U(IV)–bis(imido); however, the near-energy degeneracy between the imido 2*p*<sub>π</sub> orbitals with the 5*f* shell weakens one of the U(IV)–N<sub>imido</sub> bonds through static electron

correlation, further increasing the bond length. The partial occupation of antibonding orbitals as we observe is responsible for the asymmetric nature of the U-N bonds in this species and has not been previously reported. The resulting activation of strong uranium-element bonds, which are key components of spent nuclear fuels, could have an impact in spent nuclear fuel processing and recycling to make nuclear power more accessible and environmentally benign.

Reactivity studies with this *cis*-bis(imido) complex have also shown that this molecule will readily exchange the NTSA ligands lending more promise to finding a pathway to activate the uranium imido bonds even further. In addition to this reactivity this molecule has provided new avenues to explore for uranyl activation through the synthesis of analogous uranyl bis(NTSA) complexes to investigate whether similar activation and geometry changes can be achieved.

## 1.4 Experimental Methods

### 1.4.1 General Considerations

All air- and moisture-sensitive manipulations were performed using standard Schlenk techniques or in an MBraun inert atmosphere drybox with an atmosphere of purified nitrogen. The MBraun drybox was equipped with two  $-35\text{ }^{\circ}\text{C}$  freezers for cooling samples and crystallizations. Solvents for sensitive manipulations were dried and deoxygenated using literature procedures with a Seca solvent purification system.<sup>36</sup> Benzene- $\text{d}_6$  was purchased from Cambridge Isotope Laboratories, dried with molecular sieves and sodium, and degassed by six freeze–pump–thaw cycles. KNTSA,<sup>24</sup> potassium graphite,<sup>37</sup> and  $\text{U}_2(\text{NDIPP})_2\text{THF}_4$ <sup>23</sup> were synthesized according to literature procedures.

**Caution:** *U-238 is a weak  $\alpha$ -emitter with a half-life of  $t_{1/2} = 4 \times 10^9$  years. All manipulations were performed in an inert atmosphere glovebox in a laboratory equipped with proper detection equipment.*

$^1\text{H}$  NMR spectra were recorded at  $25\text{ }^{\circ}\text{C}$  on a Varian Inova 300, spectrometer operating at 299.96 MHz. All chemical shifts are reported relative to the peak for  $\text{SiMe}_4$ , using  $^1\text{H}$  (residual) chemical shifts of the solvent as a secondary standard. For all molecules, the NMR data are reported with the chemical shift and peak assignment, followed by the peak width at half height. Infrared spectra were recorded using a Thermo Nicolet 6700 spectrometer; samples were prepared by grinding the desired compound together with KBr salt and pressing the solid into a pellet.

Elemental analyses were performed by Midwest Microlab (Indianapolis, IN). Electronic absorption spectroscopic measurements were recorded at ambient temperature in sealed 1 cm quartz cuvettes with a Cary 6000i UV–Vis-NIR spectrophotometer.

Single crystals of  $[\text{U}(\text{NDIPP})_2(\text{NTSA})_2]\text{K}_2$  suitable for X-ray diffraction were coated with poly(isobutylene) oil in a glovebox and quickly transferred to the goniometer head of a Bruker Quest diffractometer with kappa geometry, an I- $\mu$ -S microsource X-ray tube, laterally graded multilayer (Goebel) mirror single crystal for monochromatization, a Photon-II area detector and an Oxford Cryosystems low temperature device. Examination and data collection were performed with Cu K $\alpha$  radiation ( $\lambda = 1.54178 \text{ \AA}$ ) at 150 K.

Single crystals of  $\text{UCl}_2(\text{NDIPP})_2(\text{THF})_2$  suitable for X-ray diffraction were coated with poly(isobutylene) oil in a glovebox and quickly transferred to the goniometer head of a Bruker Quest diffractometer with kappa geometry, an I- $\mu$ -S microsource X-ray tube, laterally graded multilayer (Goebel) mirror single crystal for monochromatization, a Photon-II area detector and an Oxford Cryosystems low temperature device. Examination and data collection were performed with Mo K $\alpha$  radiation ( $\lambda = 0.71073 \text{ \AA}$ ) at 100 K. See the crystallography section below for details on single-crystal structure determination.

## 1.4.2 Synthesis

### *Potassium tert-butyl(dimethyl)silylamide (KNTSA)*

A 20-mL scintillation vial was charged with benzyl-potassium (1.09 g, 8.37 mmol), a stir bar, and 10 mL diethyl ether to make a suspension. While stirring, *tert*-butyl(dimethylsilyl)amine (HNTSA)<sup>19</sup> (1.00 g, 7.62 mmol) was added dropwise to this solution until all the suspended benzyl-potassium was consumed as indicated by disappearance of the intense orange color. This orange suspension gradually changed to a pale-yellow solution. After 30 minutes of stirring, the solution was dried in vacuo leaving a pale-yellow powder (1.168 g, 91 %) assigned as potassium -butyl(dimethylsilyl)amide, KNTSA. The solid was washed with pentane and dried to further remove toluene that was formed during the reaction. <sup>1</sup>H NMR ( $\text{C}_6\text{D}_6$ , 25 °C):  $\delta$  0.32 (dd, 6.2H,  $\text{SiH}(\text{CH}_3)_2$ ), 1.28 (s, 10.1H,  $\text{C}(\text{CH}_3)_3$ ), 4.84 (sept, 1H, *SiH*). IR (KBr,  $\text{cm}^{-1}$ ): 2946 m, 2853 m, 1929 s ( $\nu_{\text{SiH}}$ ), 1861 m, 1344 m, 1240 m, 1211 m, 1190 m, 1060 m, 939 m, 877 m, 823 m, 800 m, 757 m, 742 m.



### *[U(NDIPP)<sub>2</sub>(NTSA)<sub>2</sub>]K<sub>2</sub>, 1*

A 20-mL scintillation vial was charged with  $\text{UI}_2(\text{NDIPP})_2\text{THF}_4$  (0.500 g, 0.44 mmol),<sup>23</sup> THF (10 mL), and a stir bar. While stirring, one equivalent of  $\text{KC}_8$  (0.065 g, 0.48 mmol) was slowly added as a solid, causing an immediate color change from dark brown to black. This black mixture was allowed to stir for an additional hour, upon which a solution of 3 equivalents of KNTSA (0.225 g, 1.33 mmol) dissolved in cold THF (5 mL) was added dropwise. The combined reaction was then allowed to stir for one hour longer. This mixture was then filtered through Celite on a medium frit to remove  $\text{C}_8$  and KI. The filtrate was dried *in vacuo*, and the residue was washed with pentane (3 mL) twice and dried leaving a brown/black powder (0.385 g, 94 %) assigned as  $[\text{U}(\text{NDIPP})_2(\text{NTSA})_2]\text{K}_2$ . Elemental Analysis, Theory: C 47.67, H 7.58, N 5.85, Calc: C 46.60, H 7.04, N 5.71.  $^1\text{H}$  NMR ( $\text{C}_6\text{D}_6$ , 300 MHz, 25 °C):  $\delta$  -14.62 (s,  $\text{Si}(\text{CH}_3)_2$ , 50 Hz), -2.84 (s,  $^t\text{BuCH}_3$ , 100), -2.10 (s,  $^i\text{Pr-CH}$ , 30), -0.99 (s,  $^i\text{Pr-CH}_3$ , 100), 10.34 (s, DIPP-ArH, 55), 14.14 (s, DIPP-ArH, 80), 34.15 (s, SiH, 40) (THF- $d_8$ , 300 MHz, 25 °C):  $\delta$  -3.79 (s,  $^i\text{Pr-CH}$ , 7 Hz), -2.67 (s,  $\text{Si}(\text{CH}_3)_2$ , 10), -1.32 (s,  $^i\text{Pr-CH}_3$ , 10), -0.13 (s, SiH, 10), 1.11 (s,  $^t\text{BuCH}_3$ , 8), 11.35 (t, DIPP-ArH, 8), 14.78 (d, DIPP-ArH, 14). IR (KBr pellet,  $\text{cm}^{-1}$ ): 2955 m, 2864 m, 2003 br ( $\nu_{\text{SiH}}$ ), 1574 m, 1461 m, 1401 m, 1354 m, 1322 m, 1253 m, 1196 m, 1134 m, 1107 m, 1042 m, 977 m, 899 m, 867 m, 837 m, 779 m, 752 m, 697 m, 578 m, 515 m, 489 m.

### *[U(NDIPP)<sub>2</sub>(NPh<sub>2</sub>)<sub>3</sub>]K<sub>2</sub>, 2*

In a JYoung fitted NMR tube **1** (0.015g, 0.016 mmol) was dissolved in  $\text{C}_6\text{D}_6$  (2mL). To this solution 6 equiv. of diphenylamide (0.016g, 0.097 mmol) was added, the tube was inverted several times and the combined reaction was then analyzed. After sitting overnight, crystals of  $[\text{U}(\text{NDIPP})_2(\text{NPh}_2)_3]\text{K}_2$  were isolated.  $^1\text{H}$  NMR ( $\text{C}_6\text{D}_6$ , 300 MHz, 25 °C): paramagnetic peaks are seen from -7 to 23 ppm (Appendix A, Figure 6).

## **1.4.3 Computational details.**

### *Geometry optimization*

Geometry optimizations have been performed in ADF2019<sup>38, 39</sup> using the generalized gradient approximation (GGA) functional PBE along with the slater-type basis functions (STO) TZP. The scalar relativistic effects were included by means of the zero<sup>th</sup>-order relativistic approximation (ZORA) Hamiltonian.<sup>40</sup> No geometry nor symmetry constraints were imposed for

the optimization process. To obtain the potential energy surface (PES) of the  $N_{\text{imido}} - U - N_{\text{imido}}$  angle, individual optimization steps were performed constraining the position of this angle from  $90^\circ - 180^\circ$ . The same level of theory used in the fully relaxed geometry optimization was considered for the PES scan. The PES surface was constructed from single-point energies using the hybrid functional PBE0 to correct overdelocalization errors coming from pure GGA functionals. The individual single point energies were fitted to third-order polynomial functions ( $r^2 = 0.992 - 0.999$ ).

### *Electronic structure*

The electronic structures of **M2**, **M3** (used to obtain the PES) and  $U(VI)(NPh)_2Cl_2DME_2$  were analyzed through the Complete Active Space Self Consistent Field (CASSCF). Initially, KS-DFT (Kohn-Sham density functional theory) wavefunctions were obtained at PBE0<sup>41</sup> level of theory in conjunction with the def2-TZVP basis set<sup>42</sup> for all atoms except U which was treated with the SARC-DKH-TZVP basis set.<sup>43</sup> Scalar relativistic (SR) effects were included via the second-order Douglas-Kroll-Hess (DKH2) Hamiltonian.<sup>44</sup> The resulting KS-DFT wavefunctions were subjected to state-average (SA) CASSCF calculations<sup>45</sup> that recover static and partial dynamic correlation energy. This method divides the canonical orbital space into inactive, virtual, and active subspaces, where in the latter a full-CI is carried out. A minimal active space was chosen and consisted of two electrons in seven *5f* orbitals, CAS(2,7), including triplets and singlets in case of **M2** and **M3**, and only singlets for  $U(VI)(NPh)_2Cl_2DME_2$ . Scalar relativistic effects were incorporated by the DKH2 Hamiltonian, while spin-orbit (SO) coupling through quasi-degenerate perturbation theory (QDPT). Further dynamic correlation was recovered by the N-electron valence state perturbation theory (NEVPT2), where excitations between the three subspaces were considered.<sup>46</sup> All these calculations were performed using the ORCA 4.2.1 package.<sup>47</sup> Due to the multiple-bond nature of the metal-imido ligands, the active space needs to be expanded to recover electron correlation between the metal and the ligands. Attempts to include ligand orbitals in the active space using both state-average and state-specific approximations were unsuccessful, evidencing that the same set of orbitals (state-averaged or state-specific) cannot be used for describing the electronic structure of **M2** nor  $U(VI)(NPh)_2Cl_2DME_2$ . To deal with this inconvenience, open-MOLCAS<sup>48</sup> was used because the CASSCF implementation allows to obtain different sets of orbitals for each multiplicity.

The procedure is similar to that of ORCA. The single-determinant KS-DFT wavefunction was calculated using the PBE0 functional along with the all-electron ANO-RCC Gaussian-type basis sets contracted to TZP quality.<sup>49, 50</sup> Scalar relativistic effects were included via DKH2 Hamiltonian. The resulting wavefunction was employed to perform SA-CASSCF calculations but, this time, for each multiplicity separately. The active space of **M2** consisted of four electrons in eight orbitals, CAS(4,8), where an internal orbital from one of the imido ligands was included in addition to the seven *5f* orbitals. This orbital was the only bonding orbital near-energy degenerate to the active space with considerable ligand-metal mixing. In case of U(VI)(NPh)<sub>2</sub>Cl<sub>2</sub>DME<sub>2</sub> a CAS(8,12) was performed by including 4π bonding orbitals, their antibonding counterparts and 4 non-bonding *5f* orbitals. Two of π bonding orbitals come from the U(VI) - N<sub>imido</sub>-lone pair interaction lying on the phenyl plane while the other two come from the U(VI) - N<sub>imido</sub>-lone pair interaction, but this time aligned with the π system. The expansion of the active space allowed to explore the inclusion of higher multiplicities in both systems. SO coupling was treated by state interactions between these CASSCF wavefunctions, using the restricted active space state interaction (RASSI) method.<sup>51</sup> The SO operator matrix was calculated from an atomic mean-field (AMFI) approximation.<sup>52</sup>

### Bonding

To obtain a more accurate picture of the chemical bond, NLMO and QTAIM analyses based on CAS(4,8) [**M2**] and CAS(8,12) [U(VI)(NPh)<sub>2</sub>Cl<sub>2</sub>DME<sub>2</sub>] densities were carried out. The NLMO analysis was performed in the standalone version of NBO7.0,<sup>53</sup> while the AIMAll package<sup>54</sup> was used to perform the QTAIM analysis. Since ETS-NOCV<sup>55</sup> is implemented in ADF2019<sup>38, 39</sup>, KS-DFT was used to perform the energy decomposition analysis. The ZORA/PBE0/STO-TZP level of theory was used to perform the ETS-NOCV analysis.

## 1.5 References

1. Gras, J.-M.; Quang, R. D.; Masson, H.; Lieven, T.; Ferry, C.; Poinssot, C.; Debes, M.; Delbecq, J.-M. "Perspectives on the closed fuel cycle: Implications for high-level waste matrices." *J. Nucl. Mater.* **2007**, 362, 383-394.
2. Katz, J.; Morss, L. R.; Seaborg, G. T., *The Chemistry of the Actinide Elements*. Chapman Hall: New York, 1980.
3. Jones, M. B.; Gaunt, A. J. "Recent Developments in Synthesis and Structural Chemistry of Nonaqueous Actinide Complexes." *Chem. Rev.* **2013**, 113, 1137-1198.

4. Hayton, T. W. "Metal-ligand multiple bonding in uranium: structure and reactivity." *Dalton Trans.* **2010**, 39, 1145-1158.
5. Denning, R. G., Electronic structure and bonding in actinyl ions. In *Complexes, Clusters and Crystal Chemistry*, Springer Berlin Heidelberg: 1992; Vol. 79, pp 215-276.
6. Denning, R. G. "Electronic Structure and Bonding in Actinyl Ions and their Analogs." *J. Phys. Chem. A* **2007**, 111, 4125-4143.
7. Lam, O. P.; Franke, S. M.; Nakai, H.; Heinemann, F. W.; Hieringer, W.; Meyer, K. "Observation of the Inverse Trans Influence(ITI) in a Uranium(V) Imide Coordination Complex: An Experimental Study and Theoretical Evaluation." *Inorg. Chem.* **2012**, 51, 6190-6199.
8. Lewis, A. J.; Mullane, K. C.; Nakamaru-Ogiso, E.; Carroll, P. J.; Schelter, E. J. "The Inverse Trans Influence in a Family of Pentavalent Uranium Complexes." *Inorg. Chem.* **2014**, 53, 6944-6953.
9. O'Grady, E.; Kaltsoyannis, N. "On the inverse trans influence. Density functional studies of  $[\text{MOX}_5]^n$  (M = Pa, n = 2; M = U, n = 1; M = Np, n = 0; X = F, Cl or Br)." *J. Chem. Soc., Dalton Trans.* **2002**, 1233-1239.
10. Windorff, C. J.; Celis-Barros, C.; Sperling, J. M.; McKinnon, N. C.; Albrecht-Schmitt, T. E. "Probing a variation of the inverse-trans-influence in americium and lanthanide tribromide tris(tricyclohexylphosphine oxide) complexes." *Chem. Sci.* **2020**, 11, 2770-2782.
11. Hayton, T. W.; Boncella, J. M.; Scott, B. L.; Palmer, P. D.; Batista, E. R.; Hay, P. J. "Synthesis of Imido Analogs of the Uranyl Ion." *Science* **2005**, 310, 1941-1943.
12. Anderson, N. H.; Odoh, S. O.; Yao, Y.; Williams, U. J.; Schaefer, B. A.; Kiernicki, J. J.; Lewis, A. J.; Goshert, M. D.; Fanwick, P. E.; Schelter, E. J.; Walensky, J. R.; Gagliardi, L.; Bart, S. C. "Harnessing redox activity for the formation of uranium tris(imido) compounds." *Nat. Chem.* **2014**, 6, 919-926.
13. Anderson, N. H.; Xie, J.; Ray, D.; Zeller, M.; Gagliardi, L.; Bart, S. C. "Elucidating bonding preferences in tetrakis(imido)uranate(VI) dianions." *Nat. Chem.* **2017**, 9, 850-855.
14. Arney, D. S. J.; Burns, C. J.; Smith, D. C. "Synthesis and structure of the first uranium(VI) organometallic complex." *J. Am. Chem. Soc.* **1992**, 114, 10068-9.
15. Peters, R. G.; Warner, B. P.; Burns, C. J. "The Catalytic Reduction of Azides and Hydrazines Using High-Valent Organouranium Complexes." *J. Am. Chem. Soc.* **1999**, 121, 5585-5586.
16. Peters, R. G.; Warner, B. P.; Scott, B. L.; Burns, C. J. "C-H Bond Activation with Actinides: The First Example of Intramolecular Ring Bite of a Pentamethylcyclopentadienyl Methyl Group." *Organometallics* **1999**, 18, 2587-2589.

17. Ward, R. J.; Rungthanaphatsophon, P.; Rosal, I. d.; Kelley, S. P.; Maron, L.; Walensky, J. R. "Divergent uranium- versus phosphorus-based reduction of  $\text{Me}_3\text{SiN}_3$  with steric modification of phosphido ligands." *Chemical Science* **2020**, *11*, 5830-5835.
18. Ward, R. J.; Del Rosal, I.; Chirdon, D. N.; Kelley, S. P.; Tarlton, M. L.; Maron, L.; Walensky, J. R. "Two-Electron Reduction of a U(VI) Complex with  $\text{Al}(\text{C}_5\text{Me}_5)$ ." *Inorg. Chem.* **2020**, *59*, 16137-16142.
19. Pattenau, S. A.; Coughlin, E. J.; Collins, T. S.; Zeller, M.; Bart, S. C. "Expanding the Library of Uranyl Amide Derivatives: New Complexes Featuring the tert-Butyldimethylsilylamide Ligand." *Inorg. Chem.* **2018**, *57*, 4543-4549.
20. Eedugurala, N.; Wang, Z.; Yan, K.; Boteju, K. C.; Chaudhary, U.; Kobayashi, T.; Ellern, A.; Slowing, I. I.; Pruski, M.; Sadow, A. D. " $\beta$ -SiH-Containing Tris(silazido) Rare-Earth Complexes as Homogeneous and Grafted Single-Site Catalyst Precursors for Hydroamination." *Organometallics* **2017**, *36*, 1142-1153.
21. Rees, W. S., Jr.; Just, O.; Schumann, H.; Weimann, R. "Structural characterization of a tris-agostic lanthanoid-H-Si interaction." *Angew. Chem., Int. Ed. Engl.* **1996**, *35*, 419-22.
22. Huynh, K.; Anderson, B. K.; Livinghouse, T. "Enantioselective hydroamination/cyclization of aminoalkenes by (bis)- $\text{C}_2$  symmetric and (mono)- $\text{C}_2$  symmetric anionic tetraamide complexes of La(III)." *Tetrahedron Lett.* **2015**, *56*, 3658-3661.
23. Hayton, T. W.; Boncella, J. M.; Scott, B. L.; Batista, E. R.; Hay, P. J. "Synthesis and Reactivity of the Imido Analogues of the Uranyl Ion." *J. Am. Chem. Soc.* **2006**, *128*, 10549-10559.
24. Perales, D.; Ford, S. A.; Salpage, S. R.; Collins, T. S.; Zeller, M.; Hanson, K.; Bart, S. C. "Conversion of Trivalent Uranium Anilido to Tetravalent Uranium Imido Species via Oxidative Deprotonation." *Inorg. Chem.* **2020**, *59*, 11910-11914.
25. Brennan, J. G.; Andersen, R. A. "Electron-transfer reactions of trivalent uranium. Preparation and structure of the uranium metallocene compounds  $(\text{MeC}_5\text{H}_4)_3\text{U}=\text{NPh}$  and  $[(\text{MeC}_5\text{H}_4)_3\text{U}]_2[\mu-\eta^1, \eta^2\text{-PhNCO}]$ ." *J. Am. Chem. Soc.* **1985**, *107*, 514-16.
26. Matson, E. M.; Crestani, M. G.; Fanwick, P. E.; Bart, S. C. "Synthesis of U(IV) imidos from  $\text{Tp}^*_2\text{U}(\text{CH}_2\text{Ph})$  ( $\text{Tp}^* = \text{hydrotris}(3,5\text{-dimethylpyrazolyl})\text{borate}$ ) by extrusion of bibenzyl." *Dalton Trans.* **2012**, *41*, 7952-7958.
27. Graves, C. R.; Yang, P.; Kozimor, S. A.; Vaughn, A. E.; Clark, D. L.; Conradson, S. D.; Schelter, E. J.; Scott, B. L.; Thompson, J. D.; Hay, P. J.; Morris, D. E.; Kiplinger, J. L. "Organometallic uranium(V)-imido halide complexes: from synthesis to electronic structure and bonding." *J. Am. Chem. Soc.* **2008**, *130*, 5272-5285.
28. Castro-Rodriguez, I.; Meyer, K. "Small molecule activation at uranium coordination complexes: control of reactivity via molecular architecture." *Chem. Commun.* **2006**, 1353-1368.

29. Graves, C. R.; Kiplinger, J. L. "Pentavalent uranium chemistry-synthetic pursuit of a rare oxidation state." *Chem. Commun.* **2009**, 3831-3853.
30. Bell, N. L.; Maron, L.; Arnold, P. L. "Thorium Mono- and Bis(imido) Complexes Made by Reprotonation of cyclo-Metalated Amides." *J. Am. Chem. Soc.* **2015**, *137*, 10492-10495.
31. Gillespie, R. J. "Fifty years of the VSEPR model." *Coord. Chem. Rev.* **2008**, *252*, 1315-1327.
32. King, D. M.; McMaster, J.; Tuna, F.; McInnes, E. J. L.; Lewis, W.; Blake, A. J.; Liddle, S. T. "Synthesis and Characterization of an f-Block Terminal Parent Imido [U=NH] Complex: A Masked Uranium(IV) Nitride." *J. Am. Chem. Soc.* **2014**, *136*, 5619-5622.
33. Neidig, M. L.; Clark, D. L.; Martin, R. L. "Covalency in f-element complexes." *Coord. Chem. Rev.* **2013**, *257*, 394-406.
34. Kerridge, A. "Quantification of f-element covalency through analysis of the electron density: insights from simulation." *Chem. Commun.* **2017**, *53*, 6685-6695.
35. Anderson, N. H. Controlling Electronics for the Formation of High Valent Uranium Imido Complexes. Purdue University, West Lafayette, IN, 2016.
36. Pangborn, A. B.; Giardello, M. A.; Grubbs, R. H.; Rosen, R. K.; Timmers, F. J. "Safe and Convenient Procedure for Solvent Purification." *Organometallics* **1996**, *15*, 1518-1520.
37. Chakraborty, S.; Chattopadhyay, J.; Guo, W.; Billups, W. E. *Angew. Chem. Int. Ed.* **2007**, *46*, 4486-4488.
38. ADF 2019.3, SCM, Theoretical Chemistry, <http://www.scm.com>: Vrije Universiteit, Amsterdam, The Netherlands, 2019.
39. te Velde, G.; Bickelhaupt, F. M.; Baerends, E. J.; Fonseca Guerra, C.; van Gisbergen, S. J. A.; Snijders, J. G.; Ziegler, T. "Chemistry with ADF." *J. Comp. Chem.* **2001**, *22*, 931-967.
40. van Lenthe, E.; Snijders, J. G.; Baerends, E. J. "The zero-order regular approximation for relativistic effects: The effect of spin-orbit coupling in closed shell molecules." *J. Chem. Phys.* **1996**, *105*, 6505-6516.
41. Adamo, C.; Barone, V. "Toward reliable density functional methods without adjustable parameters: The PBE0 model." *J. Chem. Phys.* **1999**, *110*, 6158-6170.
42. Weigend, F.; Ahlrichs, R. "Balanced basis sets of split valence, triple zeta valence and quadruple zeta valence quality for H to Rn: Design and assessment of accuracy." *Phys. Chem. Chem. Phys.* **2005**, *7*, 3297.
43. Pantazis, D. A.; Neese, F. "All-Electron Scalar Relativistic Basis Sets for the Actinides." *J. Chem. Theor. Comp.* **2011**, *7*, 677-684.

44. Hess, B. A. "Relativistic electronic-structure calculations employing a two-component no-pair formalism with external-field projection operators." *Phys. Rev. A* **1986**, *33*, 3742-3748.
45. Roos, B. O.; Taylor, P. R.; Sigbahn, P. E. M. "A complete active space SCF method (CASSCF) using a density matrix formulated super-CI approach." *Chem. Phys.* **1980**, *48*, 157-173.
46. Angeli, C.; Cimiraglia, R.; Malrieu, J.-P. "n-electron valence state perturbation theory: A spinless formulation and an efficient implementation of the strongly contracted and of the partially contracted variants." *J. Chem. Phys.* **2002**, *117*, 9138-9153.
47. Neese, F. "Software update: the ORCA program system, version 4.0." *WIREs Computational Molecular Science* **2018**, *8*, e1327.
48. Fdez. Galván, I.; Vacher, M.; Alavi, A.; Angeli, C.; Aquilante, F.; Autschbach, J.; Bao, J. J.; Bokarev, S. I.; Bogdanov, N. A.; Carlson, R. K.; Chibotaru, L. F.; Creutzberg, J.; Dattani, N.; Delcey, M. G.; Dong, S. S.; Dreuw, A.; Freitag, L.; Frutos, L. M.; Gagliardi, L.; Gendron, F.; Giussani, A.; González, L.; Grell, G.; Guo, M.; Hoyer, C. E.; Johansson, M.; Keller, S.; Knecht, S.; Kovačević, G.; Källman, E.; Li Manni, G.; Lundberg, M.; Ma, Y.; Mai, S.; Malhado, J. P.; Malmqvist, P. Å.; Marquetand, P.; Mewes, S. A.; Norell, J.; Olivucci, M.; Oppel, M.; Phung, Q. M.; Pierloot, K.; Plasser, F.; Reiher, M.; Sand, A. M.; Schapiro, I.; Sharma, P.; Stein, C. J.; Sørensen, L. K.; Truhlar, D. G.; Ugandi, M.; Ungur, L.; Valentini, A.; Vancoillie, S.; Veryazov, V.; Weser, O.; Wesolowski, T. A.; Widmark, P.-O.; Wouters, S.; Zech, A.; Zobel, J. P.; Lindh, R. "OpenMolcas: From Source Code to Insight." *J. Chem. Theor. Comp.* **2019**, *15*, 5925-5964.
49. Roos, B. O.; Lindh, R.; Malmqvist, P.-Å.; Veryazov, V.; Widmark, P.-O. "Main Group Atoms and Dimers Studied with a New Relativistic ANO Basis Set." *J. Phys. Chem. A* **2004**, *108*, 2851-2858.
50. Roos, B. O.; Lindh, R.; Malmqvist, P.-Å.; Veryazov, V.; Widmark, P.-O.; Borin, A. C. "New Relativistic Atomic Natural Orbital Basis Sets for Lanthanide Atoms with Applications to the Ce Diatom and LuF<sub>3</sub>." *J. Phys. Chem. A* **2008**, *112*, 11431-11435.
51. Malmqvist, P. Å.; Roos, B. O.; Schimmelpfennig, B. "The restricted active space (RAS) state interaction approach with spin-orbit coupling." *Chem. Phys. Lett.* **2002**, *357*, 230-240.
52. Heß, B. A.; Marian, C. M.; Wahlgren, U.; Gropen, O. "A mean-field spin-orbit method applicable to correlated wavefunctions." *Chem. Phys. Lett.* **1996**, *251*, 365-371.
53. Glendening, E. D.; Badenhoop, J. K.; Reed, A. E.; Carpenter, J. E.; Bohmann, J. A.; Morales, C. M.; Karafiloglou, P.; Landis, C. R.; Weinhold, F. *NBO 7.0. E. D.*, Theoretical Chemistry Institute: University of Wisconsin, Madison, WI, 2018.
54. Keith, T. A. *AIMAll (Version 19.10.12)*, TK Gristmill Software, Overland Park KS, USA (aim.tkgristmill.com): 2019.

55. Mitoraj, M. P.; Michalak, A.; Ziegler, T. "A Combined Charge and Energy Decomposition Scheme for Bond Analysis." *J. Chem. Theor. Comp.* **2009**, 5, 962-975.



## CHAPTER 2. INVESTIGATING THE STABILITY OF URANYL IMIDO COMPLEXES

### 2.1 Introduction

Uranium oxides are the primary component of nuclear fuels.<sup>1-3</sup> The reason for the prevalence of uranium oxides in nuclear fuels—besides being fissile—is the stability of the uranium oxide bonds, which are formally triple bonds, that are affected by the inverse trans influence (ITI).<sup>4-9</sup> The ITI strengthens the *trans*-oxo groups on uranyl complexes, making them relatively unreactive. This non reactivity is ideal for a fuel source, as the uranium oxides will not readily react once they are no longer being used in the nuclear fuel process. A byproduct of this strength is that uranyl compounds are generally insoluble in organic solvents, limiting the amount of chemistry that can be utilized to weaken and eventually activate the uranium-oxygen bonds in order to functionalize and reuse the uranium oxide materials. This functionalization is being sought because of one of the major issues with used nuclear fuels, they still possess extreme toxicity despite being unreactive due to the radioactive nature of the spent fuels. A way to reuse nuclear fuels is to find ways to make these unreactive uranium oxides reactive once again. One way to do this would be to disrupt the ITI. This disruption can be achieved through adding electron density to the equatorial plane, as was shown previously with the uranium(IV) *cis*-bis(imido).<sup>10</sup> Some other prominent examples of this principle are the uranium(VI) complexes  $(^{\text{Mes}}\text{PDI}^{\text{Me}})\text{U}(\text{NDIPP})_3$  and  $[\text{U}(\text{NDIPP})_4]\text{K}_2$ .<sup>11,12</sup> The axial imidos of the  $(^{\text{Mes}}\text{PDI}^{\text{Me}})\text{U}(\text{NDIPP})_3$  complex have a longer bond length than the axial imido groups on the uranium-bis(imido) made by Boncella and co-workers. For the tetrakis(imido) complex with potassium counterions, all four U=N bonds are approximately 2.05 Å showing that there is no ITI as there are no clear axial bonds.<sup>12-14</sup> These complexes demonstrate that addition of aromatic groups, specifically electron donating substituents, around the uranium center help disrupt the effects of the ITI within uranium imido complexes.

Attempts to make analogous uranyl imido complexes with the same ligands, 2,6-diisopropylphenyl, as uranium tris(imido) and tetrakis(imido) complexes have, thus far, not been successful. With these results in mind, alternate syntheses have been investigated to determine what types of ligands will facilitate imido formation on the uranyl moiety. Staying with the same types of ligand, the electron donating uranyl-NTSA complexes were synthesized from uranyl

dichloride,  $[\text{UO}_2\text{Cl}_2(\text{THF})_2]_2$ , and made with three NTSA ligands or two NTSA ligands also supported by a 4,4'-*tert*-butyl-bipyridine.<sup>15</sup> While these complexes alone did not cause any changes in the U=O bond lengths, they did provide new, useful starting materials for exchange reactions with anilines. The leaving group ability of the NTSA ligand, combined with the ability to easily remove the free, protonated HNTSA once it dissociates, allows for excellent utilization of proton exchange chemistry. This facilitated explorations with a large group of ligands with varying steric and electronic effects to determine which is more important to the stability of a uranyl imido complex.

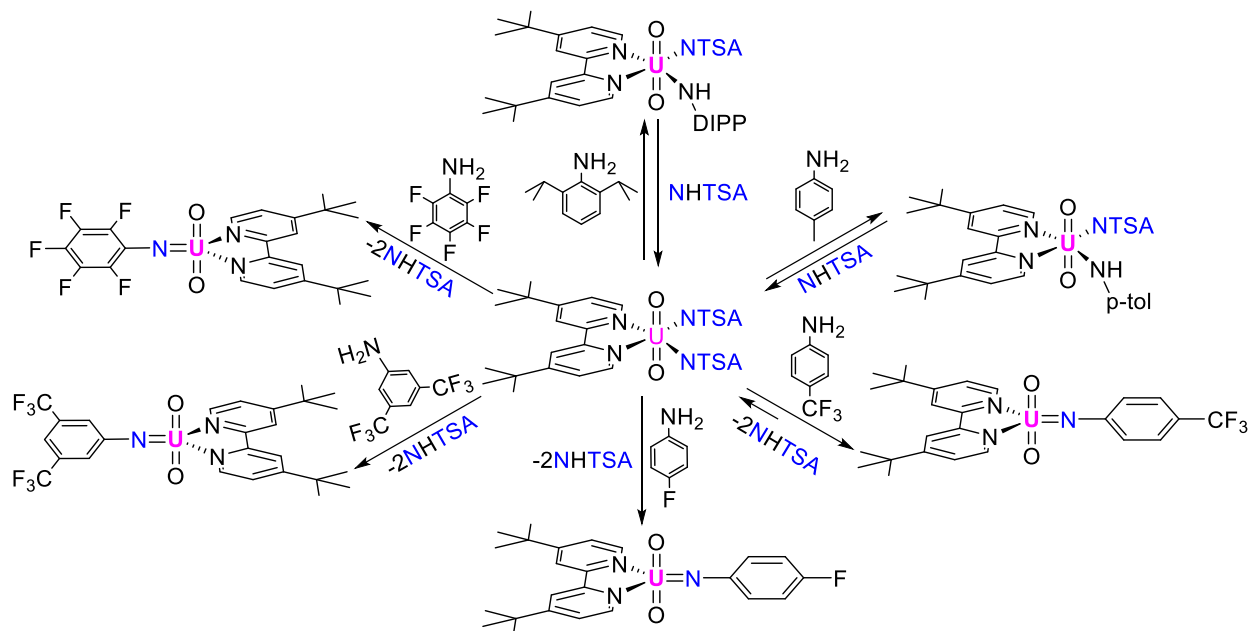
These variations in both sterics and electronics of the proposed imido ligand environment will allow for exploration of what factors are necessary for uranyl imido formation: is electron donation to the  $\pi$ -system of the complex needed, as has been previously shown uranium imido complexes, how large of an impact do steric effects have on maintaining an imido, does the steric profile of the ligand help in preventing protonation of the ligand to an amido, and how important is the connection between steric and electronic effects of the ligand is to the stabilization of imidos on the uranyl moiety are all important questions that will need to be answered.

## 2.2 Results and Discussion

The synthesis of these uranyl imido complexes is achieved through a hydride metathesis of  $\text{UO}_2(^t\text{Bubpy})(\text{NTSA})_2$  with the corresponding aniline (Scheme 2.1). The general procedure for the formation of these begins with a THF solution of  $\text{UO}_2(^t\text{Bubpy})(\text{NTSA})_2$ , followed by addition of one equivalent of aniline. This reaction mixture is then stirred for at least 15 minutes depending on the scale of reaction. For reactions with less than 100 milligrams of starting uranyl the complete exchange is complete after about 15 minutes; reactions with greater than 100 milligrams of starting uranyl should be stirred for one hour or more, depending on how much larger the reaction is than 100 milligrams, to both ensure full exchange of the NTSA ligand with the aniline and to ensure the deprotonation of the subsequent anilido product by the second NTSA ligand. It should be noted that reacting large scale reactions for shorter periods of time can result in incomplete conversion of the starting material to the uranyl imido product resulting in a mixture of imido, anilido, and amide products upon further characterization. Once the reaction is allowed to stir for the appropriate amount of time the crude product is dried *in vacuo* producing a dark red/brown solid that is washed twice with pentane and dried *in vacuo* again to ensure full removal of the free amide,

HNTSA, and eliminate as much excess solvent as possible. Once dried, the uranyl imido complexes are a lighter red/brown powder, with a slight variation in color being observed dependent on what aniline was used.

Scheme 2.1 Reaction pathways to uranyl imido products



The electronic qualities of the selected aniline appear to have a large impact on the ability to successfully form a uranyl imido but also on the resulting uranyl imido's stability. For traditionally electron donating anilines, such as DIPP and *p*-tol, are added to the  $\text{UO}_2(\text{Bubpy})(\text{NTSA})_2$  starting material a fast equilibrium can be observed between the free amine, NHTSA, the uranyl product, and the starting reactants. This fast equilibrium is supported through  $^1\text{H}$  NMR spectroscopy where free aniline and free amine are seen with an unknown uranyl product. Attempts to isolate this uranyl product, possibly a uranyl amido, simply resulted in further release of NHTSA and a mixture of other products. This can be improved with many successive washing cycles in an effort to push the equilibrium toward the new uranyl products. However, the presence of free aniline complicates the effort to fully push equilibrium toward the uranyl imido product. The free aniline can protonate the uranyl imido to a uranyl amido product, creating another equilibrium that is more complicated to control.

When electron withdrawing anilines are used the ability to form a uranyl imido dramatically increases. With fluorinated substituents in the *para*- position, such as with  $\text{NH}_2p\text{-F}$  or  $\text{NH}_2p\text{-CF}_3$ , uranyl imido products can be partially isolated. The main difference between these two anilines leading to this partial isolation are stability concerns that are observed with  $\text{UO}_2(^t\text{Bubpy})(p\text{-F})$ , **5**, and a slight equilibrium that is observed with  $\text{UO}_2(^t\text{Bubpy})(p\text{-CF}_3)$ , **6**. However, this equilibrium can be shifted toward the uranyl imido more easily than the equilibrium observed with electron donating ligands. The slight equilibrium observed with **6** may arise from inability to fully convert the starting material to a uranyl imido at room temperature. When the *p*- $\text{CF}_3$  reaction mixture is heated, a continued release of HNTSA is observed during NMR tube experiments. Suggesting that heating the reaction under a slight reduction in pressure may allow for full exchange of the NTSA ligands and formation of the desired uranyl imido product. This specific experiment was not pursued due to the success of other anilines and is not the most practical synthesis for the formation of uranyl imido complexes at this time.  $\text{UO}_2(^t\text{Bubpy})(p\text{-F})$  was more successful than  $\text{UO}_2(^t\text{Bubpy})(p\text{-CF}_3)$ . After work up of **6**, a solid was isolated and initially characterized; unfortunately, the resulting uranyl imido does not have substantial stability. The *p*-F uranyl imido complex will begin to decompose overnight, even when kept at  $-35\text{ }^\circ\text{C}$ . This decomposition can be seen by the formation of a white solid near the opening of the vial. This lack of stability does not appear to affect the formation of a uranyl imido though, as initial spectroscopic results of reactions using the *p*-F ligand show the presence of a uranyl imido. Moreover, unlike all aforementioned ligands there is no sign of bound or free HNTSA. This change in electronic environment appears to have a significant role in stabilizing the imido group on the uranyl moiety.

When using anilines with even more electron withdrawing ability,  $\text{NH}_2\text{ArF}_5$  and  $\text{NH}_23,5\text{-CF}_3$ , the resulting uranyl imido complexes,  $\text{UO}_2(^t\text{Bubpy})(\text{NArF}_5)$ , **3**, and  $\text{UO}_2(^t\text{Bubpy})(\text{N}3,5\text{-CF}_3)$ , **4**, are stable in solution at room temperature for up to several days. As a solid, and when kept in a freezer at  $-35\text{ }^\circ\text{C}$ , complexes **3** and **4** are stable for weeks. Using  $^1\text{H}$  NMR spectroscopy, complexes **3**, **4**, and **5** show no signals for bound NTSA or free HNTSA, supporting the assignment of these complexes as a uranyl imido and not an amido. Any residual HNTSA that may be seen can be easily removed with further pentane washes. There is no equilibrium between reactants and products for complexes **3** and **4**, demonstrating the importance of electronics on the stability of uranyl imido complexes. These uranyl imido complexes,  $\text{UO}_2(^t\text{Bubpy})(\text{NArF}_5)$ , **3**, and  $\text{UO}_2(^t\text{Bubpy})(\text{N}3,5\text{-CF}_3)$ , **4**, have survived preliminary decomposition studies—that will be

discussed in more detail below—with exposure to air having no adverse effects on the complexes as shown *via*  $^1\text{H}$  NMR spectroscopy, and only decomposing when directly exposed to either water or wet solvents.

### 2.2.1 NMR and Infrared spectroscopy

The  $^1\text{H}$  NMR spectra of  $\text{UO}_2(^t\text{Bubpy})(\text{NArF}_5)$ , **3** and  $\text{UO}_2(^t\text{Bubpy})(\text{N}3,5\text{-CF}_3)$ , **4** were recorded in pyridine- $d_5$  due to their insolubility in  $\text{C}_6\text{D}_6$ . The  $^1\text{H}$  NMR spectra of **3** (Figure 2.1) has three peaks corresponding to the  $^t\text{Bubpy}$  fragment, the two  $\text{C}(\text{CH}_3)_3$  moieties appear as a singlet at 1.27 ppm, and the six aromatic protons appear as three peaks, two doublets at 7.34 and 8.80 ppm, and a singlet at 8.91 ppm. There are no characteristic peaks of the -NTSA ligand—most prominent being the  $\text{SiH}$  peak of either free NHTSA (4.80 ppm) or bound -NTSA (6.59 ppm)—seen in the  $^1\text{H}$  NMR spectra for either of these compounds supporting the full protonation of the NTSA and removal once worked up.  $^{19}\text{F}$  NMR spectra of **3** has three peaks that appear at -153, -160, and -170 ppm corresponding to the fluorine on the  $\text{NArF}_5$  ring (Figure 2.2). These peaks are all shifted downfield from the free aniline peaks, at -164, -168, and -179 ppm, supporting the presence of a bound  $\text{NArF}_5$  ligand. Additionally, the  $^{19}\text{F}$  peaks seen in **3** are broader than those seen for the free aniline, suggesting that the  $\text{NArF}_5$  ligand is pulling electron density from something, most likely the uranyl moiety.

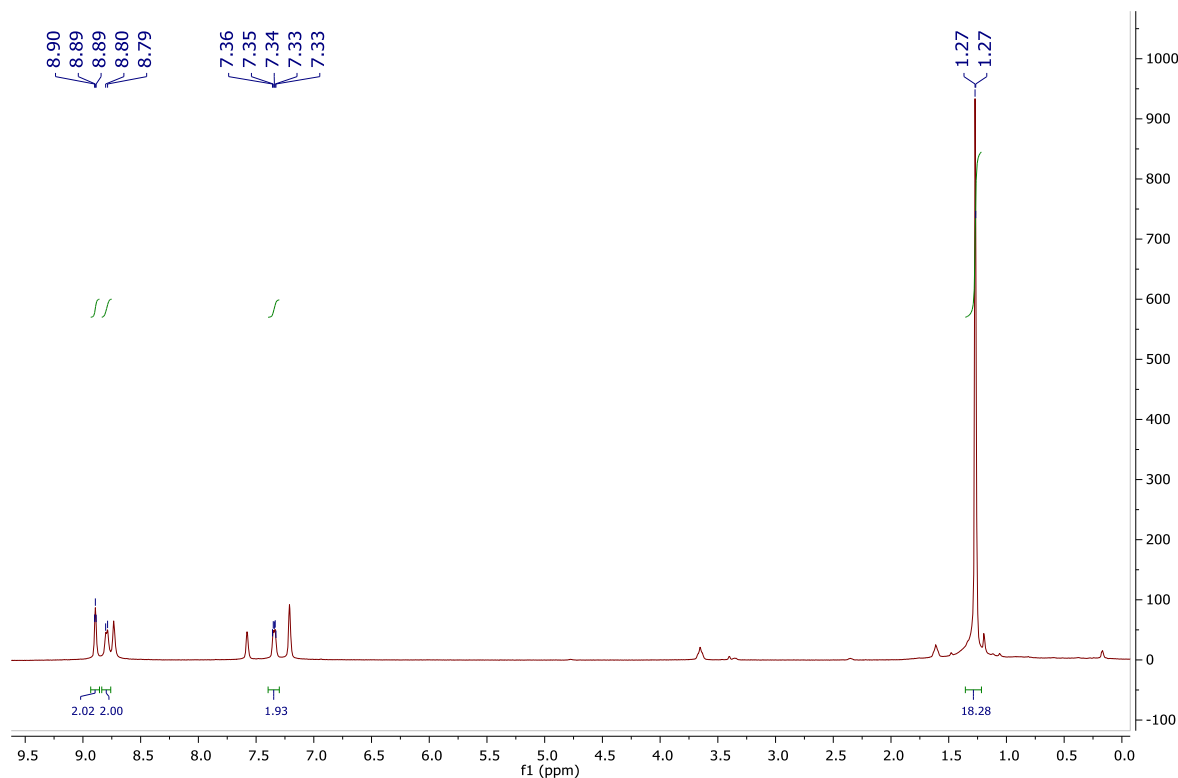


Figure 2.1  $^1\text{H}$  NMR spectra of  $\text{UO}_2(\text{tBubpy})(\text{NArF}_5)$  ( $\text{pyridine-d}_5$ )

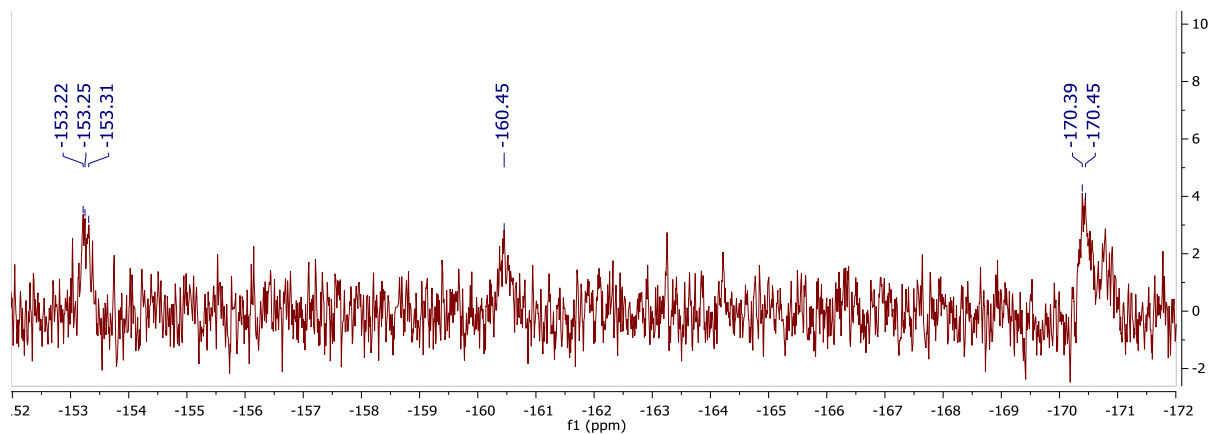


Figure 2.2  $^{19}\text{F}$  NMR Spectra for  $\text{UO}_2(\text{tBubpy})(\text{NArF}_5)$  ( $\text{pyridine-d}_5$ )

The NMR spectra of **4** has very similar peak positions when compared with **3**, at 1.28, 7.34, 8.80, and 8.90 ppm corresponding to two  $\text{C}(\text{CH}_3)_3$  and six aromatic H, respectively (Figure 1B, Appendix B). This similarity can be expected since the only difference in the proton spectra between **3** and **4** is the presence of two protons on the imido ligand. The absence of visible peaks representing the two protons on the  $\text{N}(3,5\text{-CF}_3)$  ring may be because they are eclipsed by the peaks

for either the  ${}^1\text{H}$ Bubpy moiety or the residual pyridine- $d_5$  signal. The free  $\text{H}_2\text{N}(3,5\text{-CF}_3)$  ring protons at 7.49 ppm in pyridine- $d_5$ . The spectrum for **4** does not have a peak that corresponds to the free aniline in this region and also lack the N-H peak of the free aniline (6.58 ppm) (Figure 1B, Appendix B). This information, coupled with the  ${}^{19}\text{F}$  NMR spectrum of **4** having one peak at -64 ppm—corresponding to the two  $\text{CF}_3$  groups—reinforces the presence of the  $\text{N}(3,5\text{-CF}_3)$  ligand (Figure 2B, Appendix B). This data supports the assignment as an imido as opposed to an amido or just free aniline.

Infrared spectra of **3** and **4** do not have any significant N-H absorptions as well (Figure 2.3 and Figure 2.4). The features that appear in this region are postulated to be the growth of decomposition products due to the highly sensitive nature of **3** and **4** when in the solid state. When **3** and **4** are exposed to atmosphere in the solid state immediate decomposition to a white solid is observed, this decomposition is similar to that seen for  $\text{UO}_2({}^1\text{Bubpy})(\text{Np-F})$ , **5**, when left in an inert atmosphere for a few days in the solid state.

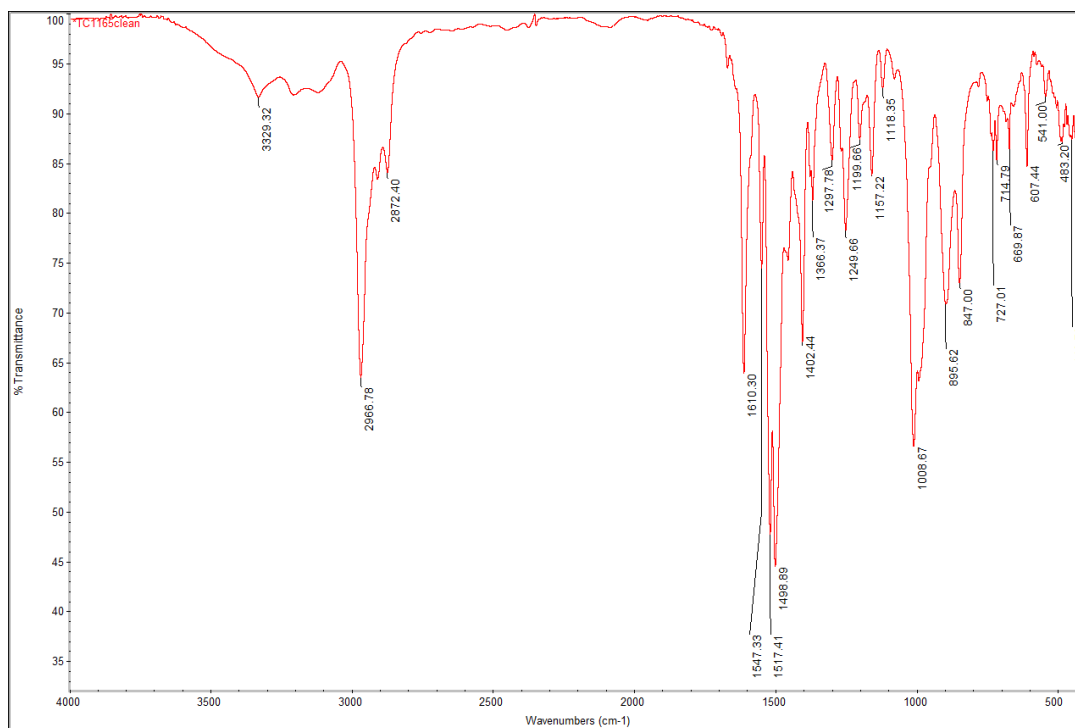


Figure 2.3 Infrared Spectra of  $\text{UO}_2({}^1\text{Bubpy})(\text{NArF}_5)$ , KBr pellet

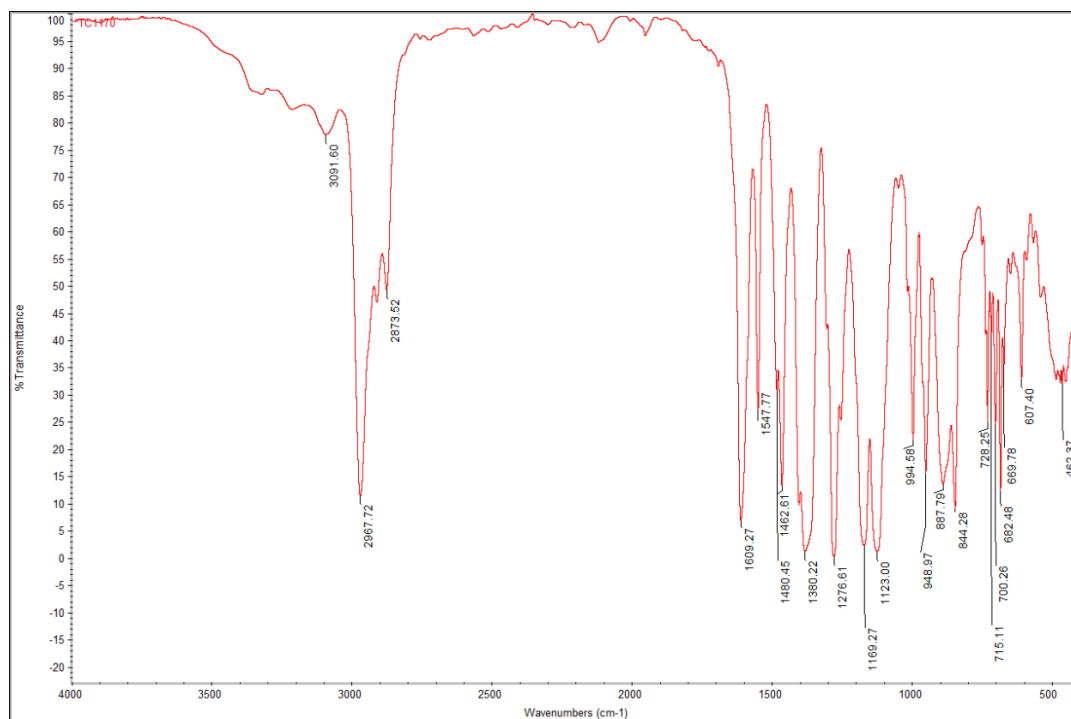


Figure 2.4 Infrared spectra of  $\text{UO}_2(\text{'Bubpy})(\text{N}3,5\text{-CF}_3)$ , KBr pellet

The last uranyl imido to be discussed for this study, **5**, was successfully synthesized but lacks the stability of **3** and **4**. Complex **5** shows visible decomposition to unidentifiable white solids after only one day, even when kept at  $-35\text{ }^{\circ}\text{C}$ .  $^1\text{H}$  NMR spectrum of freshly synthesized **5** (Figure 3B, Appendix B) matches well with other uranyl imidos **3** (Figure 2.1) and **4** (Figure 1B, Appendix B). The lack of the free aniline,  $\text{H}_2\text{N}(p\text{-F})$ , aromatic proton peaks (6.87, 7.03 ppm) and N-H peak (5.31 ppm) in the  $^1\text{H}$  NMR spectra supports assignment of a bound  $\text{-N}(p\text{-F})$  ligand in addition, the  $^{19}\text{F}$  NMR spectra of **5** (Figure 4B, Appendix B) has a peak at  $-136.50$  ppm corresponding to the bound  $\text{N}(p\text{-F})$  fluorine, representing an upfield shift of about 6 ppm from the free aniline. These changes seen by multinuclear NMR spectroscopy aid in assigning these complexes as uranyl imidos.

## 2.2.2 Literature Comparisons

A similar system to the uranyl imido complexes presented here are the uranyl bis-iminophosphoranes from Teat and coworkers<sup>16</sup> which have a range of uranyl stretches from  $908$  to  $924\text{ cm}^{-1}$  depending on ligand variations within the system. The uranyl stretches for these complexes are larger than those observed in complexes **3** and **4** because of the lower number of



multiply bound species affecting the electronic system around the uranyl center. A more comparable uranyl multiply bounded system, uranyl carbene complexes, were made by Ephritikhine and coworkers.<sup>17</sup> These have a uranyl stretching frequency of 920 cm<sup>-1</sup>, roughly 20 cm<sup>-1</sup> greater than the starting material uranyl complex used in this study, 25 cm<sup>-1</sup> greater for **3** (895 cm<sup>-1</sup>) and 53 cm<sup>-1</sup> greater for **4** (887 cm<sup>-1</sup>). This large increase in uranyl stretching frequency for the carbene likely results from the electron donating ability of the carbene; thus, when strong electron withdrawing groups are used, such as in **3** and **4**, a weakening and thus a shift to lower energy of the uranyl stretch is observed. The uranyl stretches for **3** and **4** are also very close to the U=O and O=U=O stretch seen by Liddle and co-workers for their carbene complexes at 900 and 860 cm<sup>-1</sup> respectively.<sup>18</sup> These complexes by Liddle and coworkers, containing three multiply bound species to the uranium center, support the assignment of **3** and **4** as uranyl imidos as they also have three multiply bound species to the uranium center and have similar stretches as seen by IR spectroscopy.

### 2.2.3 Discussion of uranyl imido complex stability

Initial stability experiments of box stable uranyl imido products **3** and **4** began with addition of a drop of C<sub>6</sub>D<sub>6</sub> from outside the glovebox to an NMR tube with **3** in pyridine *d*<sub>5</sub>. This resulted in the decomposition of **3** into free H<sub>2</sub>NArF<sub>2</sub> and insoluble uranyl compounds. Adding a drop of D<sub>2</sub>O to an NMR tube of **3** or **4** caused an even faster decomposition to the free aniline and intractable uranyl products, which is quantified by the rapid loss of color of the sample. This rapid decomposition is further confirmed by <sup>1</sup>H NMR, <sup>19</sup>F NMR, and, as stated, the solution color changing from a deep red to clear and colorless with a black solid precipitating out of the solution.

The stability of **3** and **4** in an inert atmosphere most likely comes from the electron withdrawing ability of the NArF<sub>5</sub> and N(3,5-CF<sub>3</sub>) ligands, which stabilizes the U=N bond by siphoning electron density from the strong O=U=O bond. This idea is supported by attempts to synthesize uranyl imido compounds with other, less electron withdrawing ligands: 2,6-diisopropylaniline (NH<sub>2</sub>DIPP), 4-methylaniline (NH<sub>2</sub>*p*-tol), and 4-trifluoromethylaniline (NH<sub>2</sub>*p*-CF<sub>3</sub>). Use of these ligands results in a fast equilibrium between the uranyl imido product and the starting uranyl material, UO<sub>2</sub>(<sup>t</sup>Bubpy)(NTSA)<sub>2</sub>. This is tracked by the presence of HNTSA in solution, as the SiH chemical shift changes by almost 2 ppm from free -NTSA (4.84ppm) to bound -NTSA (6.80 ppm). This equilibrium can be shifted toward the imido product with successive

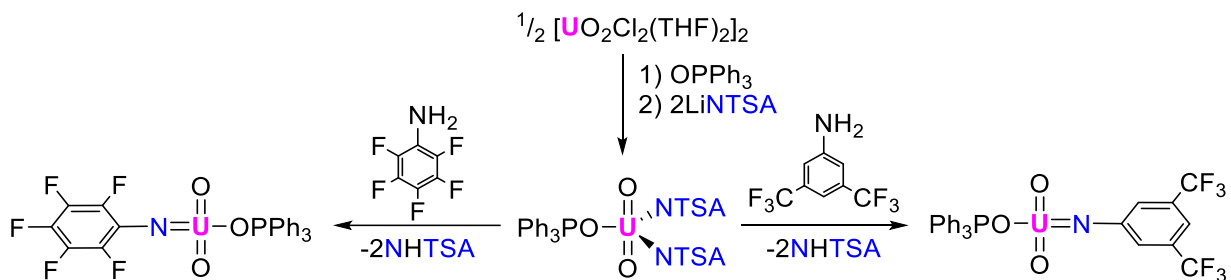
washings to remove free HNTSA. The most successful results are seen with the *para*-CF<sub>3</sub> aniline, **6**; however, the presence of -NTSA and HNTSA are still major byproducts of the reaction. Moreover, this process is time consuming, and it is unknown exactly how many washings would be needed to completely remove -NTSA and HNTSA to fully push this equilibrium toward the uranyl imido product. These results support the need for electron withdrawing substituents.

Crystallographic data of this family of uranyl imido complexes has been difficult to obtain with the excellent solubility of these complexes in polar solvents and insolubility in non-polar solvents resulting in poor quality of crystals formed and powder deposition. Crystals that have been isolated were not of high quality or not single-crystal in nature. These crystals instead look almost stringy and piled upon one another. The diminished stability of these compounds in solution at room temperature has also posed a problem for crystal growth as they appear to begin decomposing after 36 hours at room temperature while in the glovebox.

## 2.2.4 Triphenylphosphine oxide supported uranyl compounds

In an effort to increase crystallinity of the uranyl imido complexes, the supporting ligand was changed from <sup>t</sup>Bubpy to OPPh<sub>3</sub> (Scheme 2.2). This was achieved by using the same literature procedure but with OPPh<sub>3</sub> in place of <sup>t</sup>Bubpy. Triphenylphosphine oxide was chosen as the new supporting ligand because of the increased steric profile of the ligand, which should increase the ease of crystallization for the compounds. The OPPh<sub>3</sub> would also give another spectroscopic handle to probe in addition to <sup>1</sup>H and <sup>19</sup>F NMR. Comparison between OPPh<sub>3</sub> and <sup>t</sup>Bubpy will be of interest to investigate the effect that differing steric bulk and electronic profiles will have on the uranyl complexes' stabilities.

Scheme 2.2 Pathway to triphenylphosphine oxide supported uranyl imido products



The OPPh<sub>3</sub> supported complexes, **3-OPPh<sub>3</sub>** and **4-OPPh<sub>3</sub>**, were similar to the <sup>1</sup>Bubpy supported uranyl complexes (Figure 6B-9B, Appendix B). This similar reactivity supported the formation of the starting material, UO<sub>2</sub>(NTSA)<sub>2</sub>OPPh<sub>3</sub>, in absence of a crystal structure of the OPPh<sub>3</sub> supported compounds. Unfortunately, analogous to the <sup>1</sup>Bubpy compounds, all reactions with the electron withdrawing anilines proceeded in a similar manner, suggesting that the OPPh<sub>3</sub> does not affect the synthetic pathway to a uranyl imido complex. These reactions also appeared more complicated as well, as the OPPh<sub>3</sub> resonances complicate the aromatic region and obscure resonances that would also appear for free electron donating type anilines. The similar solubility of free OPPh<sub>3</sub> and the uranyl products made purification of these compounds more difficult, resulting in the isolation of oily type solids. Crystallizations that were set up for these reactions were also unsuccessful in isolating suitable crystals for diffraction studies. Overall, the change from <sup>1</sup>Bubpy to OPPh<sub>3</sub> does not exhibit any noticeable improvement to crystallizations and the additional synthetic hurdles that this change in supporting ligand has presented forced the pursuit of these compounds outside the current scope of this project.

## 2.3 Conclusions

These results have demonstrated the viability of uranyl imido complexes. There is significant spectroscopic evidence for the presence of an imido ligand bound to the uranyl moiety, with no significant N-H stretches seen by NMR and IR spectroscopy, in addition to passing EA results for both UO<sub>2</sub>(<sup>1</sup>Bubpy)(NArF<sub>5</sub>) and UO<sub>2</sub>(<sup>1</sup>Bubpy)(N3,5-CF<sub>3</sub>). These compounds are stable for long periods of time in air and moisture free environments and appear to be solution air stable as well. These characteristics further support the formation of uranyl imido complexes and demonstrate that activation of the uranyl moiety is possible through simple chemical processes. This stability is exciting for the future of uranyl activation chemistry as these compounds could be used for many applications as moisture is the only factor that needs to be considered. The lack of crystallographic details prevents in depth analysis of what effects the imido ligand has on the uranyl moiety's U=O bonds and what degree of activation is achieved. However, the lack of crystallographic data does not take away from the spectroscopic confirmation of a uranyl imido, and the activation that can be observed through these methods.

## 2.4 Experimental Methods

### 2.4.1 General Considerations

All air- and moisture-sensitive manipulations were performed using standard Schlenk techniques or in an MBraun inert atmosphere drybox with an atmosphere of purified nitrogen. The MBraun drybox was equipped with two  $-35\text{ }^{\circ}\text{C}$  freezers for cooling samples and crystallizations. Solvents for sensitive manipulations were dried and deoxygenated using literature procedures with a Seca solvent purification system.<sup>19</sup> Pyridine- $d_5$  was purchased from Cambridge Isotope Laboratories, dried with molecular sieves, and degassed by three freeze-pump-thaw cycles. 2,3,4,5,6-pentafluoro aniline, 3,5-bis(trifluoromethyl) aniline, and 4-fluoro aniline were purchased from Oakwood Chemical and degassed by three freeze-pump-thaw cycles.  $\text{UO}_2(^t\text{Bubpy})(\text{NTSA})_2$  was synthesized according to literature procedure.<sup>15</sup>

**Caution:** *U-238 is a weak  $\alpha$ -emitter with a half-life of  $t_{1/2} = 4 \times 10^9$  years. All manipulations were performed in an inert atmosphere glovebox in a laboratory equipped with proper detection equipment.*

$^1\text{H}$  NMR spectra were recorded at  $25\text{ }^{\circ}\text{C}$  on a Varian Inova 300, spectrometer operating at 299.96 MHz. All chemical shifts are reported relative to the peak for  $\text{SiMe}_4$ , using  $^1\text{H}$  (residual) chemical shifts of the solvent as a secondary standard. For all molecules, the NMR data are reported with the chemical shift, followed by the multiplicity, any relevant coupling constants, the integration value, and the peak assignment. Infrared spectra were recorded using a Thermo Nicolet 6700 spectrometer; samples were prepared by grinding the desired compound together with KBr salt and pressing the solid into a pellet or by evaporation of the sample dissolved in  $\text{C}_6\text{D}_6$  onto a KBr salt plate. Elemental analyses were performed by Midwest Microlab (Indianapolis, IN).

### 2.4.2 Synthesis

#### *Synthesis of uranyl(tert-butyl)bpy(N-2,3,4,5,6-pentafluoro-imido) 3*

The synthesis of uranyl imidos is accomplished by using  $\text{UO}_2(^t\text{Bubpy})(\text{NTSA})_2$  (0.250 g, 0.313 mmol) [NTSA=*tert*-butyl(dimethylsilyl)amide] dissolved in THF (12 mL) making a dark red solution, followed by addition of one equivalent of 2,3,4,5,6-pentafluoroaniline ( $\text{H}_2\text{NArF}_5$ ) (0.057 g, 0.311 mmol) which causes an immediate color change to dark brown. After stirring the reaction for 30 minutes, it was dried under reduced pressure leaving sticky brown residue that is

washed with *n*-pentane twice (3 mL) leaving a brown powder assigned as  $\text{UO}_2(\text{}^t\text{Bubpy})(\text{NArF}_5)$  (0.217 g, 0.301 mmol, 96% yield).  $^1\text{H}$  NMR (pyridine-*d*<sub>5</sub>, 25 °C, ppm):  $\delta$  = 1.27 (s, 18H,  $\text{CCH}_3\text{-bpy}$ ), 7.34 (dd, 2H, *ArH*-bpy), 8.80 (d, 2H, *ArH*-bpy), 8.91 (s, 2H, *ArH*-bpy).  $^{19}\text{F}$  NMR (pyridine-*d*<sub>5</sub>, 25 °C, ppm)  $\delta$  = -153.35 (s, 1F, *para*-F) -160.63 (dd, 2F, *ortho*-F) -170.48 (m, 2F, *meta*-F). IR (KBr Salt plate) ( $\text{cm}^{-1}$ ): 607 w, 670 w, 714 w, 727 w, 847 m, 895 m, 1009 m, 1118 w, 1157 w, 1200 w, 1250 m, 1297 w, 1366 w, 1402 m, 1499 s, 1517 s, 1547 w, 1610 s, 2872 m, 2967 s, 3329 w. Elemental Analysis, calculated: C 40.06%, H 3.36%, N 5.84%, found: C 38.43%, H 3.74%, N 4.33%.

#### *Synthesis of uranyl(tert-butyl)bpy(N-3,5-bis-trifluoromethyl-imido) 4*

Using the same procedure as **1** and using (0.100 g, 0.125 mmol) of  $\text{UO}_2(\text{}^t\text{Bubpy})(\text{NTSA})_2$  and one equivalent of 3,5-bis(trifluoromethyl)aniline ( $\text{H}_2\text{N}(3,5\text{-CF}_3)$ ) (0.029 g, 0.125 mmol) a dark brown residue is recovered, and once purified can be assigned as  $[\text{UO}_2(\text{}^t\text{Bubpy})(\text{N}(3,5\text{-CF}_3))](\text{THF})$  (0.092g, 0.360 mmol, 93% yield).  $^1\text{H}$  NMR (pyridine-*d*<sub>5</sub>, 25 °C, ppm ):  $\delta$  = 1.28 (s, 18H,  $\text{CCH}_3\text{-bpy}$ ), 7.34 (d, 2H, *ArH*-bpy), 8.80 (d, 2H, *ArH*-bpy), 8.90 (s, 2H, *ArH*-bpy).  $^{19}\text{F}$  NMR (pyridine-*d*<sub>5</sub>, 25 °C, ppm)  $\delta$  = -64.00 (s, 6F,  $\text{CF}_3$ ). IR (KBr Salt plate) ( $\text{cm}^{-1}$ ): 607 m, 682 m, 700 m, 728 m, 844 m, 887 m, 949 m, 995 m, 1123 s, 1169 s, 1276 s, 1380 s, 1462 s, 1548 s, 1609 s, 2873 m, 2968 s, 3092 w. Elemental Analysis, calculated: C 43.02%, H 4.21%, N 5.02%, found: C 42.58%, H 4.43%, N 5.03%.

#### *Synthesis of uranyl(tert-butyl)bpy(N-4-fluoro-imido) 5*

Using the same procedure as **1** using (0.150 g, 0.188 mmol) of  $\text{UO}_2(\text{}^t\text{Bubpy})(\text{NTSA})_2$ , THF (5 mL), and one equiv. of 4-fluoroaniline [ $\text{H}_2\text{N}(p\text{-F})$ ] (0.022 g, 0.197 mmol) resulted in a color change from dark red to brown. After stirring overnight, volatiles were removed under reduced pressure. The sticky brown residue was washed with pentane (3 mL) twice and dried, resulting in a silver brown powder assigned as  $\text{UO}_2(\text{}^t\text{Bubpy})(\text{N}(p\text{-F}))(\text{THF})_n$  (0.130 g).  $^1\text{H}$  NMR (pyridine-*d*<sub>5</sub>, 25 °C, ppm ):  $\delta$  = 1.28 (s, 18H,  $\text{CCH}_3\text{-bpy}$ ), 7.34 (dd, 2H, *ArH*-bpy), 8.79 (d, 2H, *ArH*-bpy), 8.91 (s, 2H, *ArH*-bpy).  $^{19}\text{F}$  NMR (pyridine-*d*<sub>5</sub>, 25 °C, ppm)  $\delta$  = -136.50 (s, 1F). IR (KBr salt plate) ( $\text{cm}^{-1}$ ): 607 w, 682 m, 700 w, 728 w, 844 m, 887 br, 948 m, 994 m, 1123 s, 1169 s, 1276 s, 1380 s, 1462 m, 1480 m, 1547 m, 1609 m, 2873 m, 2967 s.

*Synthesis of uranyl(tert-butyl)bpy(N-4-trifluoromethyl-imido) 6*

Using the same general procedure, reaction was stirred for two hours before work up. Heating at 60 °C alone does not dramatically improve yield, a combination of heating followed by repeated pentane washes was determined to slightly improve yield and conversion to the imido. <sup>1</sup>H NMR (C<sub>6</sub>D<sub>6</sub>, 25 °C, ppm): δ = 1.11 (s, CCH<sub>3</sub>-NTSA), 1.13 (s), 1.39 (s, CCH<sub>3</sub>-bpy), 3.57 (s, NH-CF<sub>3</sub>), 6.93 (s, SiH-NTSA), 8.64 (s, ArH-bpy), 9.05 (s, ArH-bpy). <sup>19</sup>F NMR (C<sub>6</sub>D<sub>6</sub>, 25 °C, ppm): δ = -62.17

*Synthesis of uranyl(tert-butyl)bpy(N-4-tolyl-amide) 7*

Using the same general procedure, reaction was stirred for two and a half hours before work up. <sup>1</sup>H NMR (C<sub>6</sub>D<sub>6</sub>, 25 °C, ppm): δ = 0.96 (s, SiHCH<sub>3</sub>-NTSA), 1.11 (s, CCH<sub>3</sub>-NTSA), 1.13 (s), 2.26 (s), 3.56 (s), 4.85 (m), 6.79 (s), 6.91 (m), 7.73 (s), 8.63 (s), 9.05 (s), 9.82 (d).

*Synthesis of uranyl(tert-butyl)bpy(N-2,6-diisopropyl-amide) 8*

Using the same general procedure as stated above for the uranyl imido complexes, stirred for one hour before work up. <sup>1</sup>H NMR (C<sub>6</sub>D<sub>6</sub>, 25 °C, ppm): δ = 1.13 (s), 2.67 (s), 2.36 (s), 6.89 (d), 7.04 (d), 8.64 (s), 9.04 (s)

*Synthesis of uranyl(tri-phenylphosphineoxide)(N-2,3,4,5,6-pentafluoro-imido), 3-OPPh<sub>3</sub>*

Using the same general procedure as **3**, reaction was stirred for 30 minutes before work up. This afforded a dark red/brown, oily solid which was assigned as UO<sub>2</sub>(OPPh<sub>3</sub>)(NArF<sub>5</sub>). <sup>1</sup>H NMR (pyridine-*d*<sub>5</sub>, 25 °C, ppm): δ = 6.83, 7.00, 7.41, <sup>19</sup>F NMR (pyridine-*d*<sub>5</sub>, 25 °C, ppm): δ = -160.81 (m), -166.63 (t), -174.66 (t)

*Synthesis of uranyl(tri-phenylphosphineoxide)(N-3,5-bis-trifluoromethyl-phenyl-imido), 4-OPPh<sub>3</sub>*

Using the same general procedure as **4**, reaction was stirred for 30 minutes before work up. This afforded a dark red/brown oily, solid that was assigned as UO<sub>2</sub>(OPPh<sub>3</sub>)(N3,5-CF<sub>3</sub>). <sup>1</sup>H NMR (pyridine-*d*<sub>5</sub>, 25 °C, ppm): δ = 6.93, 7.03, 7.53, <sup>19</sup>F NMR (pyridine-*d*<sub>5</sub>, 25 °C, ppm): δ = -64.34 (s)

## 2.5 References

- 1 Gras, J. M.; Quang, R. Do; Masson, H.; Lieven, T.; Ferry, C.; Poinssot, C.; Debes, M.; Delbecq, J. M. Perspectives on the Closed Fuel Cycle - Implications for High-Level Waste Matrices. *J. Nucl. Mater.* **2007**, 362 (2–3), 383–394..
- 2 Joseph J. Katz, Lester R. Morss, G. T. S. *The Chemistry of the Actinide Elements*; 1980.
- 3 Jones, M. B.; Gaunt, A. J.; Jones, M. B.; Gaunt, A. J. Recent Developments in Synthesis and Structural Chemistry of Nonaqueous Actinide Complexes. *Chem. Rev.* **2013**, 113 (2), 1137–1198.
- 4 Denning R.G. *Electronic Structure and Bonding in Actinyl Ions. In: Complexes, Clusters and Crystal Chemistry. Structure and Bonding, Vol 79. Springer, Berlin, Heidelberg.*; 1992.
- 5 Denning, R. G. Electronic Structure and Bonding in Actinyl Ions and Their Analogs. *J. Phys. Chem. A* **2007**, 111 (20), 4125–4143.
- 6 Lam, O. P.; Franke, S. M.; Nakai, H.; Heinemann, F. W.; Hieringer, W.; Meyer, K. Observation of the Inverse Trans Influence (ITI) in a Uranium(V) Imide Coordination Complex: An Experimental Study and Theoretical Evaluation. *Inorg. Chem.* **2012**, 51 (11), 6190–6199.
- 7 Lewis, A. J.; Mullane, K. C.; Nakamaru-Ogiso, E.; Carroll, P. J.; Schelter, E. J. The Inverse Trans Influence in a Family of Pentavalent Uranium Complexes. *Inorg. Chem.* **2014**, 53 (13), 6944–6953.
- 8 O’Grady, E.; Kaltsoyannis, N. On the Inverse Trans Influence. Density Functional Studies of [MOX<sub>5</sub>]N<sup>–</sup> (M = Pa{,}, n = 2; M = U{,}, n = 1; M = Np{,}, n = 0; X = F{,}, Cl or Br). *J. Chem. Soc., Dalton Trans.* **2002**, No. 6, 1233–1239.
- 9 Windorff, C. J.; Celis-Barros, C.; Sperling, J. M.; McKinnon, N. C.; Albrecht-Schmitt, T. E. Probing a Variation of the Inverse-Trans-Influence in Americium and Lanthanide Tribromide Tris(Tricyclohexylphosphine Oxide) Complexes. *Chem. Sci.* **2020**, 11 (10), 2770–2782.
- 10 Collins, T. S.; Celis-Barros, C.; Beltrán-Leiva, M. J.; Anderson, N. H.; Zeller, M.; Albrecht-Schönzart, T.; Bart, S. C. Origin of Bond Elongation in a Uranium(IV) Cis-Bis(Imido) Complex. *Inorg. Chem.* **2020**, 59 (24), 18461–18468.
- 11 Anderson, N. H.; Odoh, S. O.; Yao, Y.; Williams, U. J.; Schaefer, B. A.; Kiernicki, J. J.; Lewis, A. J.; Goshert, M. D.; Fanwick, P. E.; Schelter, E. J.; et al. Harnessing Redox Activity for the Formation of Uranium Tris(Imido) Compounds. *Nat. Chem.* **2014**, 6 (10), 919–926.

- 12 Anderson, N. H.; Xie, J.; Ray, D.; Zeller, M.; Gagliardi, L.; Bart, S. C. Elucidating Bonding Preferences in Tetrakis(Imido)Uranate(VI) Dianions. *Nat. Chem.* **2017**, *9* (9), 850–855.
- 13 Anderson, N. H.; Yin, H.; Kiernicki, J. J.; Fanwick, P. E.; Schelter, E. J.; Bart, S. C. Investigation of Uranium Tris(Imido) Complexes: Synthesis, Characterization, and Reduction Chemistry of [U(NDIPP)<sub>3</sub>(Thf)<sub>3</sub>]. *Angew. Chemie - Int. Ed.* **2015**, *54* (32), 9386–9389.
- 14 Hayton, T. W.; Boncella, J. M.; Scott, B. L.; Batista, E. R.; Hay, P. J. Synthesis and Reactivity of the Imido Analogues of the Uranyl Ion. *J. Am. Chem. Soc.* **2006**, *128* (32), 10549–10559.
- 15 Pattenau, S. A. S. A.; Coughlin, E. J. E. J.; Collins, T. S. T. S.; Zeller, M.; Bart, S. C. S. C. Expanding the Library of Uranyl Amide Derivatives: New Complexes Featuring the Tert -Butyldimethylsilylamide Ligand. *Inorg. Chem.* **2018**, *57* (8), 4543–4549.
- 16 Sarsfield, M. J.; Steele, H.; Helliwell, M.; Teat, S. J. Uranyl Bis-Iminophosphorane Complexes with in- and out-of-Plane Equatorial Coordination. *J. Chem. Soc. Dalt. Trans.* **2003**, No. 17, 3443–3449.
- 17 Tourneux, J. C.; Berthet, J. C.; Cantat, T.; Thuéry, P.; Mézailles, N.; Ephritikhine, M. Exploring the Uranyl Organometallic Chemistry: From Single to Double Uranium-Carbon Bonds. *J. Am. Chem. Soc.* **2011**, *133* (16), 6162–6165.
- 18 Mills, D. P.; Cooper, O. J.; Tuna, F.; McInnes, E. J. L.; Davies, E. S.; McMaster, J.; Moro, F.; Lewis, W.; Blake, A. J.; Liddle, S. T. Synthesis of a Uranium(VI)-Carbene: Reductive Formation of Uranyl(V)-Methanides, Oxidative Preparation of a [R<sub>2</sub>C=U=O]<sup>2+</sup> Analogue of the [O=U=O]<sup>2+</sup> Uranyl Ion (R = Ph<sub>2</sub>PN(SiMe<sub>3</sub>)<sub>2</sub>), and Comparison of the Nature of U IV=C, U V=C, and U VI=C Double Bonds. *J. Am. Chem. Soc.* **2012**, *134* (24), 10047–10054..
- 19 Pangborn, A. B.; Giardello, M. A.; Grubbs, R. H.; Rosen, R. K.; Timmers, F. J. Safe and Convenient Procedure for Solvent Purification. *Organometallics* **1996**, *15* (5), 1518–1520.



## CHAPTER 3. SYNTHESIS OF URANIUM(VI) PENTAKIS(IMIDO) COMPLEXES

### 3.1 Introduction

Understanding uranium-element multiple bonds has become an increasingly important topic in not just fundamental actinide chemistry, but also in actinide separations chemistry.<sup>1</sup> This is not just because these relatively stable bonds have been historically understudied but also because the need to recycle spent nuclear fuels has significantly grown as investigations into alternative energy sources not based on fossil fuels continues to gain momentum. The uranyl moiety,  $(\text{UO}_2)^{2+}$ , is one of the most common forms of uranium found in spent nuclear fuels. Uranium dioxides are extremely stable, making spent fuel quite inert as the strong, *trans* U-O bonds are unreactive and insoluble in most organic solvents.<sup>2-4</sup> These qualities make finding conditions to study uranium element multiple bonds difficult; therefore, analogs of the uranyl moiety have been sought out to probe chemistry that may be applied to uranyl materials. One of the most similar, and reactive analogs to the uranyl moiety is the uranium(VI) bis(imido),  $[\text{U}(\text{NR})_2]^{2+}$ , first isolated and characterized by Boncella and co-workers.<sup>5</sup> Uranium multiple-imido chemistry has proved to be a useful avenue for understanding uranium element multiple bonds as both of these complexes exhibit similar bonding motifs with strong *trans*-multiple bond species. The synthesis of uranium tris(imido) and tetrakis(imido) complexes have shown that the Inverse Trans-Influence (ITI) can be disrupted; in the case of the tetrakis(imido) complex the ITI has been rendered completely ineffective as there is no longer a distinct *trans* moiety like is observed in the uranyl and uranium(VI) bis(imido) complexes.<sup>5-8</sup>

This disruption of the ITI and subsequent activation of the uranium imido bonds demonstrates that U-O bonds on the uranyl moiety can be activated, expanding the potential uses for spent nuclear fuel. The activation of the uranium imido bonds can be quantified from the increase of the average U-N<sub>imido</sub> bond distance as the number of imido substituents increases: from 1.859(2) Å for the bis(imido) to 2.064(3) Å for the tetrakis(imido). This lengthening of uranium imido bonds is caused by the increased electron donation from the imido substituents into the  $\pi$  system of the complex.

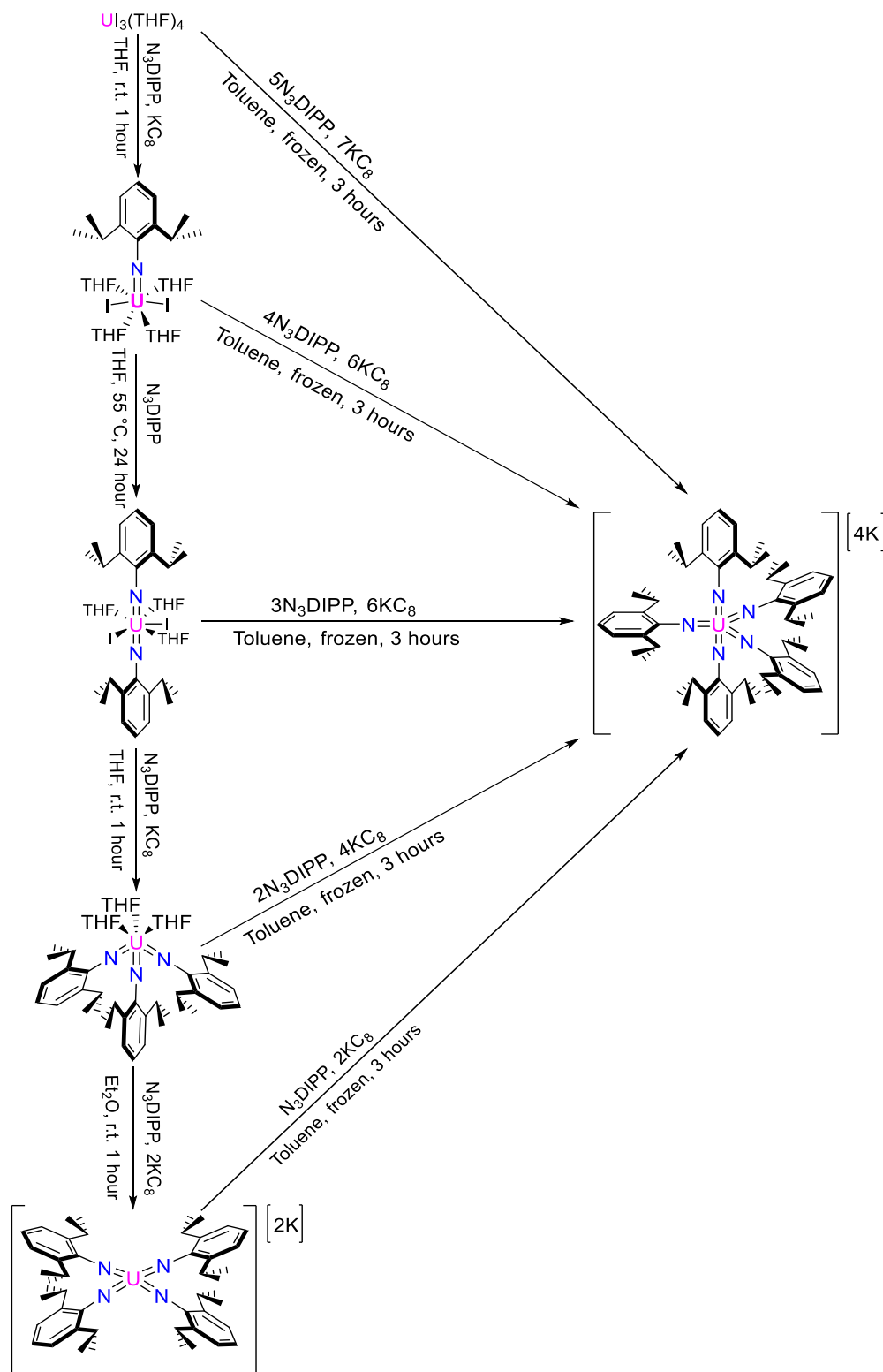
Looking at the resulting geometries obtained from crystallographic data for the tris- and tetrakis(imido), the coordination spheres of both complexes are not fully saturated and space there

appears to be available for another imido substituent to coordinate to the uranium center. The tetrakis(imido) takes on a pseudo square planer geometry leaving two open coordination sites along the axial plane of the molecule. The presence of these open coordination sites left open allowed for investigation toward a pentakis(imido) that could be synthesized using these open sites. If a pentakis(imido) could be isolated, it should show an even greater activation of uranium imido bonds, which has been observed previously with each increase in the number of imido substituents.

### **3.2 Synthesis and discussion of uranium 2,6-diisopropylphenyl pentakis(imido)**

When synthesizing the uranium pentakis(imido) there is some freedom in choosing which uranium precursor to begin the synthesis. The potassium cation supported pentakis(imido) can be successfully synthesized from uranium triiodide and every other uranium multiple-imido precursor leading to the pentakis(imido) in high yield (61-77 %) (Scheme 3.1). The versatility in synthesis that is exhibited by this uranium pentakis(imido) complex demonstrates the stability and reproducibility of the compound.

Scheme 3.1 Synthetic pathways for the formation of  $[\text{U}(\text{NDIPP})_5]\text{K}_4(\text{Et}_2\text{O})_4$



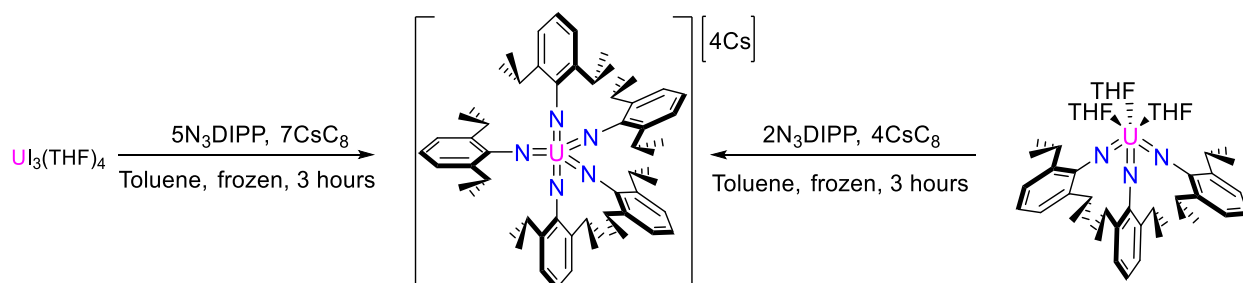
The synthesis of  $[U(NDIPP)_5]K_4(Et_2O)_4$ , **9**, from uranium triiodide starts with  $UI_3(THF)_4$  being mixed with five equivalents of the organoazide,  $N_3DIPP$ , in toluene (15 mL), stirred for 20 minutes, then frozen. Once frozen, seven equivalents of  $KC_8$  are added to the thawing mixture over less than five minutes. There are no  $N_2$  bubbles seen for the pentakis(imido) synthesis unlike when  $KC_8$  is added for the tris- and tetrakis(imido) complexes. The combined reaction mixture is then stirred for three hours as it warms to room temperature. Then the reaction is then filtered through Celite on a fine fritted flask to remove graphite and KI, the Celite layer in the frit is washed with toluene—usually no more than 10mL—until the resulting filtrate is clear. The filtrate is then dried under reduced pressure, dissolved in diethyl ether, and dried once again. To remove as much toluene as possible drying the filtrate down to a powder is advised before transferring to a vial with diethyl ether and drying *in vacuo* again. The resulting matte black powder is recovered in appreciable yield (77%) and can be assigned as  $[U(NDIPP)_5]K_4(Et_2O)_4$ .  $^1H$  NMR spectroscopy assists with determining what solvents and how much may still be bound to the compound. Crystallography confirms the presence of bound solvent by showing there is four solvent molecules, one per potassium. As a matte black powder, the pentakis(imido) can be dissolved in both coordinating ( $THF$ ,  $Et_2O$ ,  $pyridine-d_5$ ) and non-coordinating (toluene) solvents without disrupting the coordination environment.

The synthesis of the  $DIPP$  pentakis(imido) is most successfully carried out in a non-coordinating solvent such as toluene where the  $UI_3(THF)_4$  and  $N_3DIPP$  is allowed to pre-coordinate before being frozen, followed by the fast addition of  $KC_8$  to the thawing pre-mixed mixture. In coordinating solvents like  $THF$ , the uranium tetrakis(imido) becomes a large impurity and a thermodynamic sink preventing significant formation of the pentakis(imido) complex. Another hinderance to pentakis(imido) formation is adding the equivalents of  $KC_8$  over longer periods of time or to room temperature mixtures of  $UI_3(THF)_4$  and  $N_3DIPP$ . Doing this forms only a small amount pentakis(imido) with the major product(s) being the tetrakis(imido) or tris(imido). The slight pentakis(imido) is only quantified in these reactions by the resulting complication of the final reaction mixture  $^1H$  NMR spectra.

With the successful synthesis of a pentakis(imido) complex achieved using  $KC_8$  as the reductant, previous work has demonstrated the ability to use other alkali metal reductants so experiments using  $CsC_8$  as a reductant were carried out.<sup>8</sup> These experiments focused on the change from potassium to cesium rather than the number of initial imido substituents around uranium.

When beginning from either  $\text{UI}_3(\text{THF})_4$  or the tris(imido) using the optimized synthetic route developed for **9** and stoichiometric equivalents of organic azide and  $\text{CsC}_8$ , the pentakis(imido) product, **10**, is produced in good yield (80%). When characterized by  $^1\text{H}$  NMR spectroscopy it was determined that the pentakis(imido) was the only complex that was formed with no indication of the tetrakis(imido) complex as a side product of the reaction.

Scheme 3.2 Synthetic routes to  $[\text{U}(\text{NDIPP})_5]\text{Cs}_4$



Unlike **9**, the cesium metalated pentakis(imido) lacks the same solubility, similar to the cesium metalated tetrakis(imido). This lack of solubility resulted in NMR spectroscopy needing to be carried out in pyridine- $d_5$  and work up needing THF to fully recover **10** from the graphite layer when filtering *in vacuo*. Therefore, pentakis(imido) complexes can be made in good yield, either when using  $\text{UI}_3(\text{THF})_4$  and  $\text{KC}_8$  (77%) and when using  $\text{UI}_3(\text{THF})_4$  and  $\text{CsC}_8$  (80%), regardless of the alkali metal that is used as the reductant, which is a testament to the stability of the resultant compound and the reliability of the synthesis.

### 3.2.1 NMR and IR spectroscopy of uranium 2,6-diisopropylphenyl-pentakis(imido)

The  $^1\text{H}$  NMR spectrum obtained for the pentakis(imido) has six characteristic resonances (Figure 3.1); the isopropyl- $\text{CH}_3$  groups from the axial and equatorial imido substituents appear in a roughly 3:2 ratio from 1.12-1.22 ppm, the isopropyl-CH groups appear at 4.16 ppm and 5.03 ppm, the later overlapping slightly with one of the axial imido aromatic CH groups at 5.11 ppm, the second axial aromatic CH appears at 5.99 ppm, the two aromatic CH groups for the equatorial imido groups appear at 7.74 and 8.00 ppm.

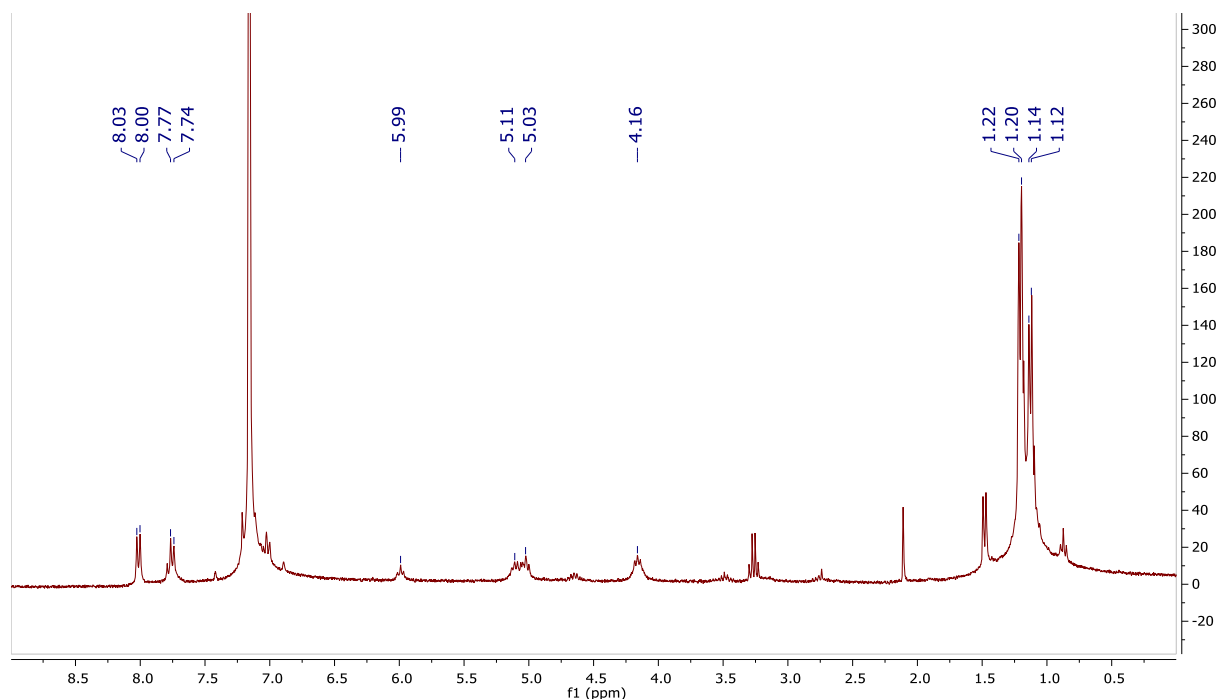


Figure 3.1  $^1\text{H}$  NMR spectra of  $[\text{U}(\text{NDIPP})_5]\text{K}_4(\text{Et}_2\text{O})_4$

The ability of the complex to be in either the trigonal bipyramidal or square pyramidal geometry is the presumed reason for the slightly larger integration values of the imido groups in the equatorial plane. The chemical shifts are found in these regions because of the temperature independent paramagnetic behavior (TIP) associated with uranium(VI); Burns and co-workers also note the unique shifts of organic components surrounding a uranium(VI) metal center.<sup>9</sup> In addition to unique chemical shifts associated with TIP, **9** also has unique shifts from the tetra(imido) with the *i*Pr-CH groups being shifted downfield, and some DIPP ArH peaks shifting upfield relative to their chemical shifts as seen for the tetrakis(imido). These shifts come from the increased electron donation to the uranium center, and further shielding from the fifth imido substituent being bound to the uranium center.

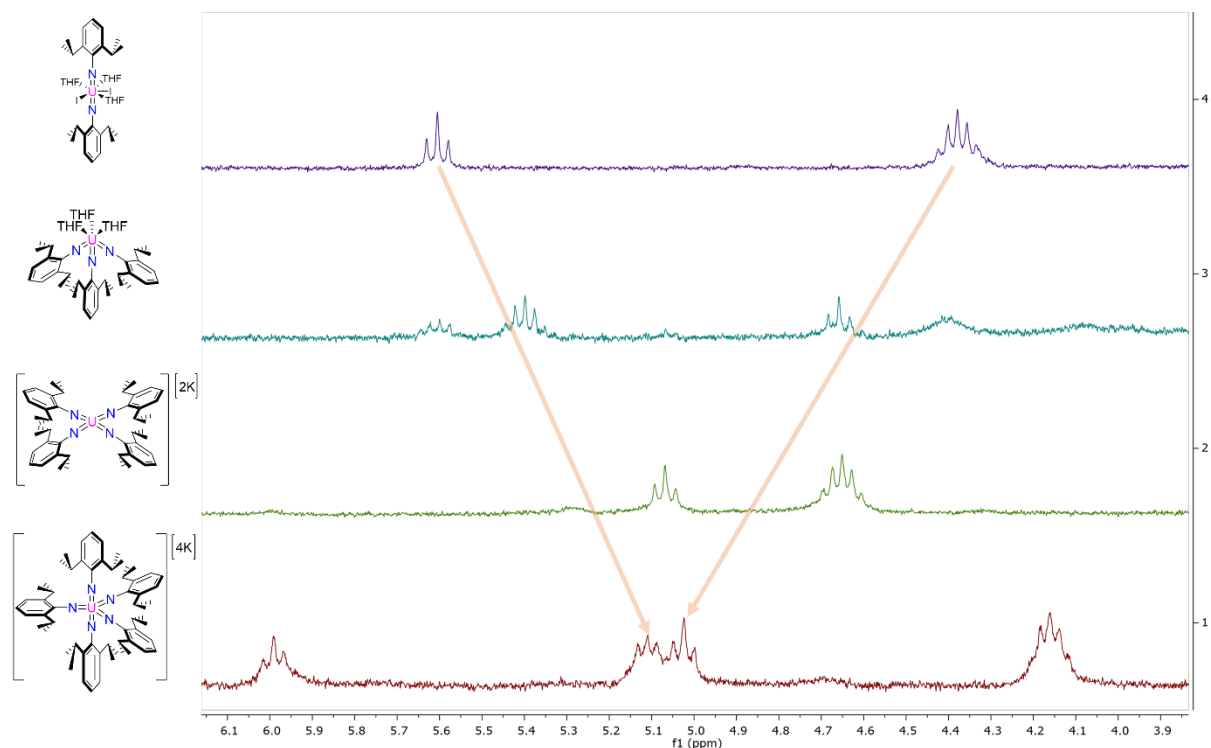


Figure 3.2 NMR trends for uranium multiple imido complexes.

The IR spectra obtained for the pentakis(imido) show a U-N-C stretch at  $1222\text{ cm}^{-1}$  for the uranium imido bonds; this frequency is approximately  $20\text{ cm}^{-1}$  lower than the U-N-C stretch observed in the uranium tetrakis(imido) complex (Figure C7, Appendix C). This weaker U-N-C stretching band makes sense given the slightly longer U-N imido bonds. Another interesting way to observe the weakening of the uranium imido bonds in the pentakis(imido) complexes is by comparing the  $^1\text{H}$  NMR spectra of the uranium multiple imido complexes bis- thru pentakis- (Figure 3.2). Doing this will demonstrate how the resonances for the imido ligands change as more electron density is donated to the  $\pi$ -system of the complex. As the electron density increases, the aromatic protons are shifted up-field while the isopropyl arms of the imido groups are shifted downfield since the electron density is being concentrated in the  $\pi$ -system.

$^1\text{H}$  NMR spectroscopy of **10** reveals a similar spectra to that of **9**, with the same number, ratio, and relative positioning of peaks given change from  $\text{C}_6\text{D}_6$  to pyridine- $d_5$  (Figure 3.3). These same characteristics support the assignment and successful synthesis of a pentakis(imido) with cesium supporting cations.

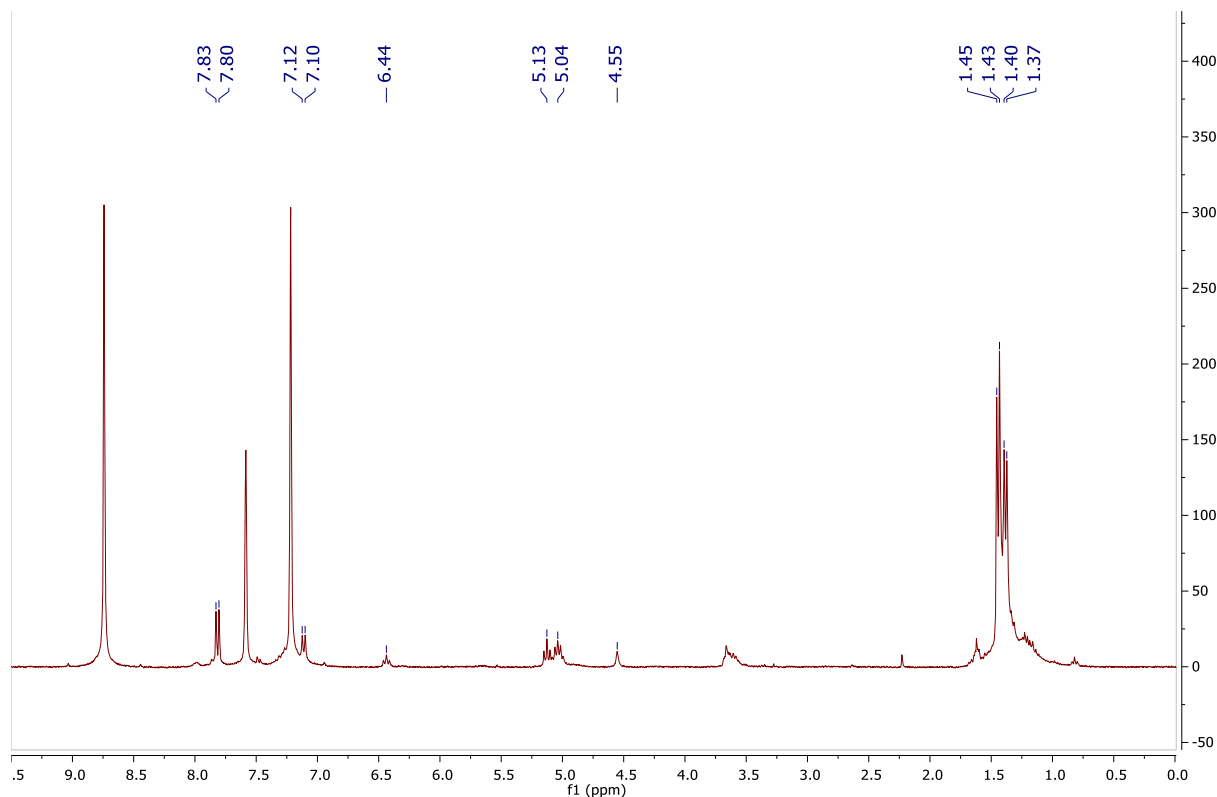


Figure 3.3  $^1\text{H}$  NMR spectra of cesium supported pentakis(imido),  $[\text{U}(\text{NDIPP})_5]\text{Cs}_4$

### 3.2.2 Crystallographic data from a uranium 2,6-diisopropylphenyl-pentakis(imido)

Refinement of crystallographic data shows the reason for the appearance of the eight unique resonances corresponding to the imido ligand in the  $^1\text{H}$  NMR spectra; the pentakis(imido) complex has a fluxional geometry between the trigonal bipyramidal and square pyramidal geometries. These geometries are both possible when looking at the experimentally determined  $\tau_5$  value of  $\tau_5=0.505$ . The molecular structure can be seen in Figure 3.4 (additional view in Appendix C, Figure C1) demonstrating how both geometries are possible. Comparisons between the angles between  $\text{N2-U-N2}_i$  of  $172.03(9)^\circ$  and  $\text{N3-U-N3}_i$  of  $141.34(9)^\circ$  (Table 3.1) demonstrates how the trigonal bipyramidal geometry is possible, as the axial bond would be along the  $\text{N2-U-N2}_i$  axis. Because there is no imido ligand that is directly *trans*- to  $\text{N1}$  the square pyramidal geometry should be easily accessible for this compound. Furthermore, looking at the structural parameters for the pentakis(imido) in Table 3.1, **9** contains the longest  $\text{U-N}_{\text{imido}}$  bond lengths of any of the multiple imido complexes of 2.0818(9), 2.1502(16), and 2.2071(16) Å. These imido bonds are approximately 0.15 Å longer than imido bonds in both the tetrakis(imido) and tris(imido) complexes. These longer imido bonds correlate with the increased electron donation to the  $\pi$ -



system from the DIPP ligands. With each additional imido ligand around the uranium center there is an increase in imido bond length; therefore, an activation of the uranium imido bonds are observed. As will be discussed later, this activation of the uranium-imido bond can be experimentally observed by using the pentakis(imido) as an imido donor complex.

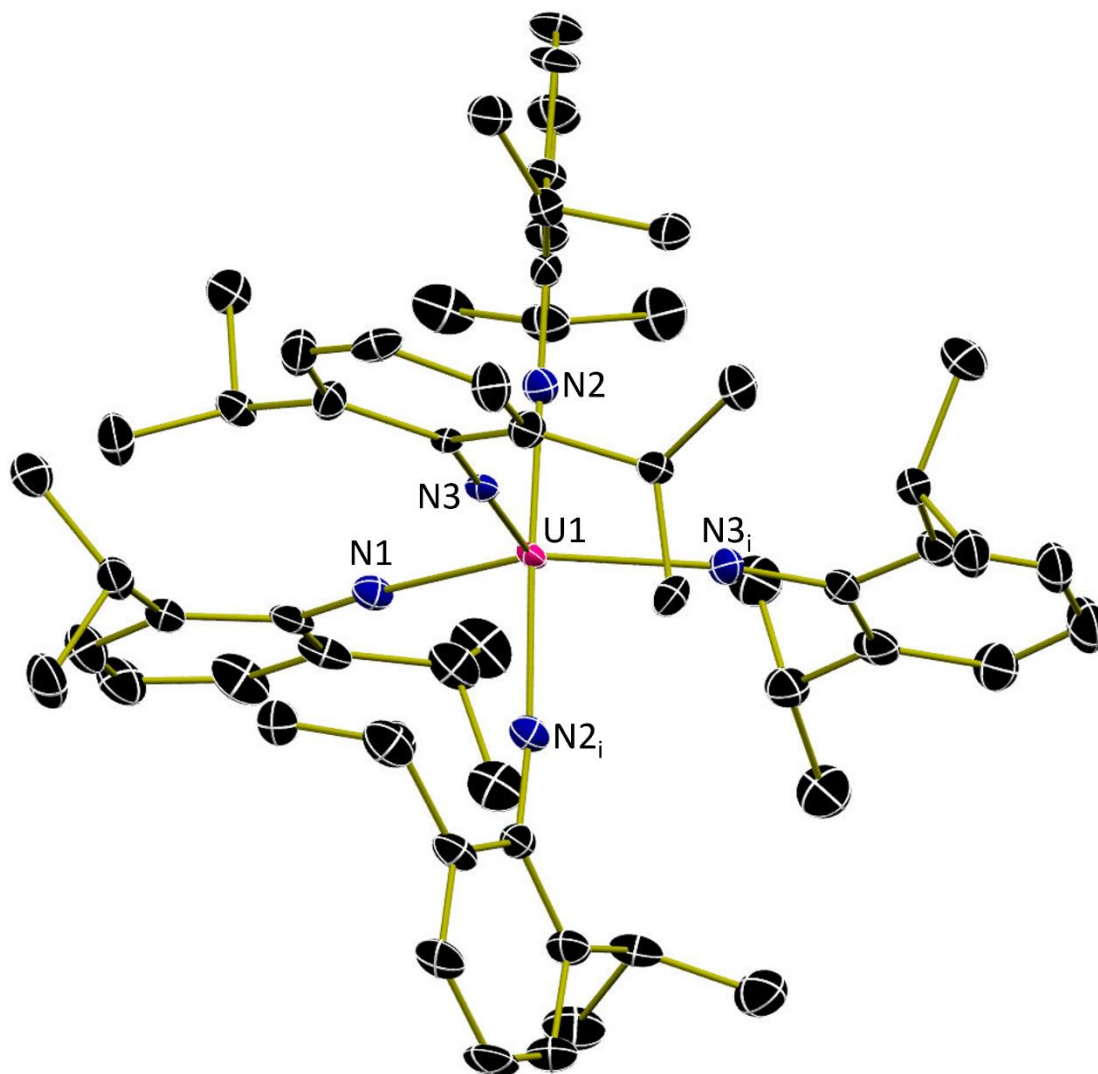


Figure 3.4 Molecular Structure of [U(NDIPP)<sub>5</sub>]K<sub>4</sub>(Et<sub>2</sub>O)<sub>4</sub> shown with 30% probability ellipsoids. Hydrogen atoms, potassium counter ions, and coordinated solvent molecules have been removed for clarity.

Table 3.1 Structural parameters for [U(NDIPP)<sub>5</sub>]K<sub>4</sub>(Et<sub>2</sub>O)<sub>4</sub>

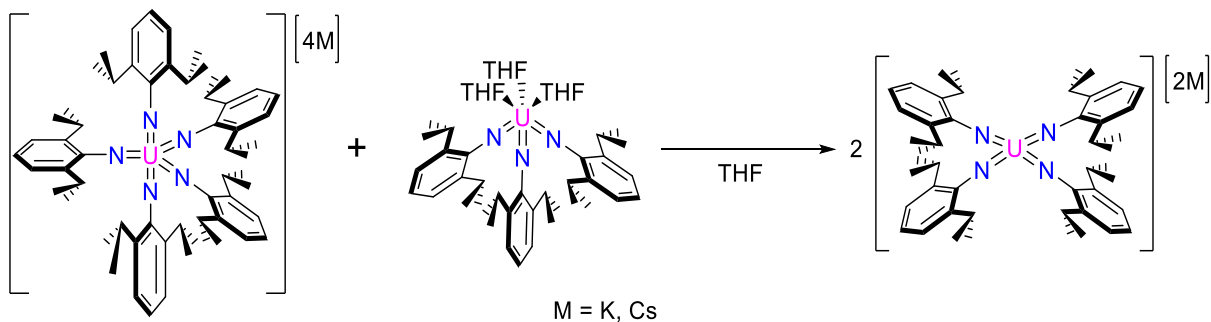
Selected Atoms	Bond Distance/Angle (Å/ °)
U-N1	2.0818(19)
U-N2	2.1502(16)
U-N3	2.2071(16)
N1-U-N2	93.99(4)
N1-U-N3	109.33(4)
N2-U-N2 <sub>i</sub>	172.03(9)
N2-U-N3	88.69(6)
N3-U-N3 <sub>i</sub>	141.34(9)
U-N1-C1	180.0(0)
U-N2-C8	169.65(14)
U-N3-C20	168.59(14)

With a crystal structure of the complex collected, the next question was whether the potassium ions that are present between the imido ligands of N2, N3, N2<sub>i</sub>, and N3<sub>i</sub> are affecting the geometry of the molecule in the solid state. Attempts to sequester the potassium ions from the coordination sphere with 18-crown-6, dibenzo-18-crown-6, and 2,2,2-cryptand failed to produce quality crystals for X-ray diffraction. Dibenzo-18-crown-6 did not readily react with the pentakis(imido) leaving large amounts of solid dibenzo-18-crown-6 in the solution preventing clean crystallization conditions. When using 18-crown-6, the resulting sequestered product was isolated as an oil, with attempts to make this oil into a powder unsuccessful. Reactions and crystallizations with 2,2,2-cryptand had dramatic sequestration of the potassium ions; however, the resulting black solid is insoluble in most organic solvents. The only solvent that was found to solubilize this crypted pentakis(imido) product is pyridine; however, this was a blessing in disguise as it is difficult to crystallize the crypted pentakis(imido) complex from pyridine due to the excellent solubility of the complex in pyridine. The best attempts to grow quality crystals have involved dissolving the pentakis(imido) in a polar solvent followed by a clean non-polar layer, layered with a non-polar solvent that has been mixed with dissolved 2,2,2-cryptand. Crystalline solids that have been recovered from the crypted pentakis(imido) are thin, fine, needles that appear to have a wispy quality to them and are not of sufficient quality for x-ray diffraction studies. Attempts to isolate crystals for diffraction studies are ongoing.

### 3.2.3 2,6-diisopropyl imido donation reactivity

An interesting point of reactivity that demonstrates the activation of the uranium-nitrogen bonds is when the uranium pentakis(imido) is used as an imido donor complex. When uranium tris(imido) and pentakis(imido) are mixed together in THF the reaction produces uranium tetrakis(imido) as the major product.

Scheme 3.3 Imido donation observed with DIPP pentakis(imido) complexes



This reactivity shows how activated the uranium-imido bonds are in the pentakis(imido), in that an imido ligand, and two potassium ions, are transferred to the tris(imido) to form a tetrakis(imido) without an external reductant. This reactivity is interesting for its applications to other chemical species, and for explorations into what else could accept an imido ligand from the pentakis complex. It will be interesting to see whether this donation process can be used to create new mixed imido species to investigate how the changes from homoleptic to heteroleptic imido complexes affects bond distances and geometry.

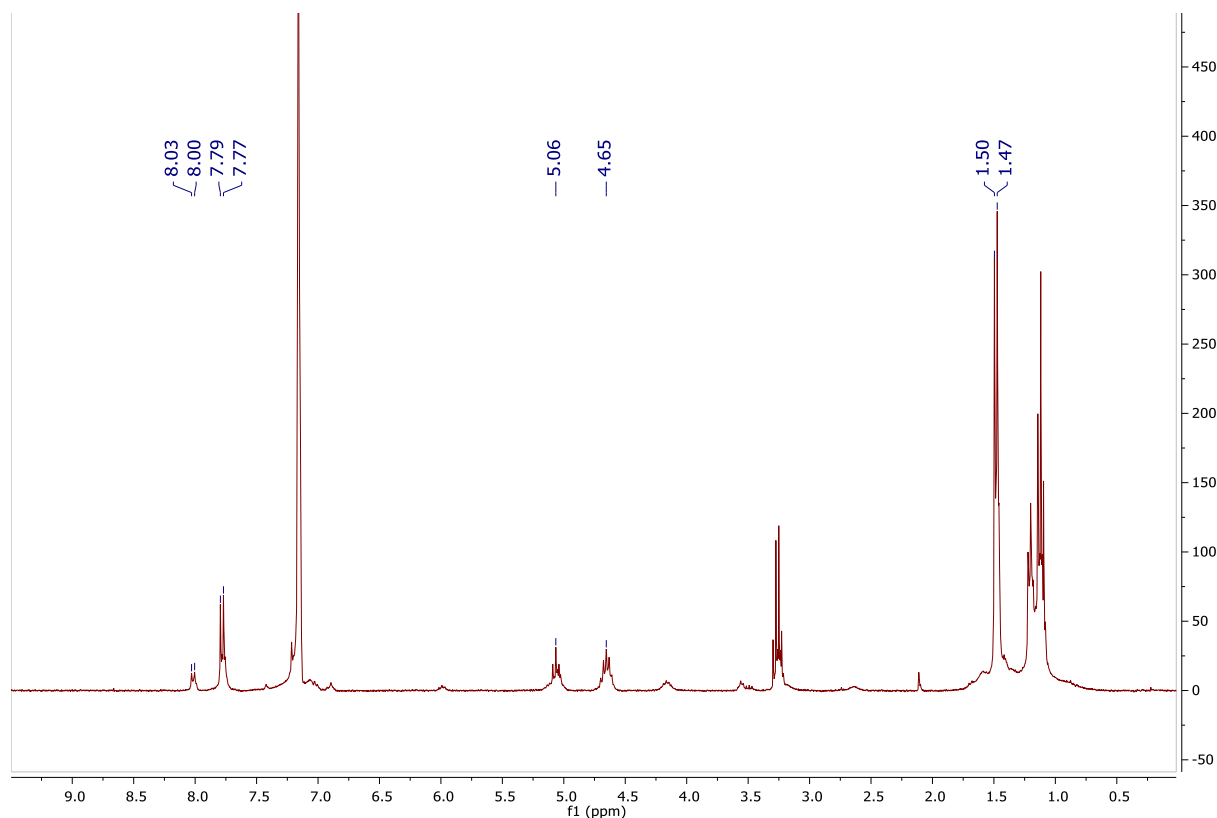


Figure 3.5  $^1\text{H}$  NMR spectra of  $[\text{U}(\text{NDIPP})_5]\text{K}_4(\text{Et}_2\text{O})_4$  imido donation reaction.

Another interesting reaction is that of the pentakis(imido) with the bis(imido) complex. During this reaction, some type of imido donation occurs; however, it is difficult to determine what products are formed, but there is no evidence for the starting materials (Appendix C, Figure C6).

### 3.2.4 Investigations toward a uranium hexakis(imido) complex

With the success of the pentakis(imido) synthesis, attempts to make a hexakis(imido) complex from  $\text{UI}_3(\text{THF})_4$  using the same procedural techniques were carried out. The reason for these investigations comes from looking at the crystal structure obtained for the pentakis(imido). The fact that the compound does exist in the square pyramidal geometry would suggest that it may be possible to obtain a hexakis(imido) that would have octahedral geometry. However, when these experiments were carried out, it was revealed that the only product that was made was an extremely clean pentakis(imido) product with a slight excess of DIPP azide when characterized by  $^1\text{H}$  NMR spectroscopy. While these results were initially unfortunate, the recovery of the clean pentakis(imido) from these reactions was not disappointing: this demonstrates the stability of the

pentakis(imido) when exposed to an excess of  $\text{KC}_8$  during synthesis. This stability suggests the reduction potential of the pentakis(imido) is more negative than the reduction potential of  $\text{KC}_8$ , which will be tested through ongoing electrochemical experiments.

### 3.3 Progress towards uranium multiple imido complexes with non-DIPP ligands

In addition to the 2,6-diisopropylphenyl ligand, synthetic experiments have been carried out using 2,4,6-mesitylene(Mes) and 4-toluidine(*p*-tol) for formation of uranium tetrakis- and pentakis(imido) complexes. These two ligands were chosen to further probe the electronic effect of the ligand on the stability of the uranium imido bonds. Previous work that has focused on the Mes and *p*-tol uranium multiple-imido complexes has shown that the tris(imido) complexes can be synthesized. However, both the *p*-tol and Mes tris(imido) complexes lack crystallographic data to definitively determine the molecular structure of either, It is possible that the tris(imido) complexes of these two ligands could exist as a dimer as observed with the 2,6-diethylphenyl tris(imido) complex.<sup>10</sup> With these results in mind, experiments to synthesize the Mes and *p*-tol tetrakis-, and pentakis(imido) complexes were carried out.

Initially, experiments to synthesize the tetrakis(imido) complexes utilizing the Mes and *p*-tol ligands beginning from  $\text{UI}_3(\text{THF})_4$  did not proceed as had previously been observed when using the DIPP ligand. The recovered products from these synthetic attempts were either a complicated paramagnetic product or the tris(imido) complex and free aniline, necessitating another route. With the knowledge of the Mes and *p*-tol tris(imido) complexes, the tetrakis(imido) complexes were then synthesized with the same method as the DIPP tetrakis(imido); starting from the tris(imido) with one equivalent of azide, and reduced by two equivalents of  $\text{KC}_8$ .<sup>8</sup> Currently, it appears that some combination of the difference in sterics and electronics prevents the formation of the tetrakis- and pentakis(imido) complexes from  $\text{UI}_3(\text{THF})_4$  when using the Mes, and *p*-tol ligands instead of the DIPP ligand.

NMR analysis of reactions to make the tetrakis(imido) complexes with the Mes and *p*-tol ligands so far has shown the presence of the tris(imido) for both compounds along with free aniline. This suggests that three equivalents of the azide can coordinate to the uranium center, with the fourth equivalent being reduced by the  $\text{KC}_8$  to the aniline without coordination or bonding to the uranium center. Another factor that suggests that these multiple imido complexes might be dimers either in the solid state or in solution is the changes in solubility compared to the DIPP tris(imido)

complexes. The Mes and *p*-tol compounds lack the same solubility in non-polar solvents that is observed for the DIPP compounds. The insoluble nature of these also plays a role in the difficulty crystallizing the tris-, tetrakis-, and pentakis(imido) complexes.

As previously noted, the DIPP pentakis(imido) can be made from any lesser multiple imido. It appears that this characteristic is unique to the DIPP ligand as attempts to make other multiple imido complexes from lesser multiple imido complexes has not proven effective to produce either the tetrakis- Mes or *p*-tol complexes. This fact holds true for production of the pentakis(imido) compound of these same ligands. Efforts to synthesize the Mes or *p*-tol pentakis(imido) complexes from  $\text{UI}_3(\text{THF})_4$  resulted in complicated spectra with, sometimes many, paramagnetic impurities suggesting over reduction of the uranium metal center and incomplete reduction of the organic azide. The smaller steric profile of these two ligands compared to the DIPP complex does also play a role in the characterization of these complexes as they appear to exhibit vastly different solubility than the DIPP complexes. These differences in solubility likely come from potential dimerization in the solid state of the Mes and *p*-tol complexes, which is known to occur for smaller mono(imido) complexes.<sup>6</sup>

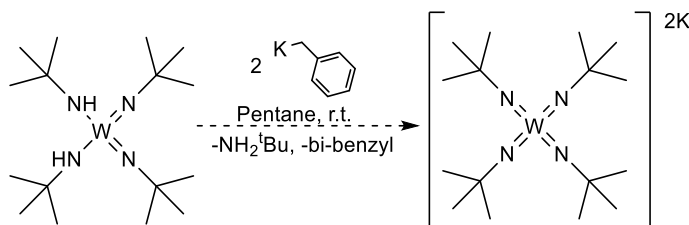
### 3.4 Investigations of analogous tungsten multiple imido complexes

Tungsten is isoelectronic with uranium and both metals can support multiple imido ligands within their coordination sphere. One of the only directly analogous uranium and tungsten compounds is a tris(imido) complex that contains the DIPP ligand. With this in mind, precedent for explorations into the synthesis of tungsten multiple imido complexes does exist.<sup>11</sup> Moreover, it would be beneficial to determine if tungsten, like uranium, can support four or more imido substituents. If this is true, then it would be prudent to explore the similarities between the complexes to determine whether tungsten could be used as a non-radioactive synthon for uranium chemistry. Starting from the tungsten(VI) complex  $\text{W}(\text{tBuN})_2(\text{tBuNH})_2$  made by Nugent and co-workers,<sup>12</sup> a deprotonation pathway was explored utilizing benzyl potassium in order to form a tungsten tetrakis(imido) complex. It has been shown that deprotonation is a viable pathway for tetrakis(imido) formation in addition to  $\text{KC}_8$  reduction, as the uranium DIPP tris(imido) can undergo a deprotonation pathway after being protonated by an equivalent of DIPP aniline.<sup>10</sup>

### 3.4.1 Experiments towards tungsten multiple imido complexes

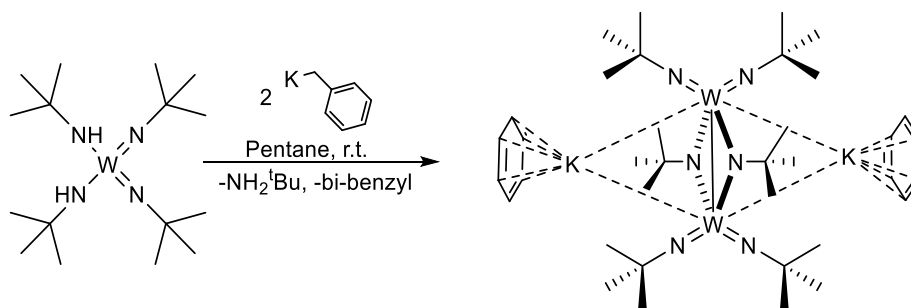
The first compound that was utilized as a potential precursor for a tungsten tetrakis(imido) complex was  $W(^t\text{BuN})_2(^t\text{BuNH})_2$ . This particular complex was chosen because if the amide ligands are able to be deprotonated, a tetrakis(imido) should be formed. Benzyl potassium was used as the deprotonating agent because the formation of toluene would be a helpful spectroscopic handle as the reactions can be carried out in pentane (Scheme 3.4). The deprotonation pathway was also considered given how the uranium tetrakis(imido) complex can also be synthesized from the tris(imido) *via* a deprotonation pathway with the bis(amido)-bis(imido) uranium complex acting as an intermediate enroute to the tetrakis(imido).<sup>8</sup>

Scheme 3.4 Proposed synthetic route for tungsten tetrakis(imido) complex



When these experiments were carried out with 2 equivalents of benzyl potassium, an orange oil was isolated upon work up, which did not appear to correspond to a tungsten tetrakis(imido) complex when characterized by  $^1\text{H}$  NMR and IR spectroscopy. Crystallization from a solution of  $\text{C}_6\text{D}_6$  allowed for characterization of this product as  $[W(\mu\text{-N}^t\text{Bu})(\text{N}^t\text{Bu})_2]_2$  (Scheme 3.5, Figure 3.6). Assignment as  $[W(\mu\text{-N}^t\text{Bu})(\text{N}^t\text{Bu})_2]_2$  aligned with the data obtained from  $^1\text{H}$  NMR and IR spectroscopy as well.

Scheme 3.5 Synthetic route to  $[W_2(^t\text{BuN})_4(\mu\text{-}^t\text{BuN})_2]\text{K}_2$



Refinement of diffraction data allowed for further assignment as a tungsten(VI) bridging amide complex  $[\text{W}_2(\text{}^t\text{BuN})_4(\mu\text{}^t\text{BuN})_2]\text{K}_2$ , **11** (Figure 3.6, Table 3.2). The structure contains three unique tungsten imido bonds making this a formal tungsten tris(imido) complex. The loss of one equivalent of *tert*-butyl amine, and lack of evidence in the spectroscopic results is contributed to the low boiling point of the amine leading to the removal of the lost equivalent during *in vacuo* work up of the reaction. The formation of free *tert*-butyl amine upon reaction is also supported by the formation of bibenzyl, which is observed in the  $^1\text{H}$  NMR spectra for **11**. This supports the benzyl potassium acting solely as a reductant, followed by a hydride shift allowing for elimination of the amine from the tungsten complex.

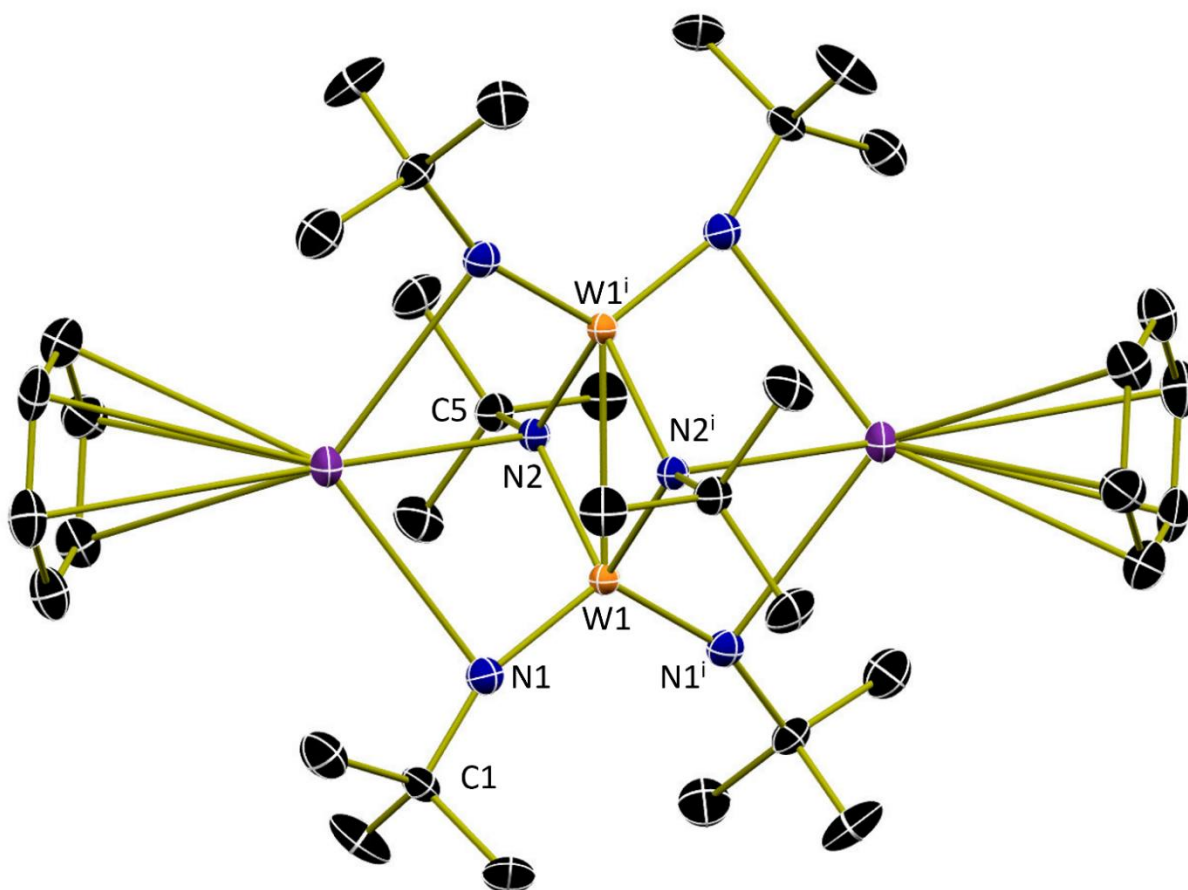


Figure 3.6 Molecular structure of  $[\text{W}_2(\text{}^t\text{BuN})_4(\mu\text{}^t\text{BuN})_2]\text{K}_2$ , shown at 30% probability ellipsoids. Hydrogen atoms and co-crystallized solvent molecules have been omitted for clarity.



Table 3.2 Selected Bond Lengths of  $[\text{W}_2(\text{}^t\text{BuN})_4(\mu\text{}^t\text{BuN})_2]\text{K}_2$ 

Atoms	Bond Length, Å
W1-N1	1.801(4)
W1-N2	1.999(3)
W1-W1 <sup>i</sup>	2.8155(6)

Looking at the bond lengths for **11** in Table 3.2, each tungsten center has two terminal imido groups and two bridging imido groups, for a formal tungsten tris(imido) complex. The bonds lengths for the two distinct tungsten imido bonds are both within the distance for a tungsten(VI) imido bond even though there is a 0.1 Å difference. The two tungsten centers are outside the ionic radius of  $\text{W}^{6+}$  meaning there is not a tungsten-tungsten bond in this complex.

The unexpected reactivity that was observed for  $\text{W}(\text{}^t\text{BuN})_2(\text{}^t\text{BuNH})_2$  made attempts to establish analogous reactivity to the uranium multiple-imido complexes difficult. Focus then changed from the *tert*-butyl amide ligand to investigations utilizing the same ligand system as the uranium multiple-imidos. Beginning from  $\text{WCl}_4$  or  $\text{WCl}_6$  and combining it with four equivalents of KNHDIPP and potassium benzyl to form a tetrakis(imido) via salt metathesis and deprotonation was then attempted. However, these reactions did not lead to the desired products, with characterization by  $^1\text{H}$  NMR and IR spectroscopy showing a mixture of products, none of which could be confidently identified as a tetrakis(imido) product.

Potassium was not the only alkali metal used to facilitate the formation of a tungsten tetrakis(imido) product. Reactions with LiNHDIPP and *n*-BuLi were also carried out; however, these reactions with  $\text{WCl}_6$  resulted in the formation of the diazene, which was confirmed by x-ray crystallography.

### 3.5 Conclusions

The successful synthesis of uranium pentakis(imido) complexes has been presented. These complexes support and demonstrate that the addition of electron donating substituents aid in the activation of uranium element multiple bonds. This is seen by the uranium imido bonds lengths of 2.08 to 2.20 Å, which are noticeably longer than those observed for the analogous tris- and tetrakis(imido) complexes. Interesting imido group donation reactivity has also been explored for the pentakis(imido) complexes experimentally demonstrating the activation of the U-N<sub>imido</sub> bonds. The various synthetic pathways available to produce the pentakis(imido) complex demonstrate the

versatility of synthesis available for these complexes. Excitingly, the pentakis(imido) complex can be generated with different alkali metals as reductants without over reducing the metal center as was observed with the tetrakis(imido) complex. The DIPP ligand appears to be a workhorse for uranium multiple imido complexes, exhibiting an ease of synthesis that is unmatched by other ligands that have been used here. Tungsten poses an interesting metal for the synthesis of an analogous *d*-block metal to uranium; however, further experiments are needed to solidify synthetic pathways and fully characterize the corresponding products. This *d*-block chemistry does appear rich with potential complexes to be synthesized for comparisons to analogous uranium imido complexes.

### 3.6 Experimental Methods

#### 3.6.1 General Considerations

All air- and moisture-sensitive manipulations were performed using standard Schlenk techniques or in an MBraun inert atmosphere drybox with an atmosphere of purified nitrogen. The MBraun drybox was equipped with two  $-35\text{ }^{\circ}\text{C}$  freezers for cooling samples and crystallizations. Solvents for sensitive manipulations were dried and deoxygenated using literature procedures with a Seca solvent purification system.<sup>13</sup> Benzene- $\text{d}_6$  was purchased from Cambridge Isotope Laboratories, dried with molecular sieves and sodium, and degassed by three freeze–pump–thaw cycles. Potassium graphite<sup>14</sup>,  $\text{UI}_2(\text{NDIPP})\text{THF}_4$ ,<sup>6</sup>  $\text{UI}_2(\text{NDIPP})_2\text{THF}_4$ ,<sup>5</sup>  $\text{U}(\text{NDIPP})_3\text{THF}_4$ ,<sup>7</sup>  $[\text{U}(\text{NDIPP})_4]\text{K}_2$ ,<sup>8</sup> 2,6-diisopropylphenyl azide<sup>15</sup> were synthesized according to literature procedures, and cesium graphite was prepared with a similar method as potassium graphite.

**Caution:** *U-238 is a weak  $\alpha$ -emitter with a half-life of  $t_{1/2} = 4 \times 10^9$  years. All manipulations were performed in an inert atmosphere glovebox in a laboratory equipped with proper detection equipment.*

$^1\text{H}$  NMR spectra were recorded at  $25\text{ }^{\circ}\text{C}$  on a Varian Inova 300, spectrometer operating at 299.96 MHz. All chemical shifts are reported relative to the peak for  $\text{SiMe}_4$ , using  $^1\text{H}$  (residual) chemical shifts of the solvent as a secondary standard. For all molecules, the NMR data are reported with the chemical shift, followed by the multiplicity, any relevant coupling constants, the integration value, and the peak assignment.

Infrared spectra were recorded using a Thermo Nicolet 6700 spectrometer; samples were prepared by grinding the desired compound together with KBr salt and pressing the solid into a pellet. Elemental analyses were performed by Midwest Microlab (Indianapolis, IN).

Single crystals of  $[U(NDIPP)_5]K_4(Et_2O)_4$  suitable for X-ray diffraction, were coated with poly(isobutylene) oil in a glovebox and quickly transferred to the goniometer head of a Bruker Quest diffractometer with a fixed chi angle, a sealed fine-focus X-ray tube, single-crystal curved graphite incident beam monochromator and a Photon100 CMOS area detector. Examination and data collection were performed with Mo  $K\alpha$  radiation ( $\lambda = 0.71073 \text{ \AA}$ ).

### 3.6.2 Synthesis

#### *Uranium-pentakis(imido)-tetra(potassium) from $UI_3(THF)_4$ , 9*

A 20-mL scintillation vial was charged with  $UI_3(THF)_4$  (0.150 g, 0.165 mmol) and toluene (10 mL), then stirred for five minutes making a royal blue solution. Five equivalents of 2,6-diisopropyl-phenyl azide ( $N_3DIPP$ ) (0.163 g, 0.802 mmol) were then added to the reaction and stirred for 15 minutes; the color changed to dark amber-red. The reaction was then frozen in the coldwell. Upon thawing, seven equivalents of  $KC_8$  (0.156 g, 1.155 mmol) were quickly added to the reaction and stirred for three hours. After this time, the black reaction mixture was filtered over Celite, and the filtrate was washed with toluene until the washings came out clear. This solution was then dried to a black residue and dissolved in diethyl ether (3 mL) and dried (x2) leaving a matte black powder assigned as  $[U(NDIPP)_5][K(Et_2O)]_4$  (0.150 g, 77 %). Elemental Analysis, calculated: C 56.71%, H 6.74%, N 5.51%, found: C 56.07%, H 7.01%, N 5.13%.  $^1H$  NMR ( $C_6D_6$ , 25 °C, ppm)  $\delta$ : 1.12-1.22 (60 H, d, *i*-Pr  $CH_3$ ), 4.16 (6 H, sext, *i*-Pr CH), 5.02 (4 H, sext, *i*-Pr CH), 5.11 (2.5 H, t, *para*-Ar-H), 5.99 (2.5 H, t, *para*-Ar-H), 7.74 (4 H, d, *meta*-Ar-H), 8.00 (6 H, d, *meta*-Ar-H). IR (KBr salt plate,  $cm^{-1}$ ): 487.90 w, 507.64 w, 568.56 w, 687.18 w, 747.55 m, 795.34 w, 856.28 m, 881.15 m, 1040.69 w, 1109.26 w, 1136.23 m, 1222.93 s ( $\nu_{N-U-N}$ ), 1318.11 s, 1339.18 s, 1460.04 m, 1577.37 s, 2864.80 m, 2957.20 s, 3032.37 w.

#### *Uranium-pentakis(imido)-tetra(cesium) from $UI_3(THF)_4$ , 10*

A 20-mL scintillation vial was charged with  $UI_3(THF)_4$  (0.100 g, 0.110 mmol) and toluene (10 mL) then stirred for five minutes making a royal blue solution. Five equivalents of 2,6-diisopropyl-phenyl azide ( $N_3DIPP$ ) (0.112 g, 0.551 mmol) were then added to the reaction and

stirred for 20 minutes; the color changed to dark amber-red. The reaction was then frozen in the coldwell. Upon thawing and seven equivalents of CsC<sub>8</sub> (0.177 g, 0.773 mmol) were slowly added to the reaction over a minute or two and stirred for three hours as the reaction warmed to room temperature. After this time, the black reaction mixture was filtered through Celite, and the filtrate was washed with THF until the washings came out clear. This solution was then dried to a black residue and dissolved in diethyl ether (3 mL) and dried leaving a matte black powder assigned as [U(NDIPP)<sub>5</sub>]Cs<sub>4</sub> (0.172 g, 80 %). <sup>1</sup>H NMR (pyridine-*d*<sub>5</sub>, 25 °C, ppm) δ: 1.37-1.46 (60 H, d, *i*-Pr CH<sub>3</sub>), 4.55 (2.5 H, m, *i*-Pr CH), 5.04 (6 H, t, *i*-Pr CH), 5.13 (2.5 H, t, *para*-Ar-H), 6.44 (2 H, t, *para*-Ar-H), 7.10 (4 H, d, *meta*-Ar-H), 7.80 (6 H, d, *meta*-Ar-H)

*Synthesis of 9 from UI<sub>2</sub>(NDIPP)(THF)<sub>3</sub>*

Using the same procedure as **9**, four equivalents of N<sub>3</sub>DIPP (0.079 g, 0.389 mmol) was added to UI<sub>2</sub>(NDIPP)(THF)<sub>3</sub> (0.100 g, 0.097 mmol), and six equivalents of KC<sub>8</sub> (0.079, 0.585 mmol) were used. A matte black powder (0.117 g, 77 %) was recovered. <sup>1</sup>H NMR (C<sub>6</sub>D<sub>6</sub>, 25 °C, ppm) δ: 1.12-1.22 (60 H, d, *i*-Pr CH<sub>3</sub>), 4.16 (6 H, sext, *i*-Pr CH), 5.03 (4 H, sext, *i*-Pr CH), 5.09 (2.5 H, t, *para*-Ar-H), 5.99 (2.5 H, t, *para*-Ar-H), 7.74 (4 H, d, *meta*-Ar-H), 8.00 (6 H, d, *meta*-Ar-H)

*Synthesis of 9 from UI<sub>2</sub>(NDIPP)<sub>2</sub>(THF)<sub>3</sub>*

Using the same procedure as **9**, three equivalents of N<sub>3</sub>DIPP (0.107 g, 0.526 mmol) were added to UI<sub>2</sub>(NDIPP)<sub>2</sub>(THF)<sub>3</sub> (0.200 g, 0.177 mmol), and six equivalents of KC<sub>8</sub> (0.143 g, 1.06 mmol) were used. A matte black powder (0.177 g, 64 %) was recovered. <sup>1</sup>H NMR (C<sub>6</sub>D<sub>6</sub>, 25 °C, ppm) δ: 1.12-1.22 (60 H, d, *i*-Pr CH<sub>3</sub>), 4.18 (6 H, sext, *i*-Pr CH), 5.02 (4 H, sext, *i*-Pr CH), 5.11 (2.5 H, t, *para*-Ar-H), 5.99 (2.5 H, t, *para*-Ar-H), 7.74 (4 H, d, *meta*-Ar-H), 8.00 (6 H, d, *meta*-Ar-H)

*Synthesis of 9 from U(NDIPP)<sub>3</sub>(THF)<sub>4</sub>*

Using the same procedure as **9**, two equivalents of N<sub>3</sub>DIPP (0.083 g, 0.408 mmol) were added to (0.200 g, 0.204 mmol) of U(NDIPP)<sub>3</sub>(THF)<sub>4</sub>, and four equivalents of KC<sub>8</sub> (0.110 g, 0.814 mmol) were used. A matte black powder (0.222g, 69 %) was recovered. <sup>1</sup>H NMR (C<sub>6</sub>D<sub>6</sub>, 25 °C, ppm) δ: 1.14-1.22 (60 H, d, *i*-Pr CH<sub>3</sub>), 4.17 (6 H, sext, *i*-Pr CH), 5.03 (4 H, sext, *i*-Pr CH), 5.10

( 2.5 H, t, *para*-Ar-H), 6.00 (2.5 H, t, *para*-Ar-H), 7.74 (4 H, d, *meta*-Ar-H), 8.00 (6 H, d, *meta*-Ar-H)

#### *Synthesis of 9 from [U(NDIPP)<sub>4</sub>]K<sub>2</sub>*

Using the same procedure as **10**, one equivalent of N<sub>3</sub>DIPP (0.050 g, 0.246 mmol) was added to [U(NDIPP)<sub>4</sub>]K<sub>2</sub> (0.250 g, 0.246 mmol), and two equivalents of KC<sub>8</sub> (0.060 g, 0.444 mmol) were used. A matte black powder (0.234 g, 61 %) was recovered. <sup>1</sup>H NMR (C<sub>6</sub>D<sub>6</sub>, 25 °C, ppm) δ: 1.12-1.22 (60 H, d, *i*-Pr CH<sub>3</sub>), 4.16 (6 H, sext, *i*-Pr CH), 5.02 (4 H, sext, *i*-Pr CH), 5.11 ( 2.5 H, t, *para*-Ar-H), 5.99 (2.5 H, t, *para*-Ar-H), 7.74 (4 H, d, *meta*-Ar-H), 8.00 (6 H, d, *meta*-Ar-H)

#### *Synthesis of 10 from U(NDIPP)<sub>3</sub>(THF)<sub>3</sub>*

Using the same procedure as for **10**, two equivalents of N<sub>3</sub>DIPP (0.062 g, 0.305 mmol) was added to U(NDIPP)<sub>3</sub>(THF)<sub>3</sub> (0.150 g, 0.153 mmol), and four equivalents of CsC<sub>8</sub> (0.140 g, 0.613 mmol) was used. A matte black powder was recovered.

#### *Synthesis of 10 from [U(NDIPP)<sub>4</sub>]Cs<sub>2</sub>*

Using the same procedure as for **10**, one equivalent of N<sub>3</sub>DIPP (0.015 g, 0.073 mmol) was added to [U(NDIPP)<sub>4</sub>]Cs<sub>2</sub> (0.110 g, 0.073 mmol), and four equivalents of CsC<sub>8</sub> (0.034 g, 0.149 mmol) was used. A matte black powder was recovered.

#### *Syntheis of [W<sub>2</sub>(<sup>t</sup>BuN)<sub>4</sub>(μ-<sup>t</sup>BuN)<sub>2</sub>]K<sub>2</sub>, 11*

W(<sup>t</sup>BuN)<sub>2</sub>(<sup>t</sup>BuNH)<sub>2</sub> (0.090g, 0.191 mmol) was dissolved in pentane (3 mL). While stirring this clear yellow solution, benzyl potasssium (0.053g, 0.407 mmol) was added causing a color change to cloudy orange. The reaction was stirred for one hour then solvent was removed *in vacuo* leaving an oily solid that was then redissolved in pentane and decanted. The orange decanted pentane was dried *in vacuo* leaving a red-orange oil that was assigned as [W<sub>2</sub>(<sup>t</sup>BuN)<sub>4</sub>(μ-<sup>t</sup>BuN)<sub>2</sub>]K<sub>2</sub> upon crystallization from a C<sub>6</sub>D<sub>6</sub> solution. Additional product can be recovered by filtering a pentane slurry of the original reaction vial to remove unreacted starting material and any salts that may have formed, this lead to 0.058g(59%), in total, of [W<sub>2</sub>(<sup>t</sup>BuN)<sub>4</sub>(μ-<sup>t</sup>BuN)<sub>2</sub>]K<sub>2</sub> being recovered. <sup>1</sup>H NMR (C<sub>6</sub>D<sub>6</sub>, 25 °C) δ (ppm): 1.49 (s, μ-<sup>t</sup>BuN ), 1.52 (s, <sup>t</sup>BuN). IR (salt plate) ν (wavenumbers, cm<sup>-1</sup>): 2960 s, 2894 m, 2856 m, 1589 m, 1486 m, 1454 m, 1383 w, 1350 s, 1284 s, 1250 m, 1209 s, 1069 m, 798 m, 760 m, 701 m.

### 3.7 References

- 1 Gras, J. M.; Quang, R. Do; Masson, H.; Lieven, T.; Ferry, C.; Poinssot, C.; Debes, M.; Delbecq, J. M. Perspectives on the Closed Fuel Cycle - Implications for High-Level Waste Matrices. *J. Nucl. Mater.* **2007**, 362 (2–3), 383–394.
- 2 Joseph J. Katz, Lester R. Morss, G. T. S. *The Chemistry of the Actinide Elements*; 1980.
- 3 Jones, M. B.; Gaunt, A. J.; Jones, M. B.; Gaunt, A. J. Recent Developments in Synthesis and Structural Chemistry of Nonaqueous Actinide Complexes. *Chem. Rev.* **2013**, 113 (2),
- 4 Hayton, T. W. Metal–Ligand Multiple Bonding in Uranium: Structure and Reactivity. *Dalt. Trans.* **2010**, 39 (5), 1145–1158.
- 5 Hayton, T. W.; Boncella, J. M.; Scott, B. L.; Batista, E. R.; Hay, P. J. Synthesis and Reactivity of the Imido Analogues of the Uranyl Ion. *J. Am. Chem. Soc.* **2006**, 128 (32), 10549–10559.
- 6 Jilek, R. E.; Spencer, L. P.; Kuiper, D. L.; Scott, B. L.; Williams, U. J.; Kikkawa, J. M.; Schelter, E. J.; Boncella, J. M. A General and Modular Synthesis of Monoimidouranium(IV) Dihalides. *Inorg. Chem.* **2011**, 50 (10), 4235–4237.
- 7 Anderson, N. H.; Yin, H.; Kiernicki, J. J.; Fanwick, P. E.; Schelter, E. J.; Bart, S. C. Investigation of Uranium Tris(Imido) Complexes: Synthesis, Characterization, and Reduction Chemistry of [U(NDIPP)3(Thf)3]. *Angew. Chemie - Int. Ed.* **2015**, 54 (32), 9386–9389.
- 8 Anderson, N. H.; Xie, J.; Ray, D.; Zeller, M.; Gagliardi, L.; Bart, S. C. Elucidating Bonding Preferences in Tetrakis(Imido)Uranate(VI) Dianions. *Nat. Chem.* **2017**, 9 (9), 850–855.
- 9 Arney, D. S. J.; Burns, C. J.; Smith, D. C. Synthesis and Structure of the First Uranium(VI) Organometallic Complex. *J. Am. Chem. Soc.* **1992**, 114 (25), 10068–10069.
- 10 Anderson, N. H. Controlling Electronics for the Formation of High Valent Uranium Imido Complexes, Purdue University, West Lafayette, IN, 2016.
- 11 Nugent, W. A. Synthesis of Some D0 Organoimido Complexes of the Early Transition Metals. *Inorg. Chem.* **1983**, 22 (6), 965–969.
- 12 Nugent, W. A.; Harlow, R. L. Some Bis(Tert-Butylimido) Complexes of the Group 6 Transition Metals and a Related Alkylamido Derivative. *Inorg. Chem.* **1980**, 19 (3), 777–779.
- 13 Pangborn, A. B.; Giardello, M. A.; Grubbs, R. H.; Rosen, R. K.; Timmers, F. J. Safe and Convenient Procedure for Solvent Purification. *Organometallics* **1996**, 15 (5), 1518–1520.

- 14 Chakraborty, S., Chattopadhyay, J., Guo, W. & Billups, W. E. Functionalization of Potassium Graphite. *Angew. Chemie Int. Ed.* **2007**, *46*, 4486–4488.
- 15 Barral, K., Moorhouse, A. D. & Moses, J. E. Efficient Conversion of Aromatic Amines into Azides: A One-Pot Synthesis of Triazole Linkages. *Org. Lett.* **2007**, *9*, 1809–1811.

## APPENDIX A: ADDITIONAL MATERIALS FOR ELUCIDATION OF BOND ELONGATION IN A URANIUM(IV)-*CIS*-BIS(IMIDO) COMPLEX

**PES-CASSCF.** The minimum of the PES was determined around 120 degrees regardless the level of theory employed in the calculation. Despite the minimal active space, CAS(2,7), significant deviations should not be expected in the low energy region after expanding it. According to the CASSCF natural orbital composition, as the angle is opened, an increase of the ligand contribution is observed. That is, the amount of metal  $5f$  - ligand mixing is favored. This observation is well-correlated with the splitting of the ground state obtained at CASSCF level which is retained in subsequent CASSCF-PT2 and SO-PT2 calculations. Looking for the factors responsible for the increase in the splitting, the symmetry imposed by the ligand field seems to dominate. When the angle is smaller, most of the  $5f$  orbitals are hardly able to form symmetry adapted interactions with imido  $2p$  orbitals, therefore reducing the ligand contribution. The opposite occurs when approaching the *trans*-position of the imido ligands, where the  $5f_{\sigma}$  interactions become more favorable enhancing the metal-ligand interaction. Consequently, the interacting  $5f$  orbitals separate from the non-interacting ones, which is mirrored in the increased  $5f$ -orbital splitting. This is also reflected in the splitting of the spin-free states belonging to the ground multiplet ( $^3H$ ) that is afterwards reduced by inclusion of the SOC. Thus, it is important to point out the importance of the interplay between electron repulsion, ligand field, and spin-orbit coupling in the proper description of the electronic structure of actinide compounds.

**U(IV)-NTSA bonds.** The interaction between U(IV) and NTSA ligands is weaker than the interaction with the bis(imido) ligands, however, covalency is not negligible. The  $\sigma$ -bonds are highly polarized (4% U(IV)) with greater contribution of U(IV)  $6d$  orbitals over the  $5f$  contribution. On the other hand,  $\pi$ -bonds have more  $5f$  involvement than the  $\sigma$ -bonds, thus the hybrid is more balanced in terms of  $5f$  and  $6d$  contributions (50/50) which is expected for this type of bonds. A similar perspective is obtained by QTAIM, where polarization is increased by more than 10% with respect to U(IV)-N<sub>imido</sub> (a) and concentration of the electron density is significantly decreased. From the ETS-NOCV perspective, the interaction with NTSA ligands is mainly described by  $\Delta\rho_8$  and  $\Delta\rho_9$ , whose stabilization energies are rather small compared to the rest of the deformation densities.



**Energy decomposition Analysis.** The energy of interaction between U(IV) and the ligands in **M1** was decomposed into steric (electrostatic + Pauli) and orbital terms. The results show that the main contribution to the total energy of interaction is the electrostatic component (76%), while orbital (covalent/charge transfer) interactions correspond to 45%. This means that covalent interactions play an important role in the nature of the chemical bond. The deformation densities ( $\Delta\rho_i$ ) associated with the bond formation are depicted in Figure 4A, where  $\sigma$ - and  $\pi$ -interactions can be distinguished. According to their associated energies,  $\pi$ -bond formation provides most of the stability of the complex with  $\Delta\rho_1$  ( $\Delta E_1 = -763.8$  kJ/mol) being the most important. Under this framework, it is also possible to see differences between the two U–N<sub>imido</sub> bonds depicted in  $\Delta\rho_5$  and  $\Delta\rho_6$ , the former being  $\sim 30$  kJ/mol more stable than the latter. Although, this picture seems to be clear, the lack of correlation makes this approach more qualitative than quantitative.

### QTAIM and electron correlation

**M2.** It is well-known that DFT includes a certain amount of dynamic correlation and that topologies of KS-DFT densities usually overestimate QTAIM metrics because of inherent self-interaction error.<sup>5</sup> As it can be seen in Supplementary Table5, PBE0 densities indeed overestimate QTAIM metrics that are decreased when derived from a minimum CAS (two electrons in seven orbitals) wavefunction. This decrease occurs due to electron repulsion in the covalent region, where electron correlation allows the electron density to ‘move out’ of the interatomic region toward the atomic basins, while the opposite is true for ionic bonds.<sup>6</sup> Furthermore, the addition of one of the imido lone pairs to the active space is essential to recover static correlation with the ligands because of significant orbital mixing. This is interesting because it is commonly accepted for low-valent actinide complexes that minimal active spaces suffice to properly describe the electron density of the system.

**U(VI)(NPh)<sub>2</sub>Cl<sub>2</sub>THF<sub>2</sub>.** Overall, and as expected, U(VI)–N<sub>imido</sub> bonds are more covalent than the other interactions of U(VI). This can be seen in the higher concentration of electron density in the interatomic regions and delocalization indices. From the energy density perspective, the total energy densities are impressively large when compared to the rest of the bonds (Supplementary Table6). The *trans* position displayed by the imido ligands allows comparisons to uranyl derivatives; however, the delocalization indices (electrons shared) describing the interaction between uranium(VI) and O<sub>yl</sub> atoms are close to 2 (from a CAS(12,12) wavefunction),<sup>7</sup> while for N<sub>imido</sub> they are described as 1. This difference may stem from the fact that the phenyl ring in NPh<sup>2-</sup> allows for strong delocalization of the density localized in the N atom. In either case, the interaction is not described by a formal triple bond as indicated in the Lewis depiction of the chemical bond. It is remarkable that DFT supports this interaction as a double bond, which is corrected by static correlation (CASSCF) to a single bond in terms of pairs of electrons shared (Supplementary Table 6). This striking difference is also seen in the ellipticity of the bond, where DFT predicts  $\varepsilon(r)$  close to zero, indicative of a purely cylindrical bond, while CASSCF suggests otherwise. It is interesting that values deviating from zero imply double bonds. In this case, the strong delocalization yields non-cylindrical bonds with the strength of a single bond. From another perspective, the covalent character of the bonds between U(VI)–N<sub>imido</sub> obtained from the  $|V|/G$  ratio predicts 48% of

covalent character (partial covalent bond) in contrast to the 33% and 25% predicted for the U(IV)–N<sub>imido</sub> bonds (Table 5A). This supports the idea that the covalent character is decreased in the tetravalent bis(imido) complex with respect to the hexavalent analog.

**Ligand Field DFT.** A final approach that provides a global description of covalency as described by Lever<sup>8</sup> within the ligand-field theory, is the reduction of the interelectronic repulsion parameters of Slater-Condon  $F^k(5f, 5f)$  ( $k = 0, 2, 4, 6$ ) and the effective spin-orbit coupling parameter  $\zeta_{so}(5f)$  to assess covalent interactions taking place within the 5*f* shell. The coordination of imido and NTSA ligands induces an expansion of the 5*f*-electron cloud such that the electron repulsion is decreased to ~ 60% and the effective spin-orbit coupling to ~ 41% (Table 7A), which is certainly unexpected for an actinide compound.<sup>9</sup> This confirms the unusual effects of imido coordination to the 5*f*-shell of U(IV).

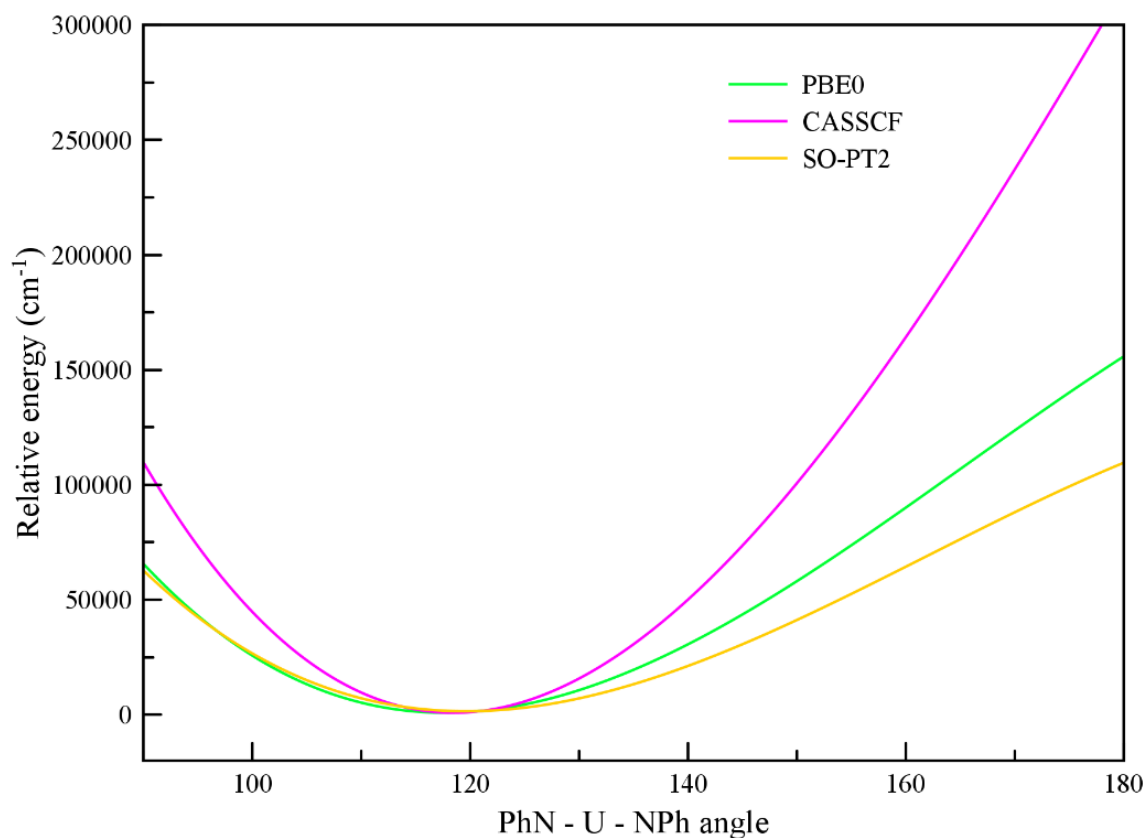


Figure 1A: Potential energy surface resulting of varying the N<sub>imido</sub>-U<sup>IV</sup>-N<sub>imido</sub> angle.

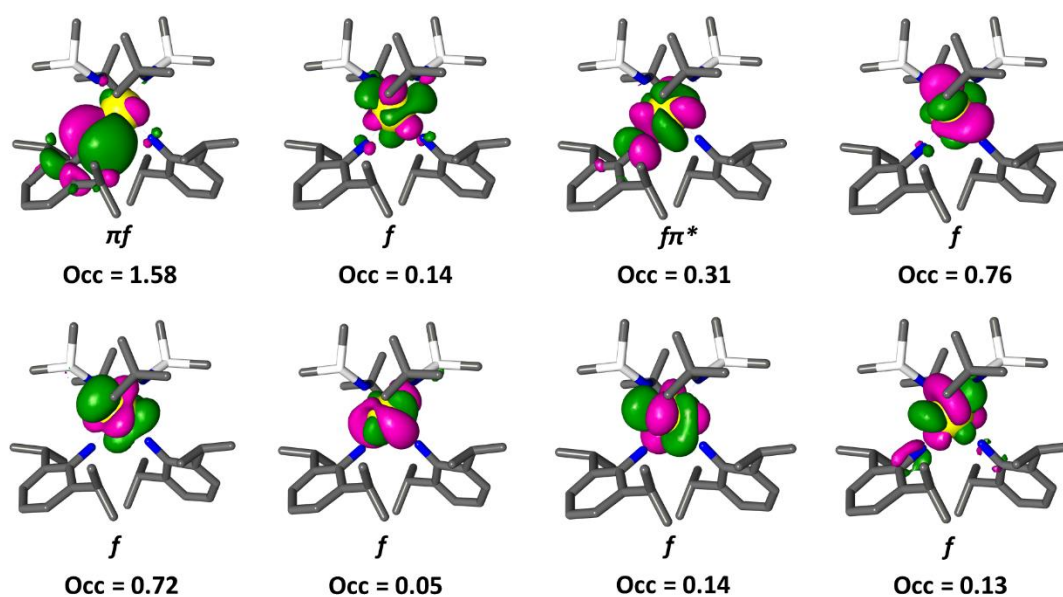


Figure 2A: CASSCF Natural Orbitals of M2 system. The occupation numbers correspond to the ground state configuration.

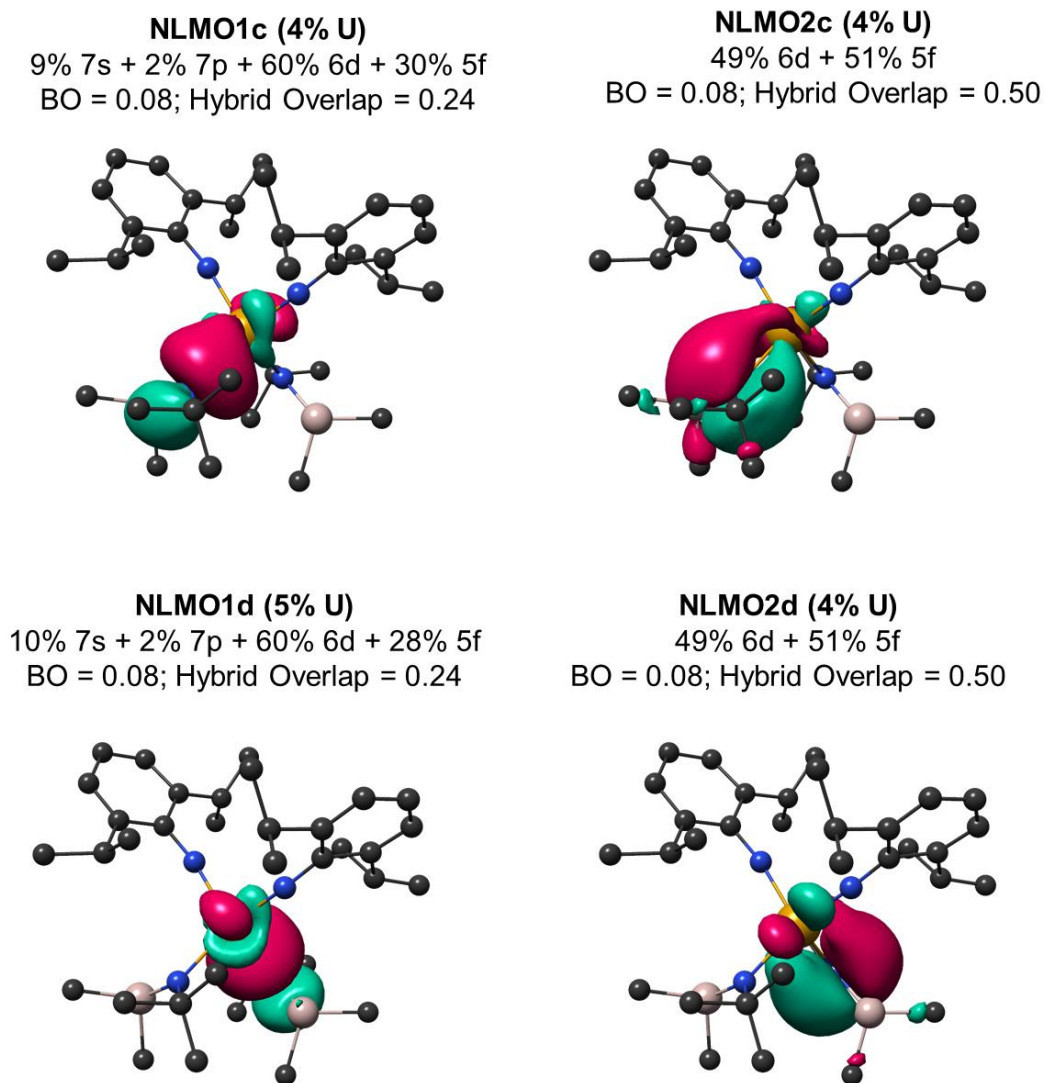


Figure 3A: Natural localized molecular orbitals (NLMOs) describing bonding interactions between U(IV) and one of the NTSA ligands. U(IV) contribution to the NLMO and its composition are given. NLMO-based bond orders (BO), and their corresponding hybrid overlap are also given.

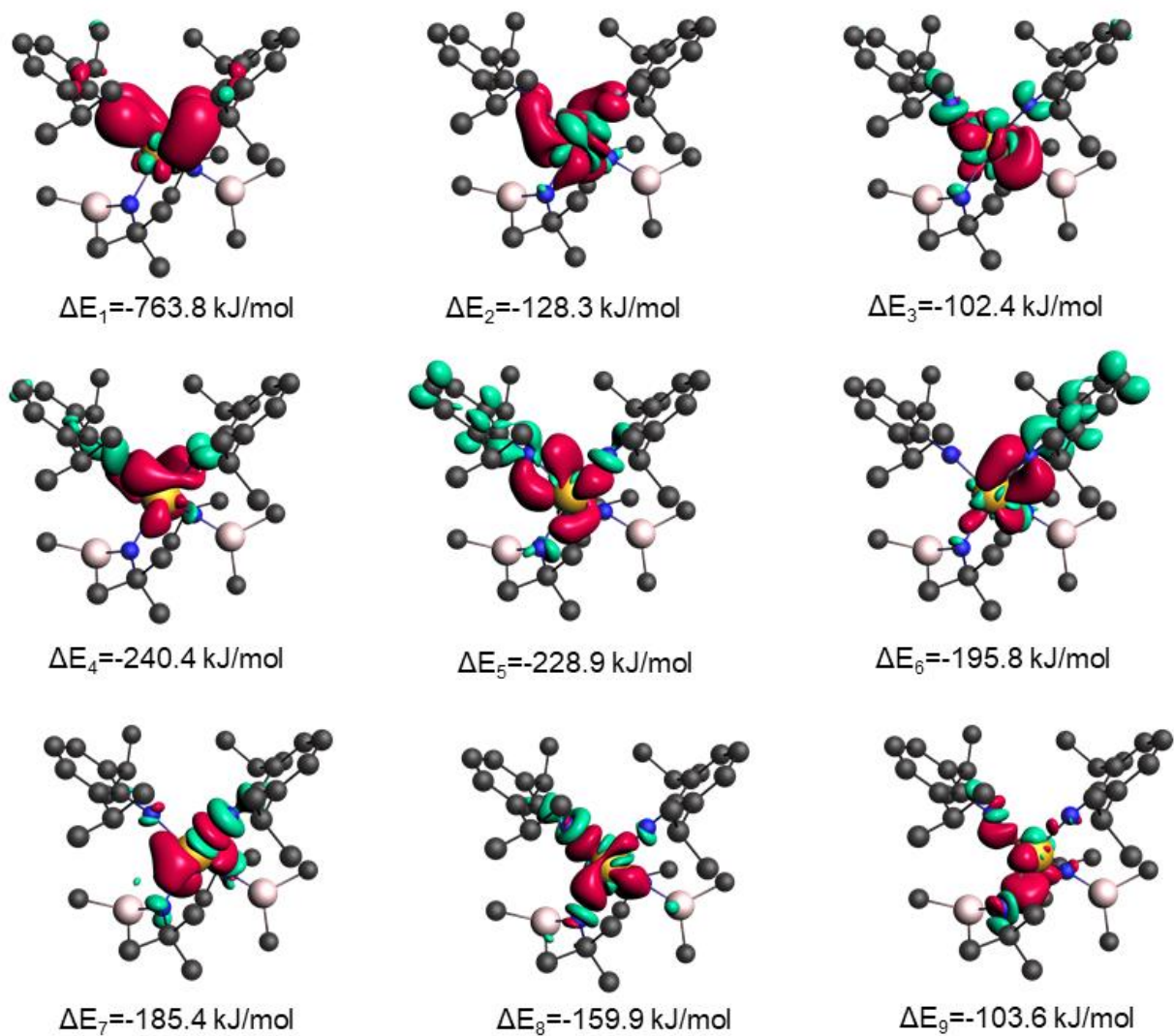


Figure 4A: Deformation densities ( $\Delta\rho_i$ ) and their corresponding energies of stabilization ( $\Delta E_i$ ) from the ETS-NOCV analysis performed under the KS-DFT formalism. The selected  $\Delta\rho_i$  cover 40% of the total orbital interaction energy. Inflow and outflow densities are depicted in red and green surfaces, respectively.

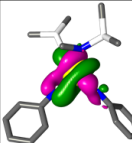
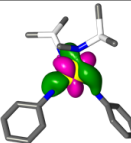
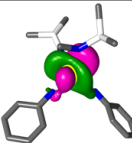
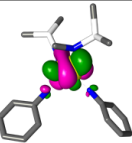
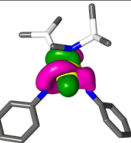
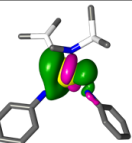
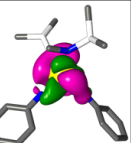
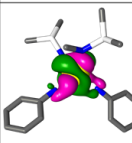
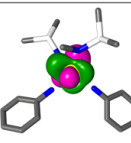
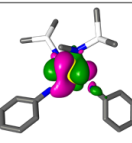
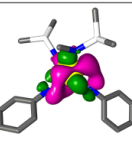
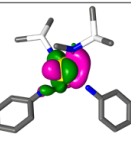
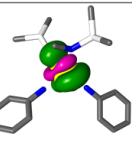
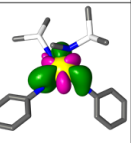
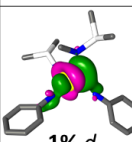
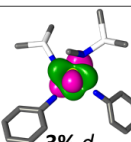
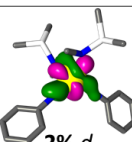
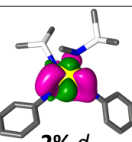
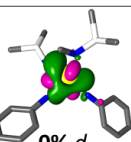
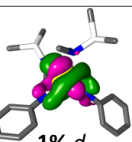
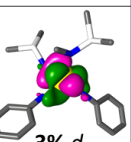

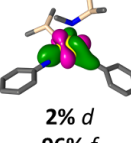
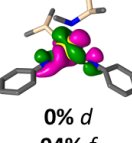
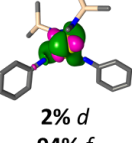
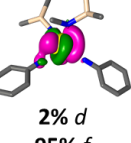
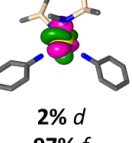
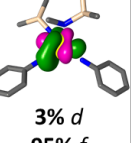
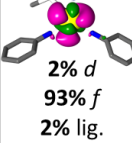
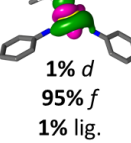
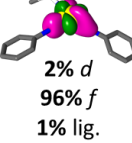
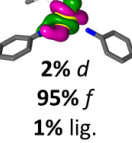
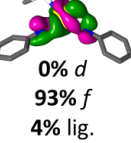
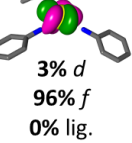
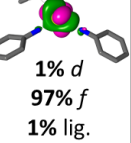
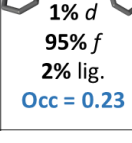
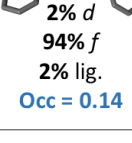
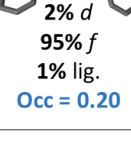
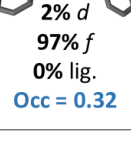
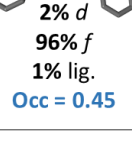
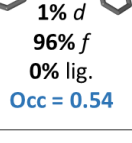
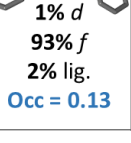
ANGLE	NATURAL CASSCF ORBITALS						
95	 2% <i>d</i> 94% <i>f</i> 3% lig. Occ = 0.05	 1% <i>d</i> 97% <i>f</i> 0% lig. Occ = 0.11	 5% <i>d</i> 94% <i>f</i> 1% lig. Occ = 0.37	 1% <i>d</i> 96% <i>f</i> 1% lig. Occ = 0.51	 4% <i>d</i> 95% <i>f</i> 0% lig. Occ = 0.64	 2% <i>d</i> 92% <i>f</i> 2% lig. Occ = 0.23	 2% <i>d</i> 94% <i>f</i> 1% lig. Occ = 0.09
105	 1% <i>d</i> 97% <i>f</i> 1% lig. Occ = 0.21	 3% <i>d</i> 96% <i>f</i> 0% lig. Occ = 0.69	 2% <i>d</i> 95% <i>f</i> 1% lig. Occ = 0.33	 2% <i>d</i> 93% <i>f</i> 3% lig. Occ = 0.06	 3% <i>d</i> 95% <i>f</i> 1% lig. Occ = 0.12	 1% <i>d</i> 94% <i>f</i> 1% lig. Occ = 0.28	 2% <i>d</i> 94% <i>f</i> 2% lig. Occ = 0.29
110	 1% <i>d</i> 95% <i>f</i> 2% lig. Occ = 0.28	 3% <i>d</i> 96% <i>f</i> 0% lig. Occ = 0.65	 2% <i>d</i> 97% <i>f</i> 1% lig. Occ = 0.36	 2% <i>d</i> 94% <i>f</i> 2% lig. Occ = 0.11	 0% <i>d</i> 93% <i>f</i> 1% lig. Occ = 0.15	 1% <i>d</i> 94% <i>f</i> 2% lig. Occ = 0.13	 3% <i>d</i> 95% <i>f</i> 1% lig. Occ = 0.31
115	 0% <i>d</i> 96% <i>f</i> 1% lig. Occ = 0.39	 2% <i>d</i> 96% <i>f</i> 1% lig. Occ = 0.25	 0% <i>d</i> 94% <i>f</i> 3% lig. Occ = 0.09	 2% <i>d</i> 94% <i>f</i> 2% lig. Occ = 0.30	 2% <i>d</i> 95% <i>f</i> 1% lig. Occ = 0.31	 2% <i>d</i> 97% <i>f</i> 0% lig. Occ = 0.44	 3% <i>d</i> 95% <i>f</i> 1% lig. Occ = 0.51
120	 2% <i>d</i> 93% <i>f</i> 2% lig. Occ = 0.10	 1% <i>d</i> 95% <i>f</i> 1% lig. Occ = 0.28	 2% <i>d</i> 96% <i>f</i> 1% lig. Occ = 0.34	 2% <i>d</i> 95% <i>f</i> 1% lig. Occ = 0.22	 0% <i>d</i> 93% <i>f</i> 4% lig. Occ = 0.02	 3% <i>d</i> 96% <i>f</i> 0% lig. Occ = 0.64	 1% <i>d</i> 97% <i>f</i> 1% lig. Occ = 0.37
125	 1% <i>d</i> 95% <i>f</i> 2% lig. Occ = 0.23	 2% <i>d</i> 94% <i>f</i> 2% lig. Occ = 0.14	 2% <i>d</i> 95% <i>f</i> 1% lig. Occ = 0.20	 2% <i>d</i> 97% <i>f</i> 0% lig. Occ = 0.32	 2% <i>d</i> 96% <i>f</i> 1% lig. Occ = 0.45	 1% <i>d</i> 96% <i>f</i> 0% lig. Occ = 0.54	 1% <i>d</i> 93% <i>f</i> 2% lig. Occ = 0.13

Figure 5A: Natural CASSCF orbitals for every single system calculated to build the PES. Occupation numbers correspond to the ground state.



Figure 5A continued

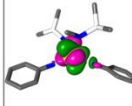

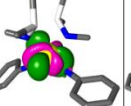
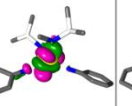
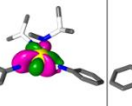
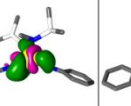
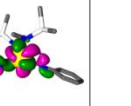

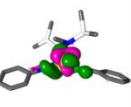
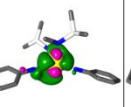
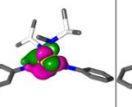
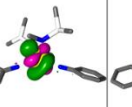
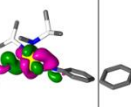
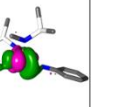


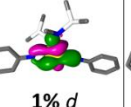
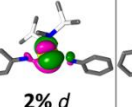
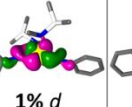
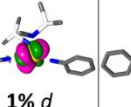
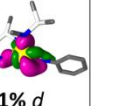

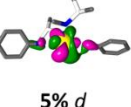

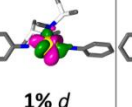
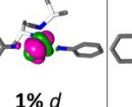
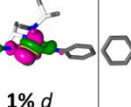
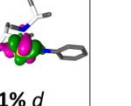
135	 1% <i>d</i> 96% <i>f</i> 1% lig. Occ = 0.36	 3% <i>d</i> 95% <i>f</i> 1% lig. Occ = 0.34	 2% <i>d</i> 96% <i>f</i> 1% lig. Occ = 0.52	 1% <i>d</i> 96% <i>f</i> 1% lig. Occ = 0.27	 2% <i>d</i> 96% <i>f</i> 1% lig. Occ = 0.26	 1% <i>d</i> 92% <i>f</i> 2% lig. Occ = 0.14	 0% <i>d</i> 93% <i>f</i> 3% lig. Occ = 0.11
145	 2% <i>d</i> 93% <i>f</i> 1% lig. Occ = 0.39	 2% <i>d</i> 93% <i>f</i> 2% lig. Occ = 0.03	 1% <i>d</i> 93% <i>f</i> 2% lig. Occ = 0.20	 1% <i>d</i> 97% <i>f</i> 1% lig. Occ = 0.49	 1% <i>d</i> 97% <i>f</i> 0% lig. Occ = 0.43	 1% <i>d</i> 92% <i>f</i> 4% lig. Occ = 0.08	 2% <i>d</i> 96% <i>f</i> 1% lig. Occ = 0.37
155	 2% <i>d</i> 94% <i>f</i> 3% lig. Occ = 0.06	 2% <i>d</i> 97% <i>f</i> 0% lig. Occ = 0.42	 1% <i>d</i> 96% <i>f</i> 1% lig. Occ = 0.32	 2% <i>d</i> 94% <i>f</i> 1% lig. Occ = 0.43	 1% <i>d</i> 90% <i>f</i> 5% lig. Occ = 0.11	 1% <i>d</i> 97% <i>f</i> 1% lig. Occ = 0.46	 1% <i>d</i> 92% <i>f</i> 2% lig. Occ = 0.18
175	 2% <i>d</i> 90% <i>f</i> 5% lig. Occ = 0.07	 5% <i>d</i> 91% <i>f</i> 3% lig. Occ = 0.16	 3% <i>d</i> 91% <i>f</i> 3% lig. Occ = 0.13	 1% <i>d</i> 98% <i>f</i> 1% lig. Occ = 0.46	 1% <i>d</i> 95% <i>f</i> 1% lig. Occ = 0.45	 1% <i>d</i> 95% <i>f</i> 2% lig. Occ = 0.29	 1% <i>d</i> 98% <i>f</i> 1% lig. Occ = 0.43

Table 1A: Comparison of selected experimental and theoretical geometry parameters.

	Exp	M1 <sup>a</sup>	M2 <sup>b</sup>	M3 <sup>c</sup>	M4 <sup>d</sup>
$\text{U}^{\text{IV}} - \text{N}_{\text{imido}}$	2.069(17)	2.133	2.089	2.083	1.942
$\text{U}^{\text{IV}} - \text{N}_{\text{imido}}$	2.149(11)	2.133	2.095	2.090	1.941
$\text{U}^{\text{IV}} - \text{NTSA}$	2.365(12)	2.403	2.471	2.377	–
$\text{U}^{\text{IV}} - \text{NTSA}$	2.365(14)	2.404	2.481	2.388	–
$\text{U}^{\text{IV}} - \text{K}^+$	3.7617(12)	3.7842	–	–	–
$\text{N}_{\text{imido}} - \text{U}^{\text{IV}} - \text{N}_{\text{imido}}$	95.2(3)	93.0	102.8	115.1	118.6

Table 2A: Morokuma-Ziegler energy decomposition analysis of the interaction between  $\text{U}^{\text{IV}}$  and the ligand environment in 1.

Component	eV
Electrostatic	-89.1
Pauli	24.4
Steric	-64.7
Orbital	-53.3
Total	-118.0



Table 3A: QTAIM metrics derived from KS-DFT and SR-CASSCF densities of M2. Electron densities are given in  $|e| \text{ \AA}^{-3}$ , and potential V, kinetic G, and total H energy densities given in  $\text{kJ mol}^{-1} \text{ \AA}^{-3}$ .

Wavefunction	Bond	$\rho(r)$	$\delta(r)$	V(r)	G(r)	H(r)	$ V /G$	$\varepsilon(r)$
PBE0	$N_{\text{imido}} \text{ (a)}$	0.9913	1.2335	-3989.9	2874.0	-1115.9	1.39	0.1137
CAS(2,7)		0.9137	0.9275	-3856.5	2852.9	-1003.6	1.35	0.1701
CAS(4,8)		0.8908	0.8822	-3793.4	2844.2	-949.2	1.33	0.1206
PBE0	$N_{\text{imido}} \text{ (b)}$	0.8388	1.1660	-3140.7	2354.6	-786.0	1.33	0.1688
CAS(2,7)		0.7700	0.8589	-3040.7	2344.1	-696.6	1.30	0.1669
CAS(4,8)		0.7389	0.6316	-3028.4	2431.8	-596.6	1.25	0.0215
PBE0	$N_{\text{NTSA}} \text{ (c)}$	0.5790	0.5979	-1719.5	1333.5	-386.0	1.29	0.1738
CAS(2,7)		0.5351	0.4716	-1721.2	1398.4	-322.8	1.23	0.1651
CAS(4,8)		0.5162	0.4798	-1701.9	1410.7	-291.3	1.21	0.0969
PBE0	$N_{\text{NTSA}} \text{ (d)}$	0.5743	0.6136	-1682.6	1298.4	-384.3	1.30	0.216
CAS(2,7)		0.5318	0.4818	-1691.4	1366.8	-324.6	1.24	0.1955
CAS(4,8)		0.5122	0.4761	-1666.8	1377.3	-289.5	1.21	0.1652

Table 4A: QTAIM metrics derived from KS-DFT and SR-CASSCF densities of U(VI)(NPh)<sub>2</sub>Cl<sub>2</sub>THF<sub>2</sub>. Electron densities are given in |e| Å<sup>-3</sup>, and potential V, kinetic G, and total H energy densities given in kJ mol<sup>-1</sup> Å<sup>-3</sup>.

Wavefunction	Bond	$\rho(r)$	$\delta(r)$	$V(r)$	$G(r)$	$H(r)$	$ V /G$	$\varepsilon(r)$
PBE0	U-N <sub>imido</sub>	1.3851	1.8368	-6352.0	4060.3	-2291.7	-1.56	0.0462
CAS(8,12)		1.2673	1.0043	-6224.0	4207.1	-2016.9	-1.48	0.1933
PBE0	U-N <sub>imido</sub>	1.3849	1.8377	-6364.1	4072.2	-2292.0	-1.56	0.0392
CAS(8,12)		1.2687	0.9996	-6219.5	4197.9	-2021.6	-1.48	0.2179
PBE0	U-Cl	0.4595	0.6955	-1160.3	916.2	-244.1	-1.27	0.0382
CAS(8,12)		0.4249	0.4491	-1216.4	1020.7	-195.7	-1.19	0.0319
PBE0	U-Cl	0.4574	0.6876	-1151.8	910.4	-241.5	-1.27	0.0470
CAS(8,12)		0.4230	0.4447	-1208.5	1015.1	-193.4	-1.19	0.0314
PBE0	U-O <sub>THF</sub>	0.3469	0.2776	-991.2	970.2	-21.0	-1.02	0.1419
CAS(8,12)		0.3328	0.2181	-1037.4	1034.3	-3.1	-1.00	0.1070
PBE0	U-O <sub>THF</sub>	0.3458	0.2750	-984.2	963.5	-20.7	-1.02	0.1484
CAS(8,12)		0.3965	0.2176	-1030.9	1028.6	-2.4	-1.00	0.1199

Table 5A: Slater-Condon  $F^k$  ( $k = 0, 2, 4, 6$ ) and effective spin-orbit coupling  $\zeta_{\text{SO}}$  parameters of the  $5f$  electrons calculated from LF-DFT for the free and complexed  $\text{U}^{\text{IV}}$  ion.

Parameter	$\text{U}^{\text{IV}}_{\text{free-ion}}$	Complex <b>1</b>	Reduction
$F^0(5f, 5f)$	17.4418	6.9874	59.94%
$F^2(5f, 5f)$	8.7422	3.3862	61.27%
$F^4(5f, 5f)$	5.7021	2.1807	61.76%
$F^6(5f, 5f)$	4.1805	1.5902	61.96%
$\zeta_{\text{SO}}(5f)$	0.2477	0.1455	41.26%

Table 6A: Ground state splitting for the ten systems used to build the PES. Results are given in wavenumbers ( $\text{cm}^{-1}$ ).

Angle	CASSCF	SO-CASSCF	SO-PT2
95	2313.1	1673.6	1504.1
105	2359.3	1819.6	1589.8
110	2515.8	2009.7	1671.6
115	2594.3	2072.3	1680.6
120	2801.5	2256.9	1771.8
125	2941.8	2310.6	1826.1
135	3647.5	2939.6	2229.5
145	4283	3480.3	2599.1
155	4948.6	4060.1	2998.4
175	6060.8	5016.5	3832.4

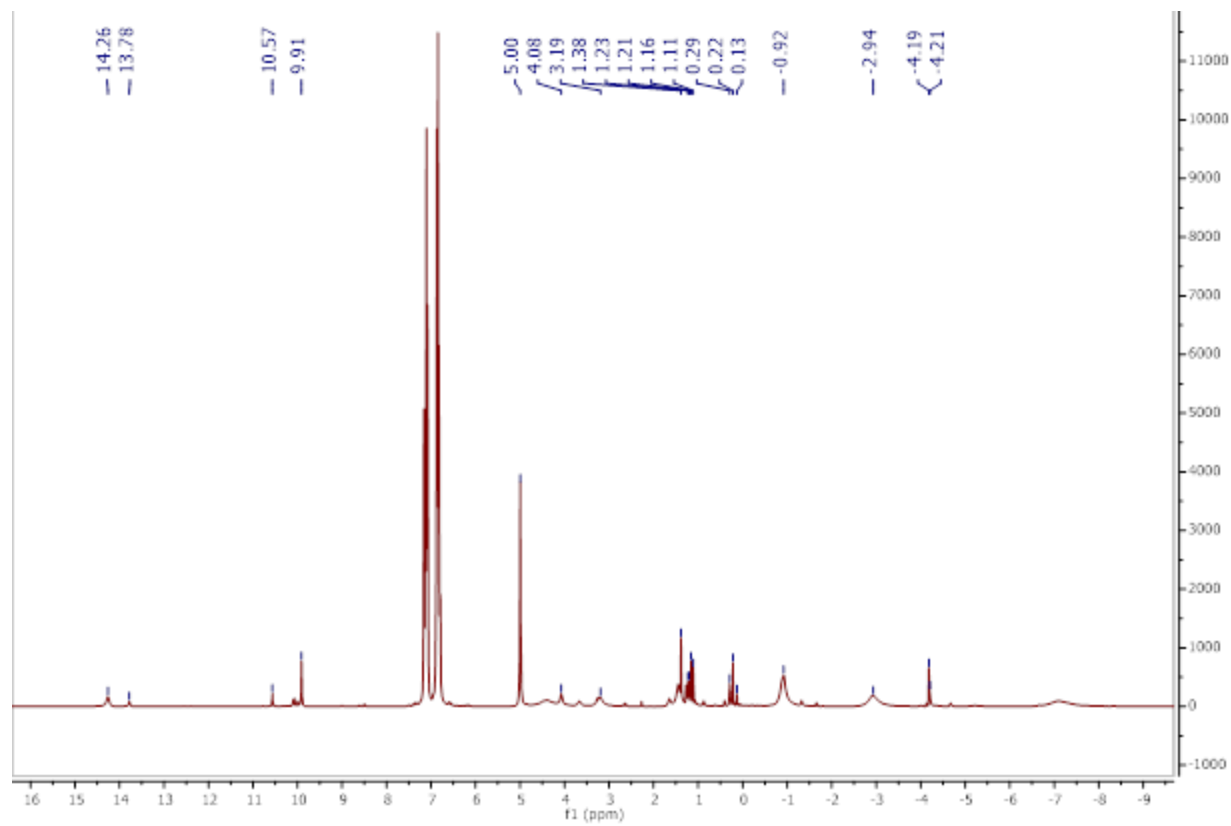


Figure 6A:  $^1\text{H}$  NMR of  $[\text{U}(\text{NDIPP})_2(\text{NPh}_2)_3]\text{K}_2$

## APPENDIX B: ADDITIONAL MATERIALS FOR INVESTIGATING THE STABILITY OF URANYL IMIDO COMPLEXES

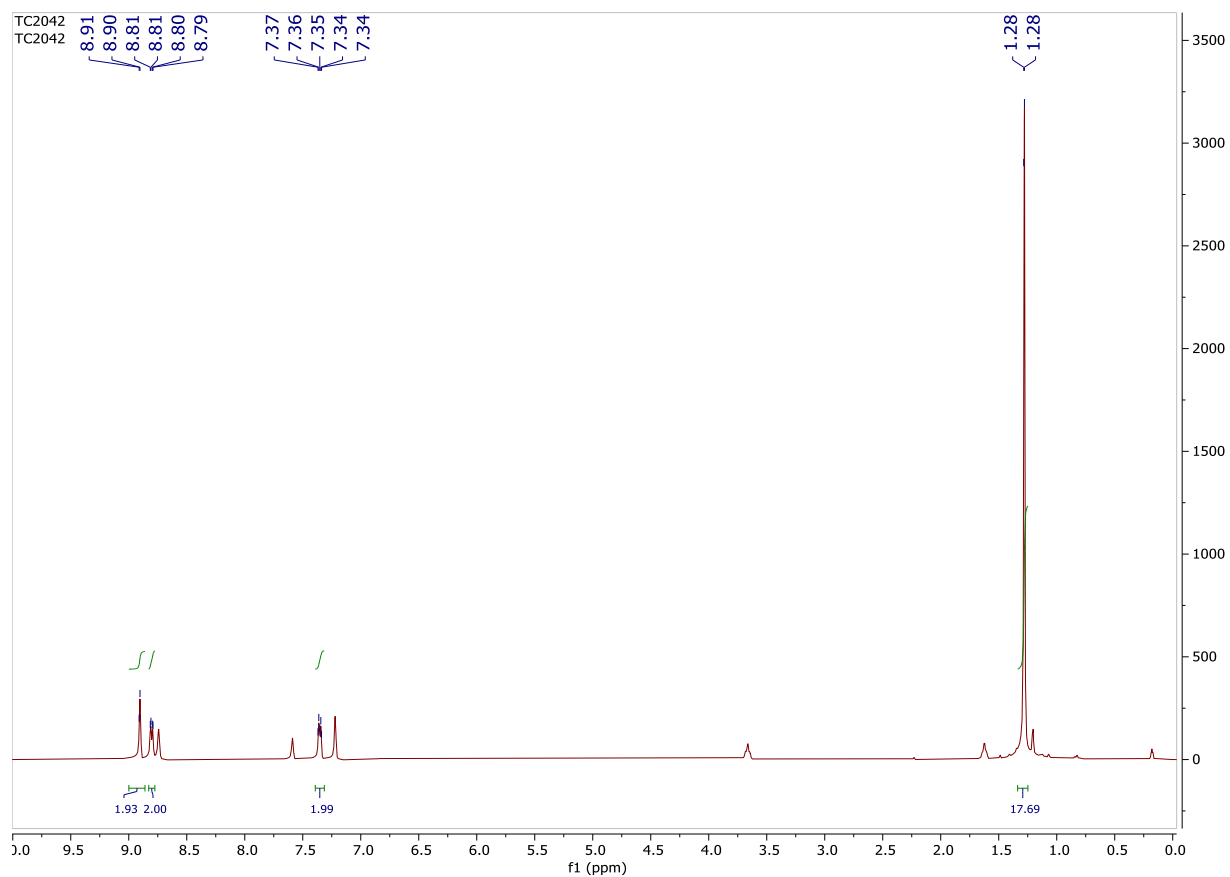


Figure 1B:  $^1\text{H}$  NMR spectrum of  $\text{UO}_2(^1\text{Bubpy})(\text{N}3,5\text{ CF}_3)$ , **4**

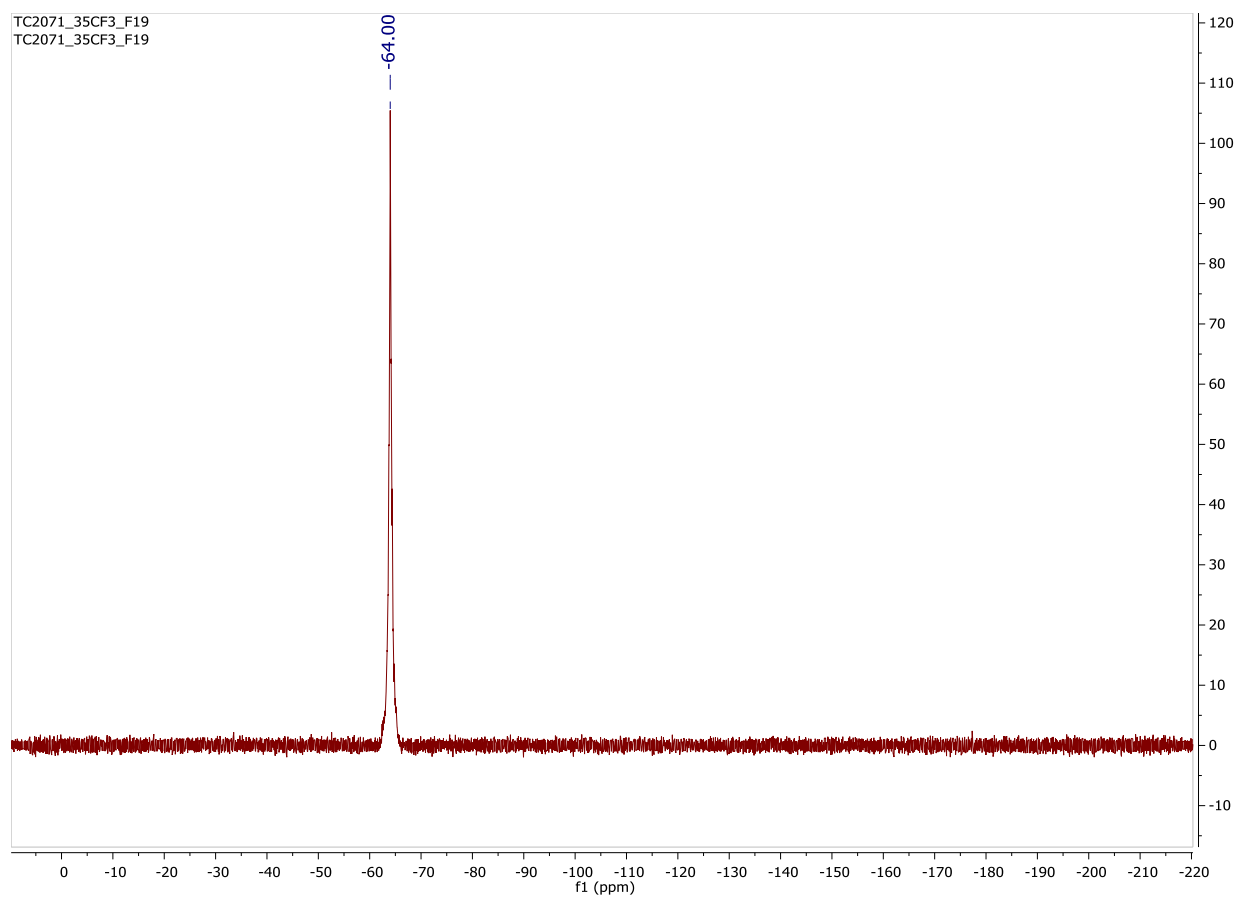


Figure 2B:  $^{19}\text{F}$  NMR spectrum of  $\text{UO}_2(^4\text{Bubpy})(\text{N}3,5\text{ CF}_3)$ , **4**

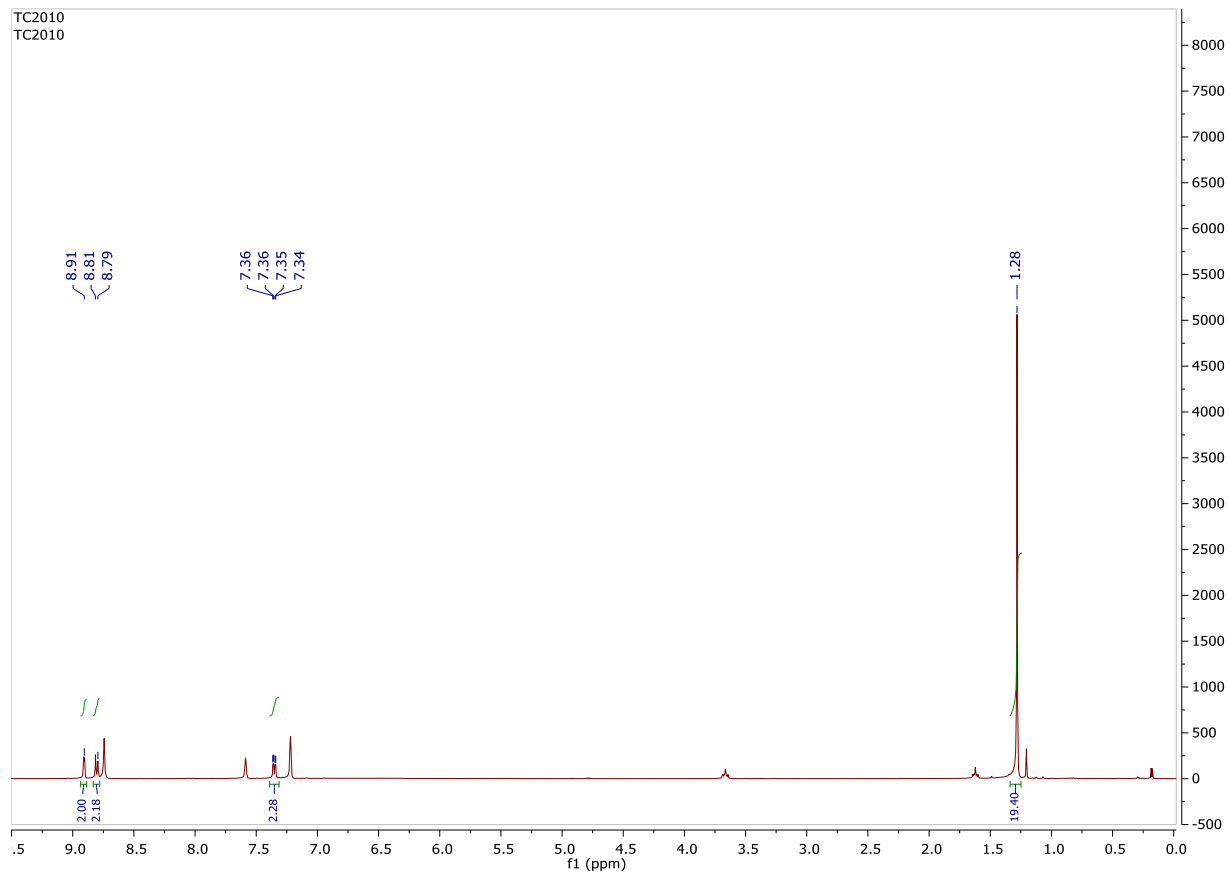


Figure 3B:  $^1\text{H}$  NMR spectrum of  $\text{UO}_2(\text{tBubpy})(\text{Npara-F})$ , **5**

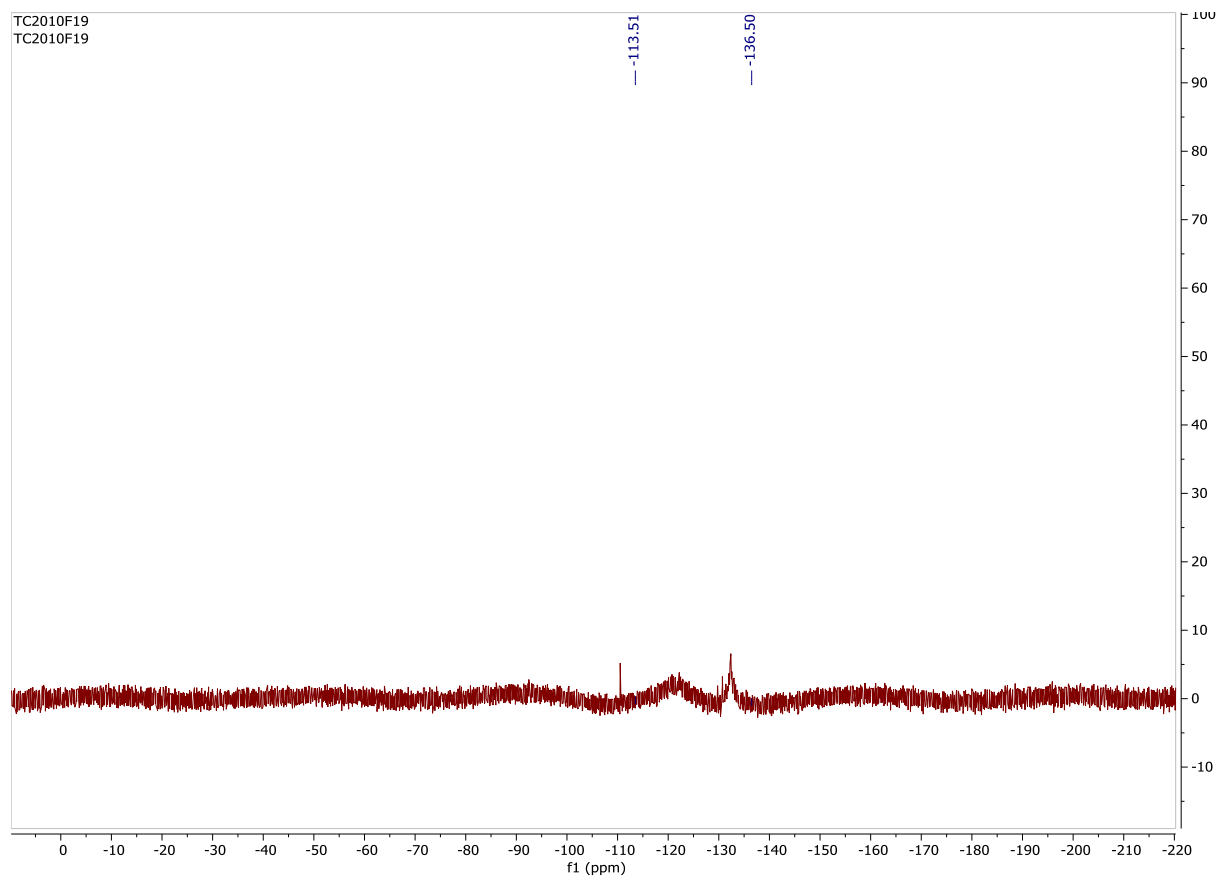


Figure 4B:  $^{19}\text{F}$  NMR spectrum of  $\text{UO}_2(\text{tBubpy})(\text{Npara-F})$ , **5**



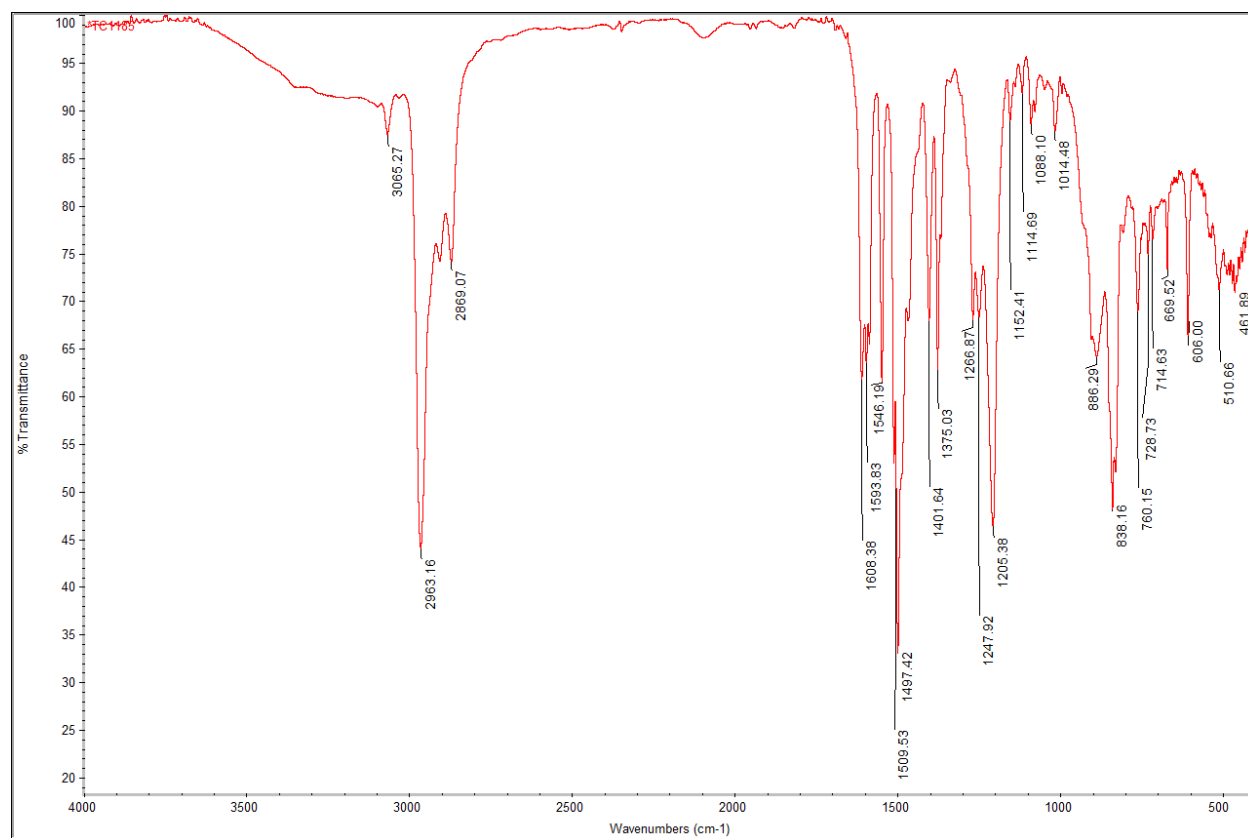


Figure 5B: IR spectrum of  $\text{UO}_2(4\text{Bubpy})(\text{Npara-F})$ , **5**

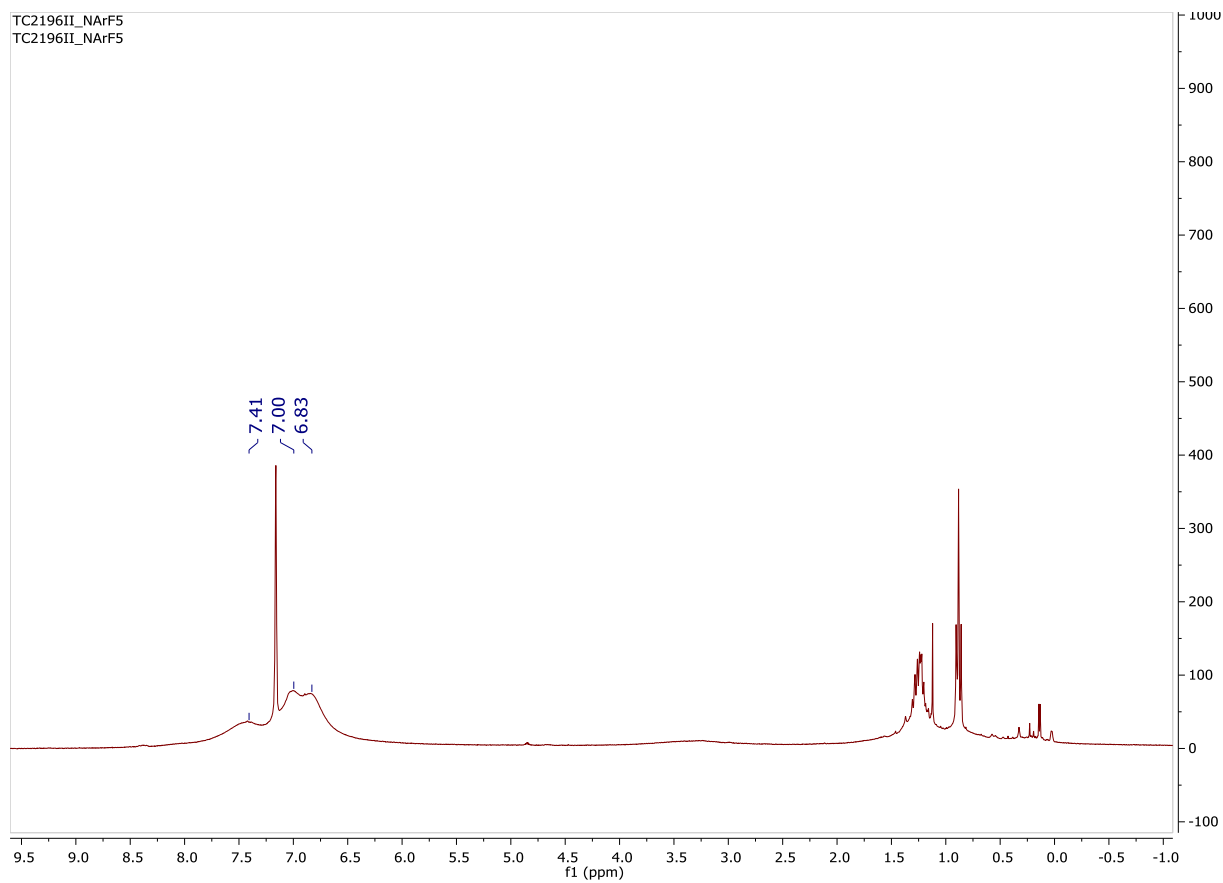


Figure 6B:  $^1\text{H}$  NMR spectrum of  $\text{UO}_2(\text{OPPh}_3)(\text{NArF})_5$ , **3-OPPh<sub>3</sub>**

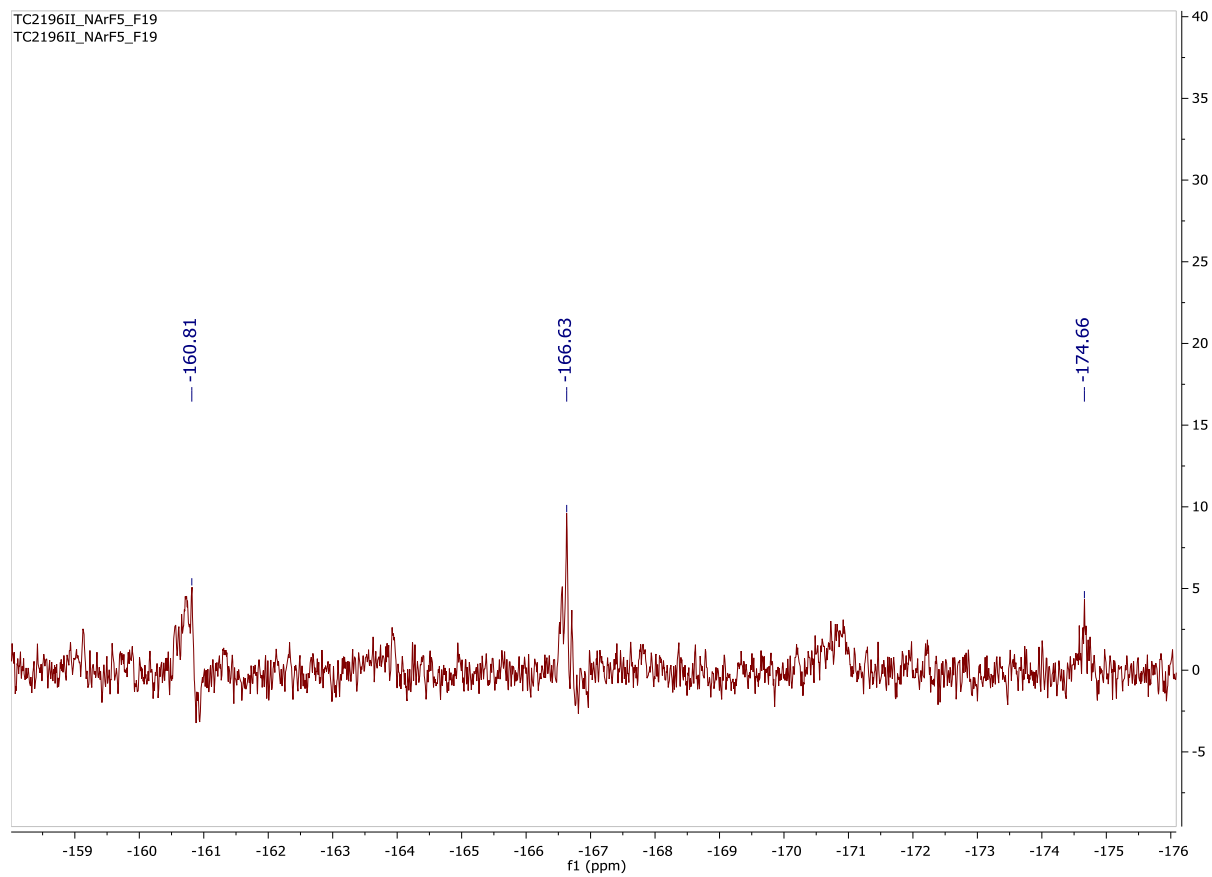


Figure 7B:  $^{19}\text{F}$  NMR spectrum of  $\text{UO}_2(\text{OPPh}_3)(\text{NArF})_5$ , **3-OPPh<sub>3</sub>**

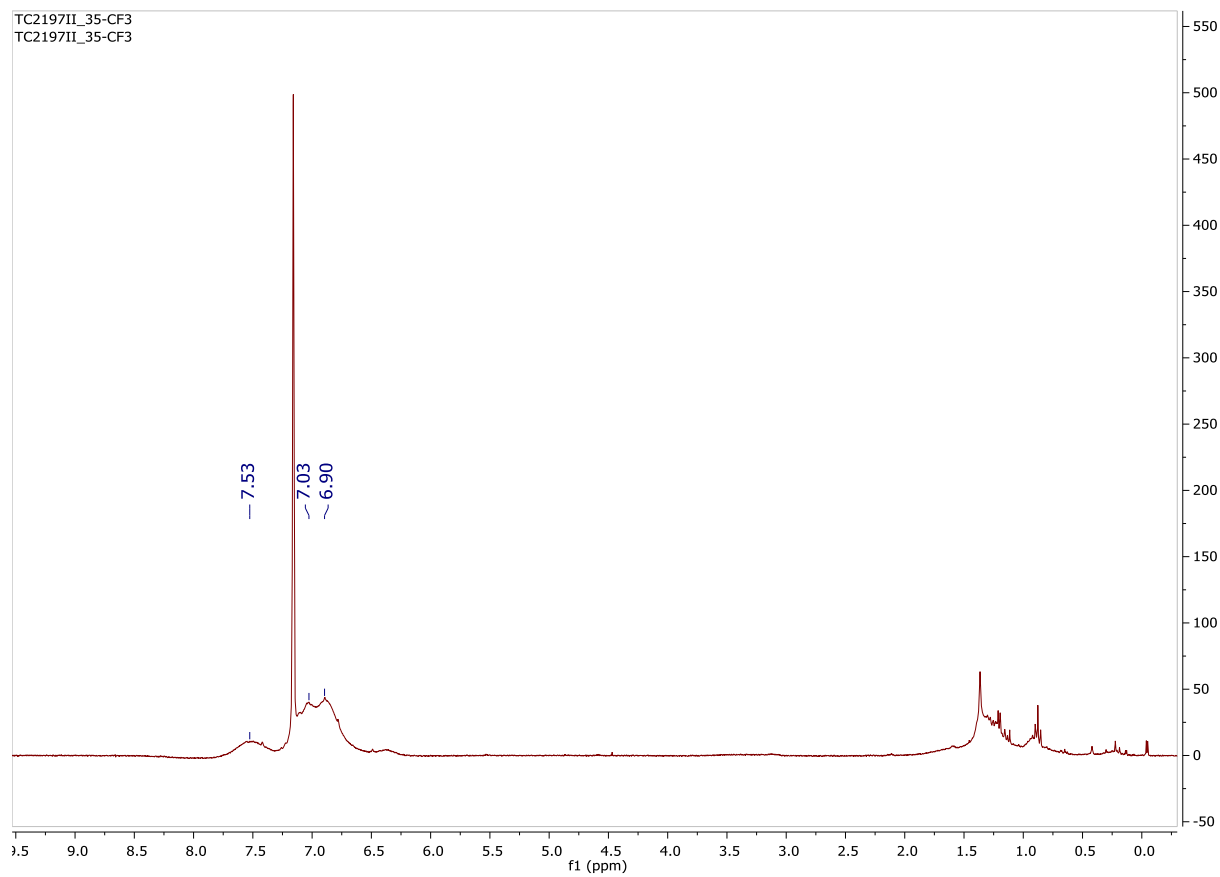


Figure 8B:  $^1\text{H}$  NMR spectrum of  $\text{UO}_2(\text{OPPh}_3)(\text{N}3,5\text{-CF}_3)$ , 4- $\text{OPPh}_3$

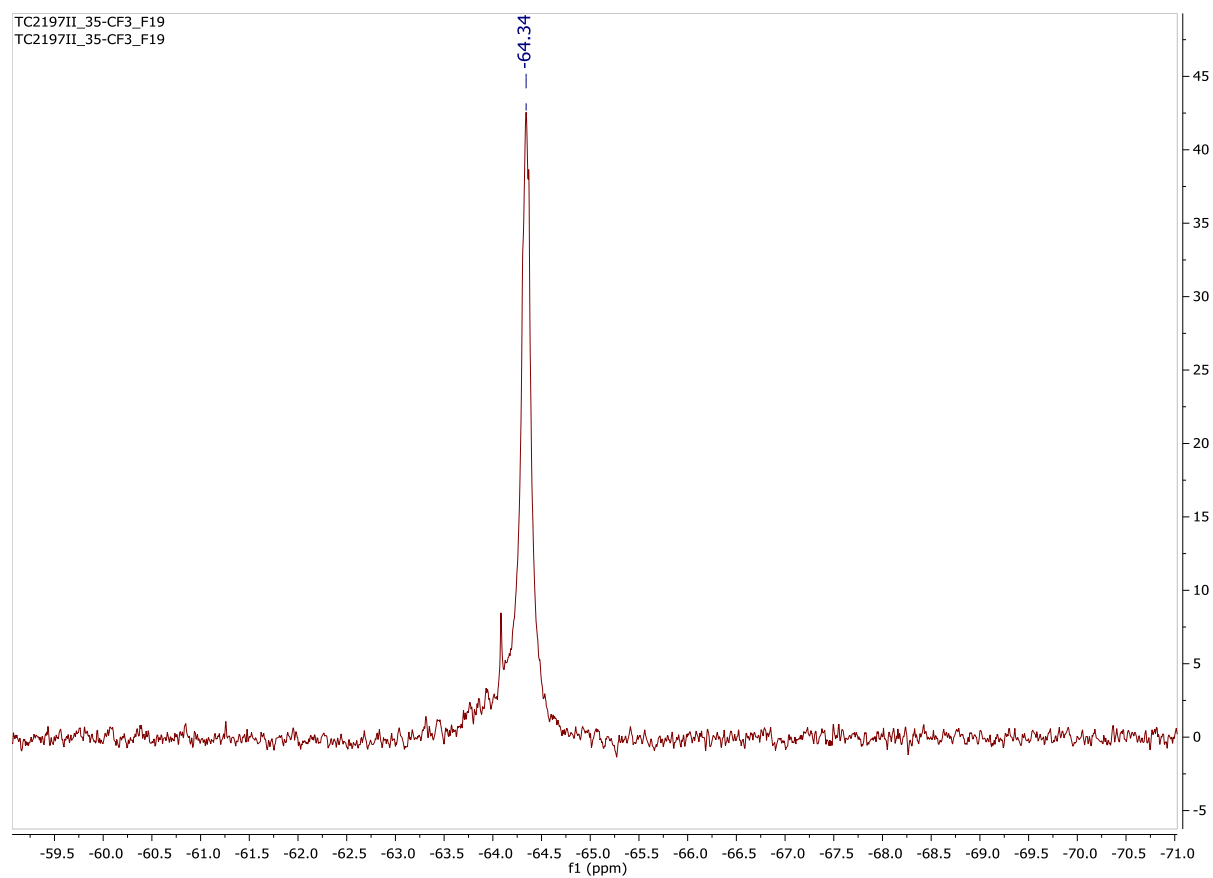


Figure 9B:  $^{19}\text{F}$  NMR spectrum of  $\text{UO}_2(\text{OPPh}_3)(\text{N}3,5\text{-CF}_3)$ , **4-OPPh<sub>3</sub>**

## APPENDIX C: ADDITIONAL MATERIALS FOR SYNTHESIS OF URANIUM(VI) PENTAKIS(IMIDO) COMPLEXES

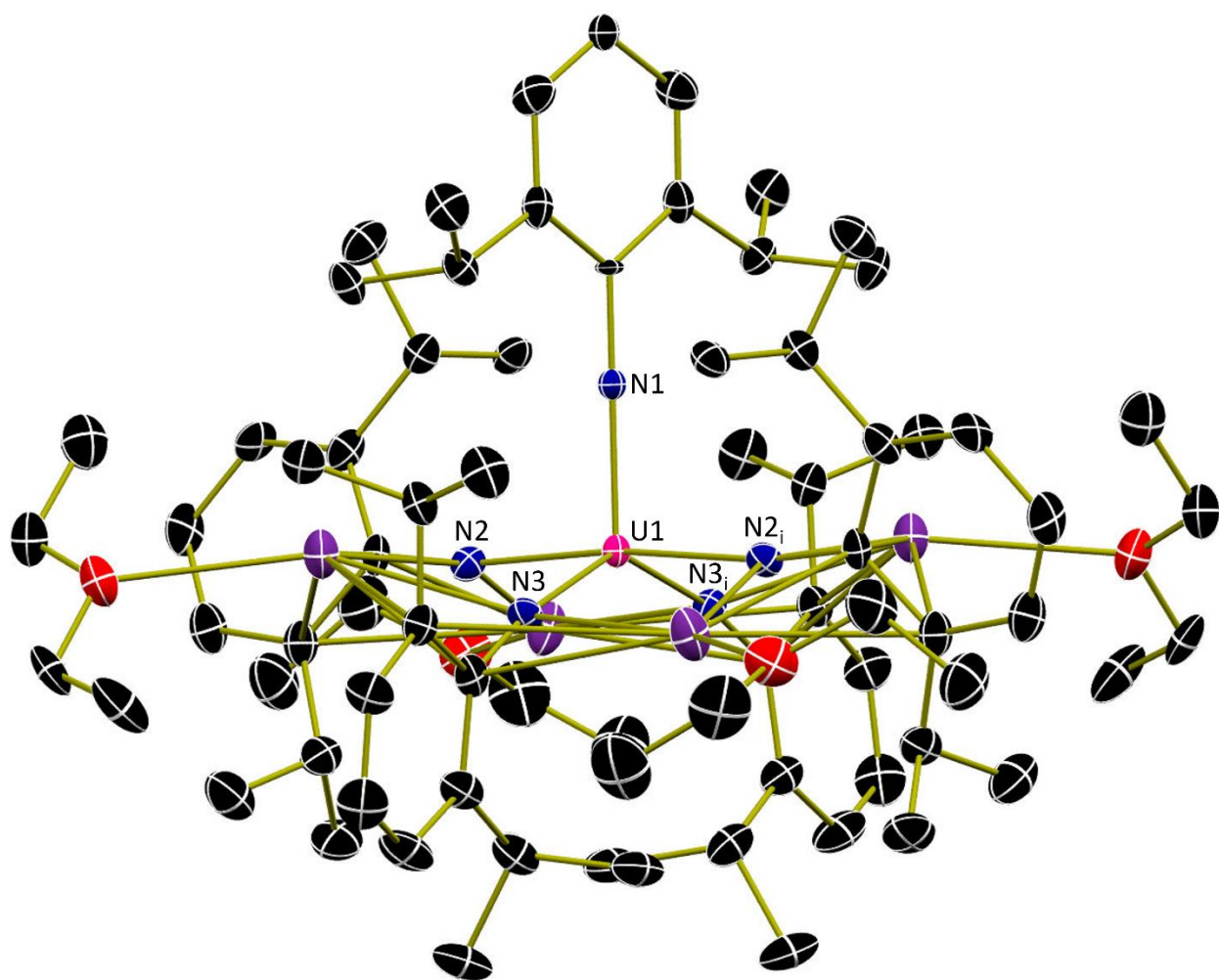


Figure C1: Molecular Structure of **9** shown with 30% probability ellipsoids. Hydrogen atoms have been removed for clarity.

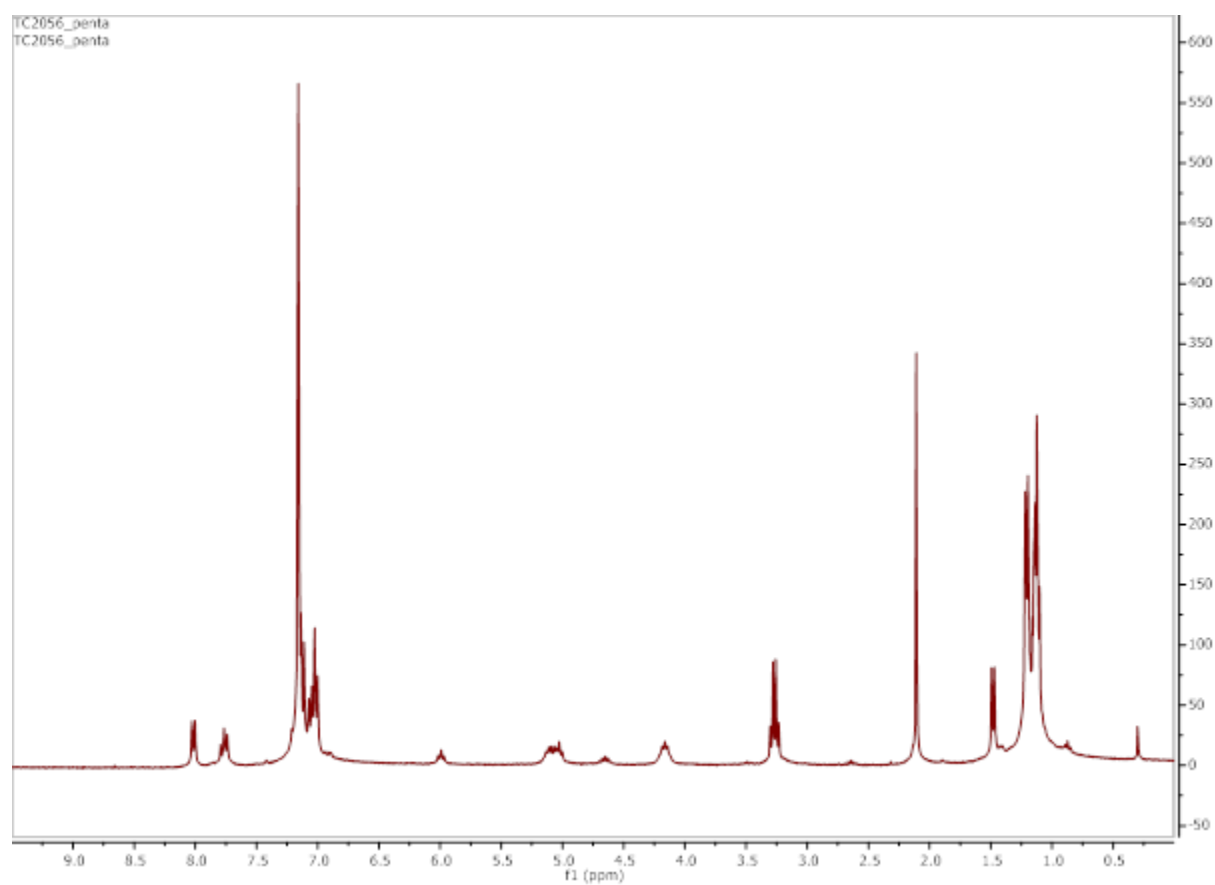


Figure C2:  $^1\text{H}$  NMR spectra of mono(imido) to pentakis(imido) reaction

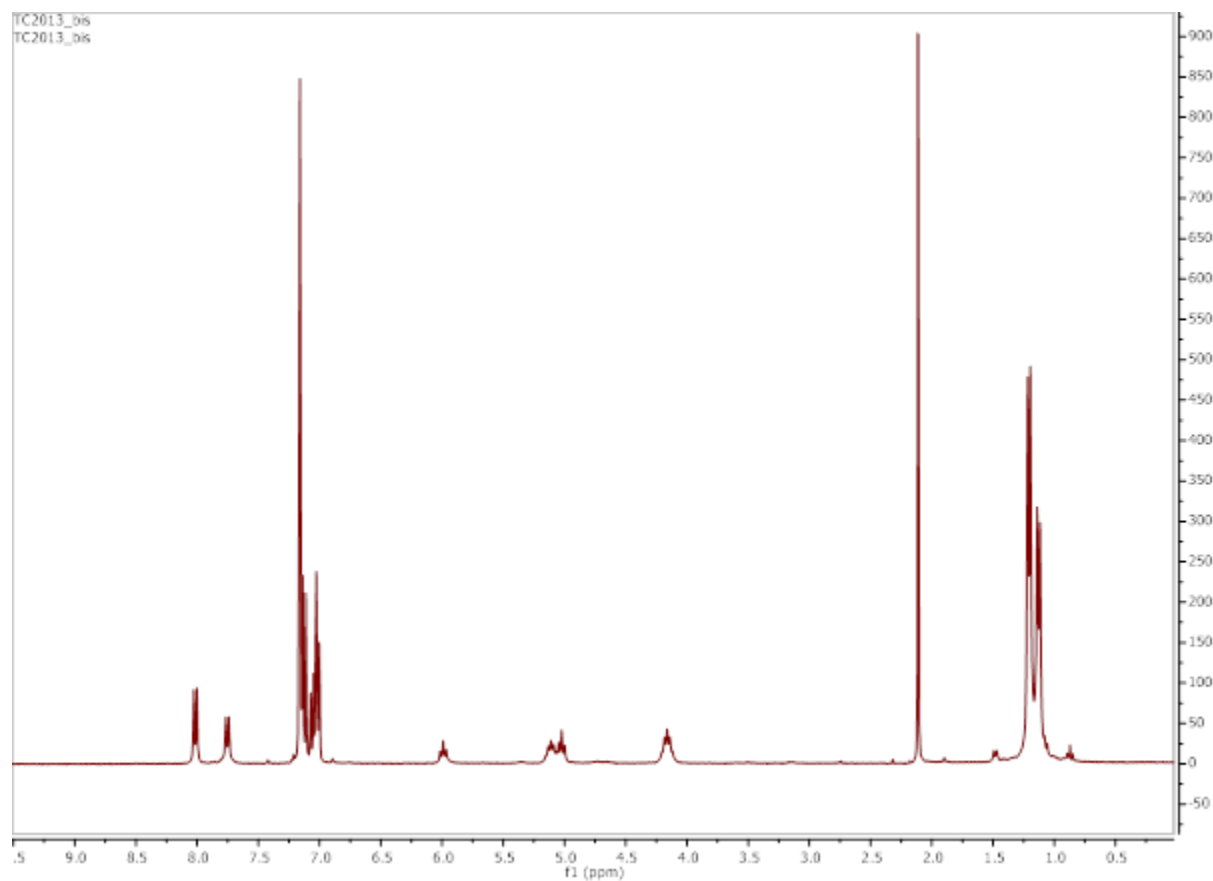


Figure C3:  $^1\text{H}$  NMR spectra of bis(imido) to pentakis(imido) reaction



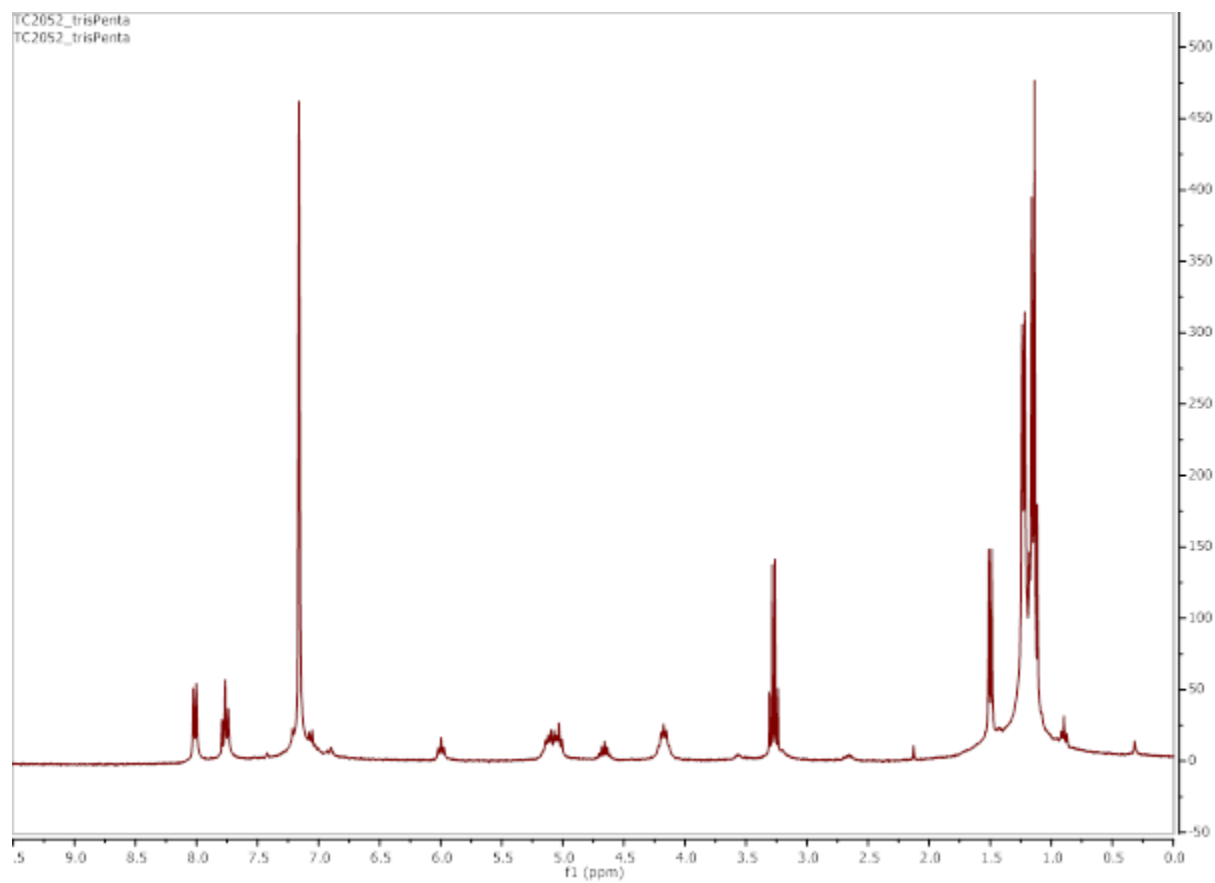


Figure C4:  $^1\text{H}$  NMR spectra of tris(imido) to pentakis(imido) reaction

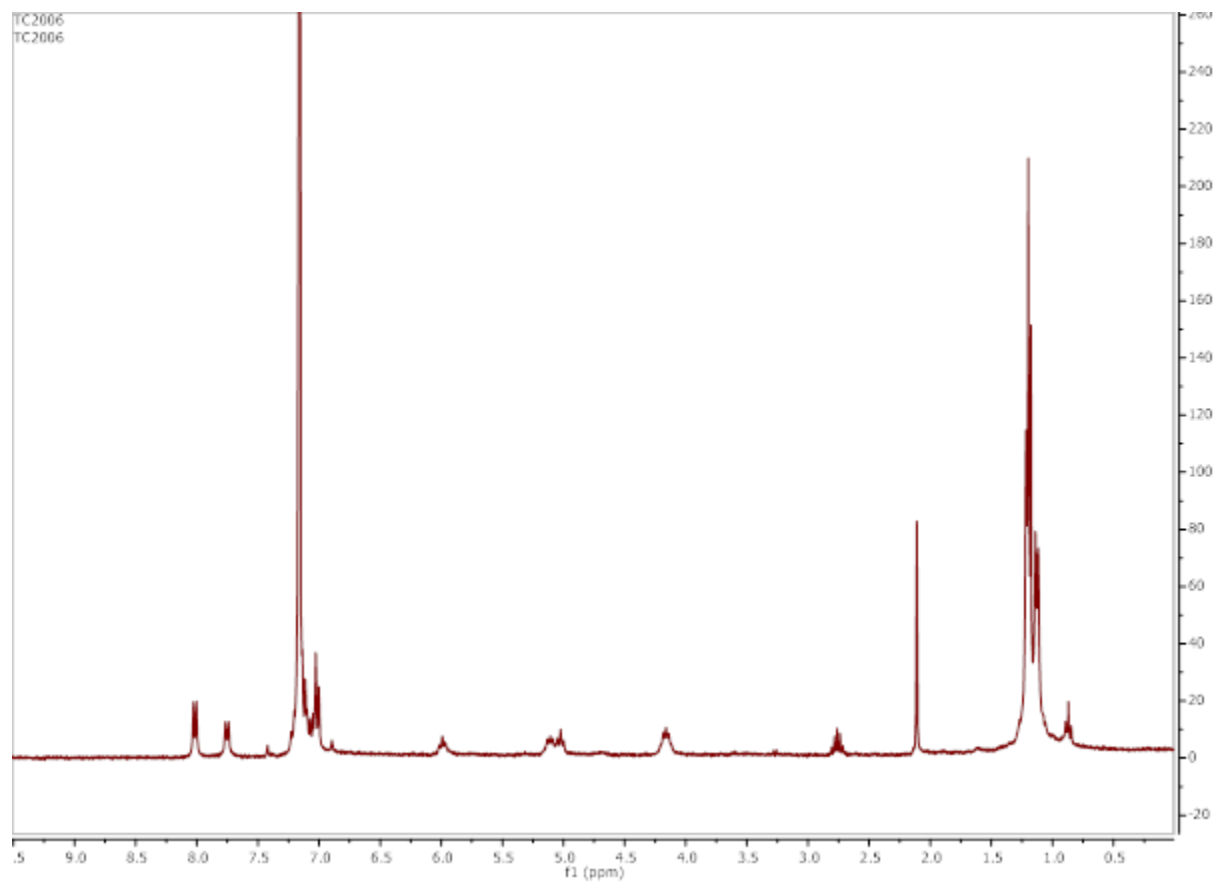


Figure C5:  $^1\text{H}$  NMR spectra of tetrakis(imido) to pentakis(imido) reaction

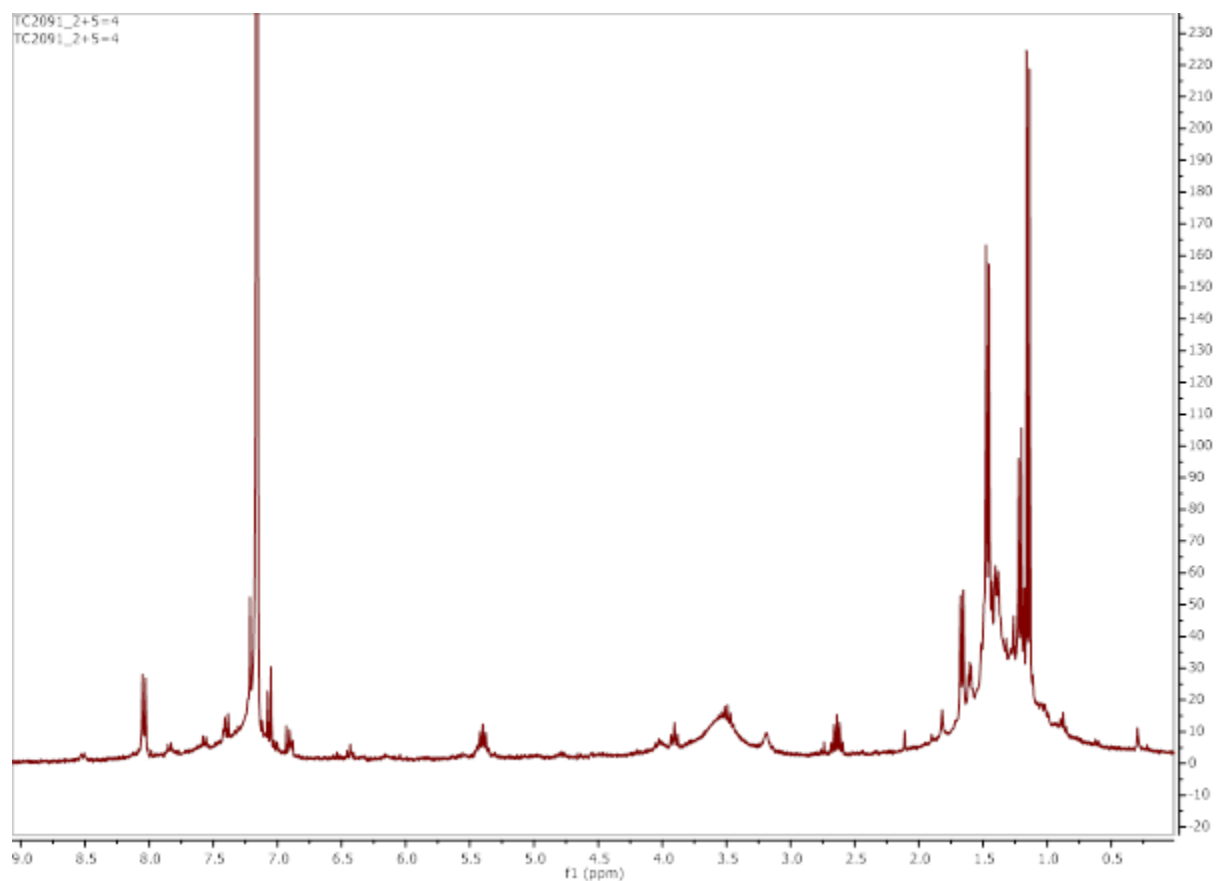


Figure C6:  $^1\text{H}$  NMR spectra of bis(imido) and pentakis(imido) reaction, to investigate how many imido ligands can be donated.

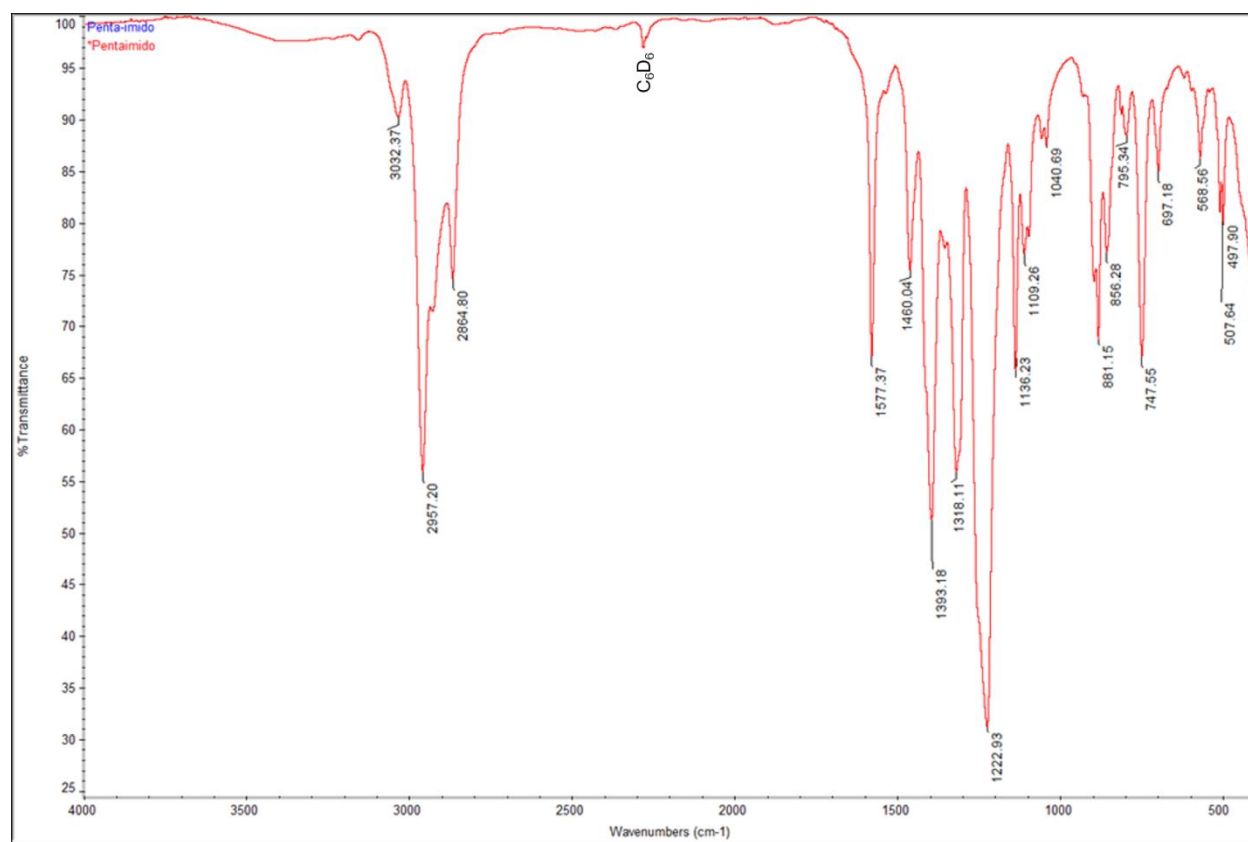


Figure C7: Infrared spectra of **9**, (KBr salt plate)

## VITA

Tyler received his B.S. in Chemistry in 2016 from Michigan State University. While at Michigan State Tyle worked in the laboratory of Professor James K. McCusker. While in the McCusker group he worked with iron(II) bipyridyl complexes with a focus on ligand design for use in dye sensitized solar cells.

After graduating from MSU and spending the summer continuing his work in the McCusker group Tyler took a position as a supplementary instructor at Davenport University in Lansing, MI. While at Davenport he worked with students in math and in various science laboratory classes. This work was a catalyzing factor to continue his education to work toward becoming an instructor himself. This is when Tyler moved on to Purdue University to work in the laboratory of Professor Suzanne Bart. While in the Bart group he initially worked on the synthesis of uranyl complexes with the focus being investigations into the activation of uranyl oxygen bonds with amide links and eventually with imido substituents. The work that Tyler has done with uranyl complexes has allowed him to present this work at Department of Energy-Energy Frontier Research Center-All hands meetings in Washington D.C., and smaller meetings at the ACS Meeting in Orlando, Florida, at the University of Pennsylvania, and at the Purdue-Indiana-Notre Dame Inorganic Conference. This initial work with uranyl amides and uranyl imidos lead to working with uranium element multiple bond complexes. Working with uranium element multiple bond complexes grew from analogous compounds to his uranyl chemistry to synthesizing a uranium(IV) *cis*-bis(imido) complex, and a uranium(VI) pentakis(imido) complex.

All of the work Tyler has done with Professor Bart has involved the use of temperature-, air-, and moisture- sensitive inorganic synthetic and characterization techniques. Some of the characterization methods that he has learned while at Purdue are paramagnetic and diamagnetic multinuclear NMR, single crystal x-ray crystallography, and UV-vis-NIR absorption spectroscopy. This work has also allowed him to work with collaborators from UPenn and Florida State University.

Origin of Bond Elongation in a Uranium(IV) *cis*-Bis(imido) Complex

Tyler S. Collins, Cristian Celis-Barros, María J. Beltrán-Leiva, Nickolas H. Anderson, Matthias Zeller, Thomas Albrecht-Schönzart, and Suzanne C. Bart\*

Cite This: *Inorg. Chem.* 2020, 59, 18461–18468

Read Online

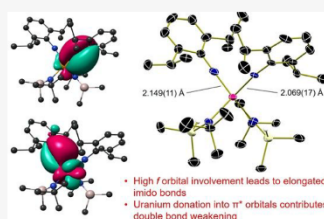
ACCESS |

Metrics &amp; More

Article Recommendations

Supporting Information

**ABSTRACT:** The activation of U–N multiple bonds in an imido analogue of the uranyl ion is accomplished by using a system that is very electron-rich with sterically encumbering ligands. Treating the uranium(VI) *trans*-bis(imido)  $\text{U}(\text{NDIPP})_2(\text{THF})_2$  (DIPP = 2,6-diisopropylphenyl and THF = tetrahydrofuran) with *tert*-butyl(dimethylsilyl)amide (NTSA) results in a reduction and rearrangement to form the uranium(IV) *cis*-bis(imido)  $[\text{U}(\text{NDIPP})_2(\text{NTSA})_2]\text{K}_2$  (**1**). Compound **1** features long U–N bonds, pointing toward substantial activation of the  $\text{N}=\text{U}=\text{N}$  unit, as determined by X-ray crystallography and  $^1\text{H}$  NMR, IR, and electronic absorption spectroscopies. Computational analyses show that uranium(IV)–imido bonds in **1** are significantly weakened multiple bonds due to polarization toward antibonding and nonbonding orbitals. Such geometric control has important effects on the electronic structures of these species, which could be useful in the recycling of spent nuclear fuels.



## INTRODUCTION

Efficient chemical processing of spent nuclear fuels represents a major hurdle in the nuclear fuel cycle, preventing its widespread use and contributing to the overall cost of this fuel source.<sup>1–3</sup> Understanding how to close this fuel loop with an eye toward recycling has been a strong driver within the actinide community for elucidation of the electronic structures of actinide derivatives with metal–element multiple bonds.<sup>4</sup> Of particular interest is gaining new insight into fundamental bonding trends and harnessing the redox properties of f-block elements for transformation to more value-added materials.

Uranium–element multiple bonds are exemplified by the ubiquitous uranyl ion, which features the *trans* arrangement of  $[\text{O}=\text{U}=\text{O}]^{2+}$  multiple bonds and a hexavalent uranium ion. This moiety is postulated to be enforced by the inverse *trans* influence (ITI).<sup>5,6</sup> This thermodynamic effect has been well studied for the actinides<sup>7–10</sup> and originates from the mixing of core p orbitals with valence axial f orbitals, deemphasizing the toroid and increasing the radial extent of the lobes in the z (axial) direction.<sup>5</sup> The result is a preference for a strongly bound ligand positioned *trans* to another strongly bound ligand.

In recent years, this effect has been observed for uranium imido species, which mimic the electronic structure of uranyl ions but are easier to work with because of their tunability and monomeric nature.<sup>11–13</sup> Such is the case for the uranyl analogues synthesized by Boncella and co-workers. This family of uranium *trans*-bis(imido) compounds,  $\text{U}(\text{NR})_2\text{I}_2$  (R = Ph, 'Bu), was found to have an electronic structure similar to that of uranyl derivatives but with increased covalency in its multiple bonds compared to its oxygen congener.<sup>11</sup> Prior to

the discovery of this family of uranyl analogues, Burns and co-workers had synthesized  $\text{Cp}^*_2\text{U}(\text{NPh})_2$ , a uranium(VI) *cis*-bis(imido) that features bulky  $\text{Cp}^*$  ligands to sterically constrain the imido groups.<sup>14</sup> In this case, the large ancillary ligands disrupt this commonly observed ITI.

The latter example has also been studied for its reduction chemistry. Simultaneous two-electron reduction of multiply bonded uranium has been observed for uranyl but is fairly uncommon for bis(imido) species. Specifically, Burns and co-workers showed two-electron reduction of  $\text{Cp}^*_2\text{U}(\text{NPh})_2$  by dihydrogen, forming the corresponding uranium(IV) bis(amido)  $\text{Cp}^*_2\text{U}(\text{NHPh})_2$ .<sup>15</sup> Reduction also results simply by heating this *cis*-bis(imido), forming the cyclometalated uranium(IV) derivative, where a C–H bond of the  $\text{Cp}^*$  methyl is added across the  $\text{U}=\text{N}$  multiple bond.<sup>16</sup> Similarly, a reductive cycloaddition results for the related uranium(VI) bis(imido)  $\text{Cp}^*_2\text{U}(\text{NSiMe}_3)\text{N}[\text{P}(\text{SiMe}_3)(\text{Mes})]$ .<sup>17</sup> More recently,  $\text{Cp}^*\text{Al}$  was used to reduce a uranium(VI) bis(imido) complex to uranium(IV).<sup>18</sup>

On the basis of this interesting geometric dichotomy in the realm of imido chemistry, we proposed that it should be possible to generate other *cis*-arranged species by making use of the bulky ancillary ligands. We reasoned that using the *tert*-butyl(dimethylsilyl)amide (NTSA),<sup>19–22</sup> which is both steri-

Received: November 10, 2020

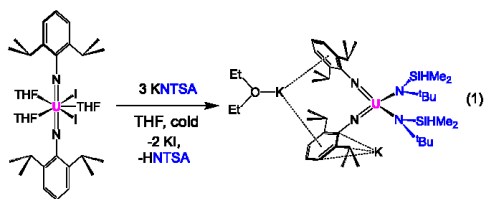
Published: December 3, 2020



cally bulky and synthetically straightforward, may make it possible to form a uranium *cis*-bis(imido) species in a lower oxidation state than Burns' example. This electron-rich species should show activated U–N multiple bonds that may lend themselves to increased reactivity and functionalization. Herein, we report the synthesis and characterization of an elusive uranium(IV) bis(imido) species, which has an interesting electronic structure. Also reported is a comparison with a hexavalent derivative, which gives insight into the differences in covalency between oxidation states. Having this type of geometric control over actinide multiply bonded species could have important effects on the electronic structures of these species.

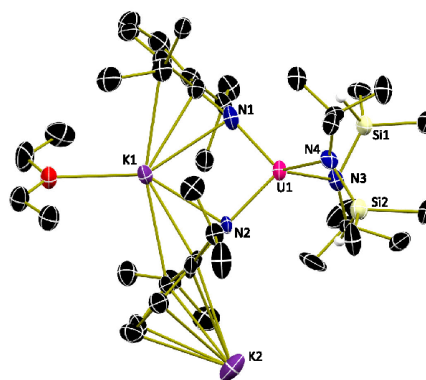
## RESULTS AND DISCUSSION

**Synthesis and Characterization.** Treating 1 equiv of a thawing tetrahydrofuran (THF) solution of uranium(VI) bis(2,6-diisopropylphenyl)imido,  $\text{U}(\text{NDIPP})_2(\text{THF})_3$ ,<sup>23</sup> with 3 equiv of KNTSA in cold THF, followed by stirring for 1 h and workup, furnished a dark-brown powder (eq 1).<sup>24</sup>



Purification was achieved by dissolution of this material in diethyl ether and layering with pentane, which resulted in the precipitation of blocks of dark-red crystals. The  $^1\text{H}$  NMR spectroscopic data clearly revealed several broadened and shifted peaks, consistent with a paramagnetic species. Also present was a resonance consistent with the free amine, HNTSA, indicating that some of the base likely served as a reductant. The multiplicity associated with the diamagnetic uranium(VI) starting material was noticeably absent, supporting reduction from uranium(VI) occurring during the course of the reaction. The presence of imido ligands was supported by the absence of an N–H absorption by IR spectroscopy. The bonding of the NTSA moiety was also confirmed by a  $70\text{ cm}^{-1}$  shift in the SiH band, as seen by IR spectroscopy, from  $1929\text{ cm}^{-1}$  in KNTSA to  $2003\text{ cm}^{-1}$  in this new product.<sup>24</sup>

Single crystals were grown in a fashion analogous to that of the purification procedure, and analysis by X-ray crystallography revealed a tetrahedral uranium compound,  $[\text{U}(\text{NDIPP})_2(\text{NTSA})_2]\text{K}_2$  (**1**; Figure 1 and Table 1). The  $\text{U}-\text{N}_{\text{imido}}$  bond distances in **1** are  $2.069(17)$  and  $2.149(11)\text{ \AA}$ , which are  $0.2\text{--}0.3\text{ \AA}$  shorter than the  $\text{U}-\text{NTSA}$  distances of  $2.365\text{ \AA}$ , supporting the presence of two imido and two amido bonds. The U–N bonds are consistent with those for other uranium(IV) imidos, including  $(\text{MeC}_6\text{H}_4)_3\text{UNPh}$  [ $2.019(6)\text{ \AA}$ ],<sup>25</sup>  $\text{Tp}^*\text{UNMes}$  [ $1.976(3)\text{ \AA}$ ],<sup>26</sup>  $\text{Tp}^*\text{UNAd}$  [ $1.953(3)\text{ \AA}$ ],<sup>26</sup>  $\text{Cp}^*\text{UNMes}$  [ $1.952(12)\text{ \AA}$ ],<sup>27</sup> and  $\text{Cp}^*\text{UNDIPP}$  [ $2.006(5)\text{ \AA}$ ].<sup>27</sup> The potassium ions are in the outer sphere, with  $\text{U1}-\text{K1}$  and  $\text{U1}-\text{K2}$  distances of  $3.7627(12)$  and  $4.422(3)\text{ \AA}$ , respectively; K2 is also associated with a DIPP group in an adjacent molecule in the crystal lattice. On the basis of the charge balance in **1**, the oxidation state of the uranium ion is best described as 4+, making this the first



**Figure 1.** Molecular structure of **1** shown at 30% probability ellipsoids. Selected hydrogen atoms and cocrystallized solvent molecules have been omitted for clarity.

**Table 1.** Comparison of Structural Parameters

	$\text{I}_2\text{U}^{6+}-\text{N}_{\text{imido}}$	$\text{NTSA}_2\text{U}^{4+}-\text{N}_{\text{imido}}$	$\text{Cp}^*_2\text{U}^{4+}-\text{N}_{\text{imido}}$ <sup>2</sup>
$\text{U}-\text{N}_{\text{imido}}\text{ (}\text{\AA}\text{)}$	$1.887(2)$ , $1.889(2)$	$2.069(17)$ , $2.149(11)$	$1.952(7)$
$\text{N}_{\text{imido}}-\text{U}-\text{N}_{\text{imido}}$ (deg)	$169.35(14)$	$95.2(3)$	$98.7(4)$

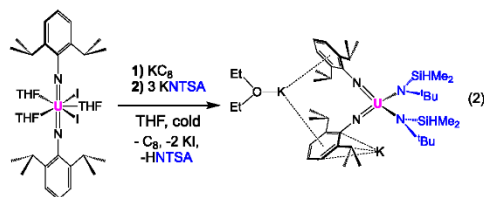
example of a crystallographically characterized uranium(IV) *cis*-bis(imido) species. With this positive identification of **1**, the formation of HNTSA is likely attributed to the fact that some of KNTSA served as a reductant and that hydrogen abstraction from a solvent molecule resulted during the reaction.

In hexavalent  $\text{Cp}^*_2\text{U}(\text{NPh})_2$ ,<sup>14</sup> the  $\text{U}-\text{N}_{\text{imido}}$  distance is  $1.952(7)\text{ \AA}$ , which is  $0.16\text{ \AA}$  longer compared to that in **1**. Similarly, that distance for **1** is approximately  $0.22\text{ \AA}$  longer than that in *trans*- $\text{U}(\text{NDIPP})_2(\text{THF})_3$ ,<sup>23</sup> which is the starting material for **1**. These differences in the bond length trend well with the increased atomic radius of uranium(IV) compared to uranium(VI). The *cis* nature of the imido groups in **1** is supported by the  $\text{N}_{\text{imido}}-\text{U}-\text{N}_{\text{imido}}$  angle as well, with **1** having an angle of  $95.2(3)^\circ$ , which is  $3.5^\circ$  shallower than that seen in the *cis*-bis(imido) complex  $\text{Cp}^*_2\text{U}(\text{NPh})_2$  at  $98.7(3)^\circ$ <sup>14</sup> and  $74.1^\circ$  more shallow than the starting *trans*-bis(imido) complex  $\text{N}_{\text{imido}}-\text{U}-\text{N}_{\text{imido}}$  angle of  $169.3(1)^\circ$ .<sup>19</sup>

Electronic absorption spectroscopy was used to assess the electronic structure of **1**. Data were acquired from 300 to  $1650\text{ nm}$  as solutions in toluene. The UV–vis region of the spectrum shows extremely broad transitions in this range, with a noticeable transition around  $\sim 325\text{ nm}$ . The near-IR (NIR) spectrum also shows broad transitions from 800 to  $1650\text{ nm}$ , which is unusual for uranium(IV)  $f^2$  ions; typically, these transitions are sharp and weakly absorbing.<sup>28</sup> However, the presence of these transitions supports the reduction from uranium(VI)  $f^0$ , which would be expected to be flat in this region. Additionally, a pentavalent uranium ion would typically show sharp transitions around  $1700\text{ nm}$ , which is not observed here, supporting the 4+ oxidation state for **1**.<sup>29</sup>

Because of the unusual reaction stoichiometries for the synthesis of **1**, an independent, rational synthesis was designed.

Reduction of  $\text{U}(\text{NDIPP})_2(\text{THF})_3$  from uranium(VI) with 1 equiv of potassium graphite for 1 h, followed by the addition of 3 equiv of KNTSA, furnished **1** in high yield (94%) after workup (eq 2). Analysis by  $^1\text{H}$  NMR spectroscopy confirmed

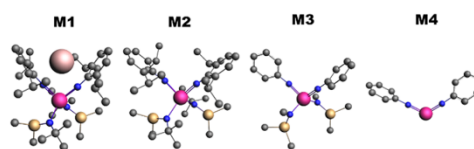


the formation of **1**, validating the need for reduction of the uranium(VI) center in the original synthesis, prior to salt metathesis. Given that this reaction proceeds in much higher yield than the original route, the efficiency of this reduction step seems to play a significant role in the formation of **1**. This supports the notion that at least 1 equiv of KNTSA acts as a reductant in the original synthesis and is the source of HNTSA.

The synthesis of **1** is significant because the *cis* arrangement of the imido substituents marks disruption of the ITI in this uranium species. On the basis of the crystallographic data, the potassium ion appears to play a role in coordination to the aryl groups, helping to stabilize the *cis* arrangement of the imido groups. Interestingly, the arrangement in **1** is quite reminiscent of  $\text{Cp}^*_2\text{U}(\text{NPh})_2$ , where the  $\text{Cp}^*$  rings, although bulky, take on the typical bent metallocene geometry. Because of the analogous nature of the U–N and U–O bonds in the respective bis(imido) and uranyl derivatives, it will be interesting to see if these results can be generally applied to uranyl complexes, which would facilitate the activation and recycling of spent nuclear fuel to generate more useful materials.

This electron-rich uranium(IV) bis(imido) dianion is reminiscent of a recent thorium example reported by Arnold and co-workers,  $[\text{K}_2(\text{S}_x)][\text{Th}(\text{NDipp})_2\text{N}']$ .<sup>30</sup> This thorium example is also dianionic, and the authors attribute the long Th–N<sub>imido</sub> bonds of 2.165(3) Å to the fact that this molecule is electron-rich, despite the thorium(IV) oxidation state. Thus, it is reasonable to expect that some of the elongation in this uranium system is also due to its anionic nature.

**Theoretical Models.** To understand the role of the counterion, steric effects, and NTSA coordination in the bis(imido) structure, four theoretical models have been considered (Figure 2). The first model, **M1**, consists of the optimized crystal structure including the counterion stacked between the two phenyl rings of the imido ligands. Model 2 (**M2**) corresponds to **M1** without inclusion of the counterion. Model 3 (**M3**) derives from **M2**, in which the substituents were simplified. Finally, model 4 (**M4**) represents the simplest model, including only two phenylimido (NPh) ligands coordinated to uranium(IV). The geometrical parameters for these models, including the experimental values for comparison, are summarized in Supplementary Table 4. From these data, clear trends emerge: the U–N<sub>imido</sub> bond lengths are shortened, and the angle defined by N<sub>imido</sub>–U<sup>IV</sup>–N<sub>imido</sub> increases when moving from **M1** to **M4**. These findings are consistent with the counterion preventing the opening of the angle of the N-phenyl rings in **1**. This occurs as steric



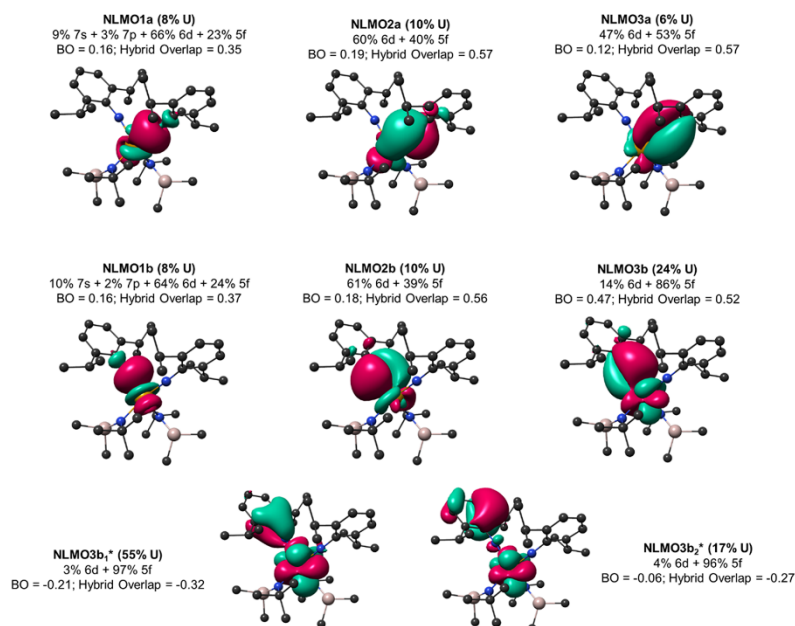
**Figure 2.** These models have been studied to understand the role of the potassium (pink sphere in **M1**) counterion and steric factors of the ligands in the coordination arrangement around the uranium(IV) metal center. Uranium(IV), nitrogen, carbon, and silicon atoms are depicted as magenta, blue, gray, and yellow balls, respectively. The geometries depicted correspond to optimizations performed at the ZORA/PBE0/STO-TZP level of theory.

constraints are removed and even further when NTSA ligands are not considered. The optimized (calculated) structure of **M4** provides insight into the interactions between uranium(IV) and the NPh ligands, where evidence of neither the trans influence nor ITI is observed (Supplementary Figure 7 and Table 4). As shown by the geometrical parameters of **M3**, the N<sub>imido</sub>–U<sup>IV</sup>–N<sub>imido</sub> angle is  $\sim 6^\circ$  larger than the  $109.5^\circ$  expected for a perfect tetrahedron due to the multiple-bond character of the U<sup>IV</sup>–NPh bonds. As a consequence, the NTSA–U<sup>IV</sup>–NTSA angle is decreased to  $\sim 106^\circ$  (Supplementary Table 4). It is very likely that, if not for the counterions and hydrocarbon substituents, the structure of **1** would best be described by valence-shell electron-pair repulsion theory.<sup>31</sup>

**Electronic Structure.** To understand the nature of the ground (GS) and excited states of **1**, spin–orbit complete-active-space self-consistent-field (SO-CASSCF) calculations were performed. According to the SO-CASSCF calculations, the GS of **M2** corresponds to a  $J = 4$  state that is composed of 96% triplet, where 66% is assigned to the expected spectroscopic term  $^3\text{H}_4$ , with 4% of singlet contributions. Interestingly, the Hartree–Fock (HF) determinant only represents 56% of the GS, while another 21% corresponds to single excitations from a bonding  $\pi$  orbital to its antibonding  $\pi^*$  counterpart. The remaining contributions arise from single and double excitations from  $\pi$  to nonbonding 5f orbitals (Supplementary Figure 8). The unusual occurrence of  $\pi \rightarrow \pi^*$  excitations in the GS highlights the importance of electron correlation in the correct description of the chemical bond in **1**. In simpler words, correlation allows the population of antibonding orbitals, which reduces the strength of one of the U(IV)–N<sub>imido</sub> bonds, which is observed experimentally.

**Bonding.** The nature of the chemical bond was investigated using the natural localized molecular orbitals (NLMOs) based on scalar relativistic (SR)-CASSCF densities. Three different types of NLMOs were identified for the interaction within the U<sup>IV</sup>–NDIPP bonds (Figure 3) but only two for the U<sup>IV</sup>–NTSA bonds (Supplementary Figure 9). The NLMOs found for U<sup>IV</sup>–N<sub>imido</sub> (Figure 3) are very similar to the natural bond orbitals (NBOs) reported previously by Liddle and co-workers for  $[\text{U}(\text{Tren}^{\text{TIPS}})(\text{NH})]^-$ ,<sup>32</sup> i.e., one  $\sigma$  type (NLMOs 1 in Figure 3) and two  $\pi$  types (NLMOs 2 and 3 in Figure 3) are present. According to King et al.,<sup>32</sup> these NBOs suggest a triple bond associated with the U<sup>IV</sup>–N<sub>imido</sub> interaction; however, despite the similar bond pattern found in our system, in the case of **1**, a formal triple-bond description for this interaction is not supported. From Figure 3, it can be seen that the  $\sigma$ -NLMOs, NLMO1a and NLMO1b, are almost identical in





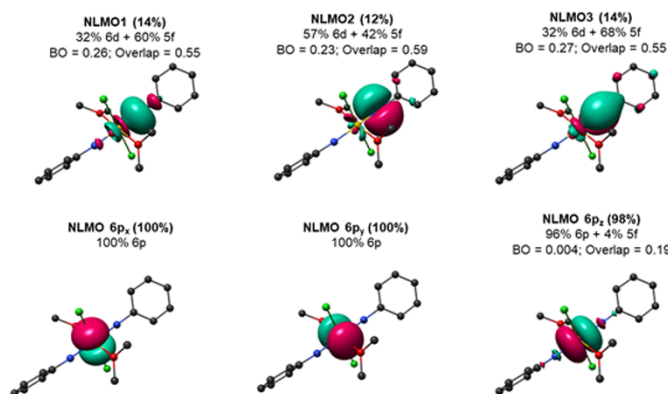
**Figure 3.** NLMOs of M2. Bonding interactions between uranium(IV) and the NDIPP ligands are shown. NLMO1a and -b display  $\sigma$ -type interactions, NLMO2a and -b in-plane  $\pi$ -bond interactions, and NLMO3a and -b the  $\pi$ -bond interactions aligned with the  $\pi$  system of the phenyl rings. Letters a and b are used to distinguish between the two imido ligands. The uranium(IV) contribution to the NLMO and its composition are given. NLMO-based BOs and their corresponding hybrid overlap are also given. NLMOs marked with a star correspond to partially occupied antibonding NLMO counterparts to NLMO3b.

polarization and composition. The same is true for the  $\pi$ -NLMOs, NLMO2a and NLMO2b, which are mainly composed of the  $N_{\text{imido}}$ -lone pair lying on the phenyl plane with 10% uranium 5f6d(40/60) hybrid orbital contribution. The second set of  $\pi$ -NLMOs, NLMO3a and NLMO3b, originates from the interaction between the  $N_{\text{imido}}$  and lone pair aligned with the  $\pi$  system and uranium ion. These  $\pi$ -type NLMOs differ from each other because they depend on the orientation of the uranium(IV) ion hybridization, resulting in significant differences in both polarization and composition. For instance, NLMO3 (Figure 3) has substantial uranium(IV) contribution with a strong 5f character that is indicative of a less polar bond. Furthermore, this is the only NLMO having an antibonding counterpart, NLMO3b<sub>1</sub>\* and NLMO3b<sub>2</sub>\* (Figure 3), indicating that the strength of the bond is affected by the population of these NLMOs. The importance of electron correlation in this bond is reflected in the occupation numbers of 1.8, 0.95, and 1.65 for NLMO3b, NLMO3b<sub>1</sub>\*, and NLMO3b<sub>2</sub>\*, respectively.

Covalency, from the orbital perspective, is discussed in terms of two main factors: the orbital overlap between the ligand and metal orbitals and the energy gap between them. The only way for a covalent bond to become stronger is to increase the orbital overlap. Energy matching enhances the orbital mixing and, consequently, the bond order (BO), but it does not lead to bond stabilization.<sup>33,34</sup> An overall qualitative picture of the bond strength can be obtained by NLMO decomposition into individual contributions to the total BO in addition to the

individual hybrid overlap. If we compare the interaction between each imido ligand with uranium(IV), it appears that they differ significantly. However, the seemingly "most covalent" bond (NLMO3b in Figure 3) is counterbalanced by the antibonding contribution to this bond. This can be seen in the total BO contribution coming from  $\sigma$  and  $\pi$  interactions, where the  $U^{\text{IV}}-N_{\text{imido}}(\text{a})$  and  $U^{\text{IV}}-N_{\text{imido}}(\text{b})$  bonds are described with 0.47 and 0.54 bond indices, respectively, in agreement with the difference in the experimentally observed bond lengths 2.069(17) and 2.149(11) Å (Supplementary Table 3), respectively. On the other hand, the hybrid overlap shows that the strength of these bonds is dominated by  $\pi$  interactions with similar values between the two imido (Figure 3) and two NTSA ligands (Supplementary Figure 9).

Another approach to assessing the covalency is mapping the electron density of 1 using the quantum theory of atoms in molecules (QTAIM) approach based on SR-CASSCF densities. It is important to note the electron correlation between uranium(IV) and one of the imido ligands; expansion of the active space was crucial to recovering the true nature of the chemical bonds (Supplementary Table 6 and Computational Details). As expected,  $U^{\text{IV}}-N_{\text{imido}}$  bonds are more covalent than  $U^{\text{IV}}-\text{NTSA}$  bonds, mainly based on the increased accumulation of the electron density at the bond critical point (BCP), as well as the increased delocalization indices and more negative energy densities. For partially covalent bonds such as actinide–ligand, the ratio between the potential ( $V$ ) and kinetic ( $G$ ) energy densities provides an



**Figure 4.** NLMOs of  $U^{VI}(NPh)_2Cl_2THF_2$ . Main interactions between uranium(VI) and one imido ligand describing the  $\sigma$  (NLMO1) and  $\pi$  (NLMO2 and NLMO3) interactions. The other imido shows the same interactions with the same BO and hybrid overlaps. The semicore 6p orbitals have been included to show polarization of the core toward the 5f shell induced by the imido ligands. This effect supports the ITI in this system similar to that seen in  $UO_2^{2+}$ .<sup>10</sup>

estimation of the degree of polarization of the bond or how covalent the bond is.  $U^{IV}-N_{imido}(a)$  displays more electron density at the BCP with 33% degree of covalency versus a value of 25% observed in  $U^{IV}-N_{imido}(b)$ . This reduction is attributed to Coulomb correlation, which allows polarization of the  $U^{IV}-N_{imido}(b)$  electron density toward the fractionally occupied 5f orbitals, agreeing well with NLMO analysis.

To elucidate the differences in the  $U^{VI,IV}-N_{imido}$  bonds, the  $U^{VI}(NPh)_2Cl_2DME_2$  (DME = dimethyl ether) model was considered based on the crystal structure of  $U^{VI}(NDIPP)_2Cl_2THF_2$ .<sup>35</sup> This model was developed to simplify the molecule as much as possible without influencing the electronic structure. Because the equatorial coordination—especially solvent coordination—does not bind covalently, the electronic structure is not affected by a change from THF to DME. NLMO analysis revealed that the  $U^{VI}-N_{imido}$  bonds are more covalent than the  $U^{IV}-N_{imido}$  ones. The most striking difference is that the  $\sigma$  bond (NLMO1 in Figure 4) is composed of 14% uranium(VI), displaying an increase of 6% with respect to the uranium(IV) bis(imido) complex M2. Furthermore, the 5f involvement in the formation of this bond is significantly higher (60% 5f). The strength of the U–N bond is also greater in the hexavalent complex, which is seen in the individual BOs of the  $\sigma$  and  $\pi$  NLMOs. Also of note is the involvement of the semicore 6p orbitals in bonding. As shown in Figure 4, NLMO 6p<sub>z</sub> shows polarization toward the 5f orbitals although with a very low contribution to the actual bond (BO = 0.004), supporting the ITI mechanism operating in this hexavalent system. This polarization has been reported for other actinide systems, including the uranyl unit, where the NLMO composition for the 6p orbital in the axis where the ITI occurs is very similar to that of Boncella's hexavalent uranium *trans*-bis(imido) complexes.<sup>10</sup> Further discussion about bonding in  $U^{VI}(NPh)_2Cl_2THF_2$  can be found in the Additional Discussion.

From the combination of natural localization, deformation densities, and electron density topology mapping, we can conclude that, despite the triple bond reported for the uranium(IV)–bis(imido) interaction,<sup>11</sup> our results support that the strength of the bond matches more closely to that of a

formal single bond. Furthermore, the bond is clearly weakened by lowering the oxidation state of uranium, whereas the involvement of semicore orbitals, and therefore observation of the ITI, is only observed in the hexavalent oxidation state (Figure 4).

## CONCLUSIONS

In summary, we have presented an unusual bent uranium(IV) bis(imido) compound. Unlike its uranium(VI) counterparts, the U– $N_{imido}$  bonds are long due, in part, to the longer ionic radius of the uranium(IV) ion but also, in part, to a unique electronic structure that was discovered by computational analyses. Full characterization using a variety of spectroscopic and crystallographic techniques supports this claim. From the theoretical viewpoint, the 5f orbitals play a crucial role in the bond formation of the uranium(IV) bis(imido); however, the near-energy degeneracy between the imido 2p <sub>$\pi$</sub>  orbitals with the 5f shell weakens one of the  $U^{IV}-N_{imido}$  bonds through static electron correlation, further increasing the bond length. The partial occupation of antibonding orbitals, as we observe, is responsible for the asymmetric nature of the U–N bonds in this species and has not been previously reported. The resulting activation of strong uranium–element bonds, which are key components of spent nuclear fuels, could have an impact in spent nuclear fuel processing and recycling to make nuclear power more accessible and environmentally benign.

## EXPERIMENTAL SECTION

**General Considerations.** All air- and moisture-sensitive manipulations were performed using standard Schlenk techniques or in an MBraun inert-atmosphere drybox with an atmosphere of purified nitrogen. The MBraun drybox was equipped with two  $-35\text{ }^\circ\text{C}$  freezers for cooling samples and crystallizations. Solvents for sensitive manipulations were dried and deoxygenated using literature procedures with a Seca solvent purification system.<sup>36</sup> Benzene-*d*<sub>6</sub> was purchased from Cambridge Isotope Laboratories, dried with molecular sieves and sodium, and degassed by six freeze–pump–thaw cycles. KNTSA,<sup>24</sup> potassium graphite,<sup>37</sup> and  $UCl_2(NDIPP)_2THF_4$ <sup>23</sup> were synthesized according to literature procedures.

**Caution!** U-238 is a weak  $\alpha$ -emitter with a half-life of  $t_{1/2} = 4 \times 10^9$  years. All manipulations were performed in an inert-atmosphere glovebox in a laboratory equipped with proper detection equipment.

<sup>1</sup>H NMR spectra were recorded at 25 °C on a Varian Inova 300 spectrometer operating at 299.96 MHz. All chemical shifts are reported relative to the peak for SiMe<sub>4</sub> using <sup>1</sup>H (residual) chemical shifts of the solvent as a secondary standard. For all molecules, the NMR data are reported with the chemical shift and peak assignment, followed by the peak width at half-height.

IR spectra were recorded using a Thermo Nicolet 6700 spectrometer; samples were prepared by grinding the desired compound together with KBr salt and pressing the solid into a pellet. Elemental analyses were performed by Midwest Microlab (Indianapolis, IN). Electronic absorption spectroscopic measurements were recorded at ambient temperature in sealed 1 cm quartz cuvettes with a Cary 6000i UV–Vis–NIR spectrophotometer.

Single crystals of **1** suitable for X-ray diffraction were coated with poly(isobutylene) oil in a glovebox and quickly transferred to the goniometer head of a Bruker Quest diffractometer with  $\kappa$  geometry, an I- $\mu$ S microsource X-ray tube, a laterally graded multilayer (Goebel) mirror single crystal for monochromatization, a Photon-II area detector, and an Oxford Cryosystems low-temperature device. Examination and data collection were performed with Cu K $\alpha$  radiation ( $\lambda = 1.54178$  Å) at 150 K.

Single crystals of UCl<sub>2</sub>(NDIPP)<sub>2</sub>(THF)<sub>2</sub> suitable for X-ray diffraction were coated with poly(isobutylene) oil in a glovebox and quickly transferred to the goniometer head of a Bruker Quest diffractometer with  $\kappa$  geometry, an I- $\mu$ S microsource X-ray tube, a laterally graded multilayer (Goebel) mirror single crystal for monochromatization, a Photon-II area detector, and an Oxford Cryosystems low-temperature device. Examination and data collection were performed with Mo K $\alpha$  radiation ( $\lambda = 0.71073$  Å) at 100 K. See the crystallography section below for details on single-crystal structure determination.

**Synthesis of [U(NDIPP)<sub>2</sub>(NTSA)<sub>2</sub>]K<sub>2</sub> (**1**).** A 20 mL scintillation vial was charged with UCl<sub>2</sub>(NDIPP)<sub>2</sub>THF<sub>2</sub> (0.500 g, 0.44 mmol),<sup>23</sup> THF (10 mL), and a stir bar. With stirring, 1 equiv of K<sub>2</sub>C<sub>8</sub> (0.065 g, 0.48 mmol) was slowly added as a solid, causing an immediate color change from dark brown to black. This black mixture was allowed to stir for an additional 1 h, upon which a solution of 3 equiv of KNTSA (0.225 g, 1.33 mmol) dissolved in cold THF (5 mL) was added dropwise. The combined reaction was then allowed to stir for 1 h longer. This mixture was then filtered through Celite on a medium frit to remove C<sub>8</sub> and KI. The filtrate was dried in vacuo, and the residue was washed with pentane (3 mL) twice and dried, leaving a brown/black powder (0.385 g, 94%) assigned as **1**. Elem anal. Theory: C, 47.67; H, 7.58; N, 5.85. Calcd: C, 46.60; H, 7.04; N, 5.71. <sup>1</sup>H NMR (C<sub>6</sub>D<sub>6</sub>, 300 MHz, 25 °C):  $\delta$  –14.62 (s, Si(CH<sub>3</sub>)<sub>2</sub>, 50), –2.84 (s, <sup>t</sup>BuCH<sub>3</sub>, 100), –2.10 (s, <sup>p</sup>PrCH, 30), –0.99 (s, <sup>p</sup>PrCH<sub>3</sub>, 100), 10.34 (s, DIPP-ArH, 55), 14.14 (s, DIPP-ArH, 80), 34.15 (s, SiH, 40). <sup>1</sup>H NMR (THF-*d*<sub>6</sub>, 300 MHz, 25 °C):  $\delta$  –3.79 (s, <sup>p</sup>PrCH, 7 Hz), –2.67 (s, Si(CH<sub>3</sub>)<sub>2</sub>, 10), –1.32 (s, <sup>p</sup>PrCH<sub>3</sub>, 10), –0.13 (s, SiH, 10), 1.11 (s, <sup>t</sup>BuCH<sub>3</sub>, 8), 11.35 (t, DIPP-ArH, *J* = 8), 14.78 (d, DIPP-ArH, *J* = 14). IR (KBr pellet, cm<sup>–1</sup>): 2955 m, 2864 m, 2003 br ( $\nu_{\text{SiH}}$ ), 1574 m, 1461 m, 1401 m, 1354 m, 1322 m, 1253 m, 1196 m, 1134 m, 1107 m, 1042 m, 977 m, 899 m, 867 m, 837 m, 779 m, 752 m, 697 m, 578 m, 515 m, 489 m.

**Computational Details. Geometry Optimization.** Geometry optimizations have been performed in ADF2019<sup>38,39</sup> using the generalized gradient approximation (GGA) Perdew–Burke–Ernzerhof (PBE) functional along with the Slater-type basis functions (STO) triple- $\zeta$  potential (TZP). The SR effects were included by means of the zeroth-order relativistic approximation (ZORA) Hamiltonian.<sup>40</sup> No geometry or symmetry constraints were imposed for the optimization process. To obtain the potential energy surface (PES) of the N<sub>imido</sub>–U–N<sub>imido</sub> angle, individual optimization steps were performed, constraining the position of this angle from 90° to 180°. The same level of theory used in the fully relaxed geometry optimization was considered for the PES scan. The PES was constructed from single-point energies using the hybrid PBE0

functional to correct the overdelocalization errors coming from pure GGA functionals. The individual single-point energies were fitted to third-order polynomial functions ( $r^2 = 0.992–0.999$ ).

**Electronic Structure.** The electronic structures of **M2**, **M3** (used to obtain the PES), and U<sup>VI</sup>(NPh)<sub>2</sub>Cl<sub>2</sub>DME<sub>2</sub> were analyzed through the CASSCF. Initially, Kohn–Sham density functional theory (KS-DFT) wave functions were obtained at the PBE0<sup>41</sup> level of theory in conjunction with the def2-TZVP basis set<sup>42</sup> for all atoms except uranium, which was treated with the SARC-DKH-TZVP basis set.<sup>43</sup> The SR effects were included via the second-order Douglas–Kroll–Hess (DKH2) Hamiltonian.<sup>44</sup> The resulting KS-DFT wave functions were subjected to state-average (SA-)CASSCF calculations<sup>45</sup> that recover static and partial dynamic correlation energies. This method divides the canonical orbital space into inactive, virtual, and active subspaces, where in the latter a full continuous integration is carried out. A minimal active space was chosen and consisted of two electrons in seven 5f orbitals, CAS(2,7), including triplets and singlets in the case of **M2** and **M3** and only singlets for U<sup>VI</sup>(NPh)<sub>2</sub>Cl<sub>2</sub>DME<sub>2</sub>. The SR effects were incorporated by the DKH2 Hamiltonian, while SO coupling induced through quasi-degenerate perturbation theory. Further dynamic correlation was recovered by the N-electron valence state perturbation theory, where excitations between the three subspaces were considered.<sup>46</sup> All of these calculations were performed using the ORCA 4.2.1 package.<sup>47</sup> Because of the multiple-bond nature of the metal imido ligands, the active space needs to be expanded to recover the electron correlation between the metal and ligands. Attempts to include ligand orbitals in the active space using both state-average and state-specific approximations were unsuccessful, evidencing that the same set of orbitals (state-averaged or state-specific) cannot be used for describing the electronic structure of **M2** or U<sup>VI</sup>(NPh)<sub>2</sub>Cl<sub>2</sub>DME<sub>2</sub>. To deal with this inconvenience, open MOLCAS<sup>48</sup> was used because CASSCF implementation allows one to obtain different sets of orbitals for each multiplicity.

The procedure is similar to that of ORCA. The single-determinant KS-DFT wave function was calculated using the PBE0 functional along with the all-electron ANO-RCC Gaussian-type basis sets contracted to TZP quality.<sup>49,50</sup> The SR effects were included via the DKH2 Hamiltonian. The resulting wave function was employed to perform SA-CASSCF calculations but this time for each multiplicity separately. The active space of **M2** consisted of four electrons in eight orbitals, CAS(4,8), where an internal orbital from one of the imido ligands was included, in addition to the seven 5f orbitals. This orbital was the only bonding orbital near-energy degenerate to the active space with considerable ligand–metal mixing. In the case of U<sup>VI</sup>(NPh)<sub>2</sub>Cl<sub>2</sub>DME<sub>2</sub>, CAS(8,12) was performed by including 4 $\pi$  bonding orbitals, their antibonding counterparts and four nonbonding 5f orbitals. Two of the  $\pi$  bonding orbitals come from the U<sup>VI</sup>–N<sub>imido</sub>–lone pair interaction lying on the phenyl plane, while the other two come from the U<sup>VI</sup>–N<sub>imido</sub>–lone pair interaction but this time aligned with the  $\pi$  system. Expansion of the active space allowed one to explore the inclusion of higher multiplicities in both systems. SO coupling was treated by state interactions between these CASSCF wave functions, using the restricted-active-space state interaction method.<sup>51</sup> The SO operator matrix was calculated from an atomic mean-field approximation.<sup>52</sup>

**Bonding.** To obtain a more accurate picture of the chemical bond, NLMO and QTAIM analyses based on the CAS(4,8) (**M2**) and CAS(8,12) [U<sup>VI</sup>(NPh)<sub>2</sub>Cl<sub>2</sub>DME<sub>2</sub>] densities were carried out. NLMO analysis was performed in the standalone version of NBO7.0,<sup>53</sup> while the AIMAll package<sup>54</sup> was used to perform QTAIM analysis. Because the extended transition state natural orbitals for chemical valence (ETS-NOCV)<sup>55</sup> approximation was implemented in ADF2019,<sup>38,39</sup> KS-DFT was used to perform the energy decomposition analysis. The ZORA/PBE0/STO-TZP level of theory was used to perform the ETS-NOCV analysis.

## ■ ASSOCIATED CONTENT

## ■ Supporting Information

The Supporting Information is available free of charge at <https://pubs.acs.org/doi/10.1021/acs.inorgchem.0c03340>.

Supplementary figures and tables, crystallographic data, computational section, and additional discussion (PDF)

## Accession Codes

CCDC 1997658 and 2033982 contain the supplementary crystallographic data for this paper. These data can be obtained free of charge via [www.ccdc.cam.ac.uk/data\\_request/cif](http://www.ccdc.cam.ac.uk/data_request/cif), or by emailing [data\\_request@ccdc.cam.ac.uk](mailto:data_request@ccdc.cam.ac.uk), or by contacting The Cambridge Crystallographic Data Centre, 12 Union Road, Cambridge CB2 1EZ, UK; fax: +44 1223 336033.

## ■ AUTHOR INFORMATION

## Corresponding Author

Suzanne C. Bart – H. C. Brown Laboratory, Department of Chemistry, Purdue University, West Lafayette, Indiana 47907, United States; [orcid.org/0000-0002-8918-9051](https://orcid.org/0000-0002-8918-9051); Email: [sbart@purdue.edu](mailto:sbart@purdue.edu)

## Authors

Tyler S. Collins – H. C. Brown Laboratory, Department of Chemistry, Purdue University, West Lafayette, Indiana 47907, United States; [orcid.org/0000-0003-1026-4379](https://orcid.org/0000-0003-1026-4379)

Cristian Celis-Barros – Department of Chemistry and Biochemistry, Florida State University, Tallahassee, Florida 32306, United States; [orcid.org/0000-0002-4685-5229](https://orcid.org/0000-0002-4685-5229)

Maria J. Beltrán-Leiva – Department of Chemistry and Biochemistry, Florida State University, Tallahassee, Florida 32306, United States; [orcid.org/0000-0003-3221-3118](https://orcid.org/0000-0003-3221-3118)

Nickolas H. Anderson – H. C. Brown Laboratory, Department of Chemistry, Purdue University, West Lafayette, Indiana 47907, United States

Matthias Zeller – H. C. Brown Laboratory, Department of Chemistry, Purdue University, West Lafayette, Indiana 47907, United States; [orcid.org/0000-0002-3305-852X](https://orcid.org/0000-0002-3305-852X)

Thomas Albrecht-Schönzart – Department of Chemistry and Biochemistry, Florida State University, Tallahassee, Florida 32306, United States; [orcid.org/0000-0002-2989-3311](https://orcid.org/0000-0002-2989-3311)

Complete contact information is available at:

<https://pubs.acs.org/doi/10.1021/acs.inorgchem.0c03340>

## Notes

The authors declare no competing financial interest.

## ■ ACKNOWLEDGMENTS

This research was supported by the Center for Actinide Science and Technology, an Energy Frontier Research Center funded by the U.S. Department of Energy, Office of Science, Basic Energy Sciences, under Award DE-SC0016568. Funding for the single-crystal X-ray diffractometer was provided by the National Science Foundation through the Major Research Instrumentation Program under Grant CHE1625543.

## ■ REFERENCES

- (1) Gras, J.-M.; Quang, R. D.; Masson, H.; Lieven, T.; Ferry, C.; Poinssot, C.; Debes, M.; Delbecq, J.-M. Perspectives on the closed fuel cycle: Implications for high-level waste matrices. *J. Nucl. Mater.* **2007**, *362*, 383–394.
- (2) Katz, J.; Moss, L. R.; Seaborg, G. T. *The Chemistry of the Actinide Elements*; Chapman Hall: New York, 1980.
- (3) Jones, M. B.; Gaunt, A. J. Recent Developments in Synthesis and Structural Chemistry of Nonaqueous Actinide Complexes. *Chem. Rev.* **2013**, *113*, 1137–1198.
- (4) Hayton, T. W. Metal-ligand multiple bonding in uranium: structure and reactivity. *Dalton Trans.* **2010**, *39*, 1145–1158.
- (5) Denning, R. G. Electronic structure and bonding in actinyl ions. *Complexes, Clusters and Crystal Chemistry*; Springer: Berlin, 1992; Vol. 79, pp 215–276.
- (6) Denning, R. G. Electronic Structure and Bonding in Actinyl Ions and their Analogs. *J. Phys. Chem. A* **2007**, *111*, 4125–4143.
- (7) Lam, O. P.; Franke, S. M.; Nakai, H.; Heinemann, F. W.; Hieringer, W.; Meyer, K. Observation of the Inverse Trans Influence (ITI) in a Uranium(V) Imide Coordination Complex: An Experimental Study and Theoretical Evaluation. *Inorg. Chem.* **2012**, *51*, 6190–6199.
- (8) Lewis, A. J.; Mullane, K. C.; Nakamaru-Ogiso, E.; Carroll, P. J.; Schelter, E. J. The Inverse Trans Influence in a Family of Pentavalent Uranium Complexes. *Inorg. Chem.* **2014**, *53*, 6944–6953.
- (9) O'Grady, E.; Kallitsayannis, N. On the inverse trans influence. Density functional studies of  $[\text{MOX}_3]^{n-}$  ( $\text{M} = \text{Pa}$ ,  $n = 2$ ;  $\text{M} = \text{U}$ ,  $n = 1$ ;  $\text{M} = \text{Np}$ ,  $n = 0$ ;  $\text{X} = \text{F}$ ,  $\text{Cl}$  or  $\text{Br}$ ). *J. Chem. Soc., Dalton Trans.* **2002**, 1233–1239.
- (10) Windorff, C. J.; Celis-Barros, C.; Sperling, J. M.; McKinnon, N. C.; Albrecht-Schmitt, T. E. Probing a variation of the inverse-trans-influence in americium and lanthanide tribromide tris(tricyclohexylphosphine oxide) complexes. *Chem. Sci.* **2020**, *11*, 2770–2782.
- (11) Hayton, T. W.; Boncella, J. M.; Scott, B. L.; Palmer, P. D.; Batista, E. R.; Hay, P. J. Synthesis of Imido Analogs of the Uranyl Ion. *Science* **2005**, *310*, 1941–1943.
- (12) Anderson, N. H.; Odoh, S. O.; Yao, Y.; Williams, U. J.; Schaefer, B. A.; Kiernicki, J. J.; Lewis, A. J.; Goshert, M. D.; Fanwick, P. E.; Schelter, E. J.; Walensky, J. R.; Gagliardi, L.; Bart, S. C. Harnessing redox activity for the formation of uranium tris(imido) compounds. *Nat. Chem.* **2014**, *6*, 919–926.
- (13) Anderson, N. H.; Xie, J.; Ray, D.; Zeller, M.; Gagliardi, L.; Bart, S. C. Elucidating bonding preferences in tetrakis(imido)uranate(VI) dianions. *Nat. Chem.* **2017**, *9*, 850–855.
- (14) Arney, D. S. J.; Burns, C. J.; Smith, D. C. Synthesis and structure of the first uranium(VI) organometallic complex. *J. Am. Chem. Soc.* **1992**, *114*, 10068–9.
- (15) Peters, R. G.; Warner, B. P.; Burns, C. J. The Catalytic Reduction of Azides and Hydrazines Using High-Valent Organouranium Complexes. *J. Am. Chem. Soc.* **1999**, *121*, 5585–5586.
- (16) Peters, R. G.; Warner, B. P.; Scott, B. L.; Burns, C. J. C–H Bond Activation with Actinides: The First Example of Intramolecular Ring Bite of a Pentamethylcyclopentadienyl Methyl Group. *Organometallics* **1999**, *18*, 2587–2589.
- (17) Ward, R. J.; Rungthanaphatsophon, P.; Rosal, I. d.; Kelley, S. P.; Maron, L.; Walensky, J. R. Divergent uranium- versus phosphorus-based reduction of  $\text{Me}_3\text{SiN}_3$  with steric modification of phosphido ligands. *Chem. Sci.* **2020**, *11*, 5830–5835.
- (18) Ward, R. J.; Del Rosal, I.; Chirdon, D. N.; Kelley, S. P.; Tarlton, M. L.; Maron, L.; Walensky, J. R. Two-Electron Reduction of a U(VI) Complex with  $\text{Al}(\text{C}_2\text{Me}_5)_3$ . *Inorg. Chem.* **2020**, *59*, 16137–16142.
- (19) Pattenaude, S. A.; Coughlin, E. J.; Collins, T. S.; Zeller, M.; Bart, S. C. Expanding the Library of Uranyl Amide Derivatives: New Complexes Featuring the tert-Butyldimethylsilylamide Ligand. *Inorg. Chem.* **2018**, *57*, 4543–4549.
- (20) Eedugurala, N.; Wang, Z.; Yan, K.; Boteju, K. C.; Chaudhary, U.; Kobayashi, T.; Ellern, A.; Slowing, I. L.; Pruski, M.; Sadow, A. D.  $\beta$ -SiH-Containing Tris(silazido) Rare-Earth Complexes as Homogeneous and Grafted Single-Site Catalyst Precursors for Hydroamination. *Organometallics* **2017**, *36*, 1142–1153.
- (21) Rees, W. S., Jr.; Just, O.; Schumann, H.; Weimann, R. Structural characterization of a tris-agostic lanthanoid-H-Si interaction. *Angew. Chem., Int. Ed. Engl.* **1996**, *35*, 419–22.
- (22) Huynh, K.; Anderson, B. K.; Livinghouse, T. Enantioselective hydroamination/cyclization of aminoalkenes by (bis)- $\text{C}_2$  symmetric



- and (mono)-C<sub>2</sub> symmetric anionic tetraamide complexes of La(III). *Tetrahedron Lett.* **2015**, *56*, 3658–3661.
- (23) Hayton, T. W.; Boncella, J. M.; Scott, B. L.; Batista, E. R.; Hay, P. J. Synthesis and Reactivity of the Imido Analogues of the Uranyl Ion. *J. Am. Chem. Soc.* **2006**, *128*, 10549–10559.
- (24) Perales, D.; Ford, S. A.; Salpage, S. R.; Collins, T. S.; Zeller, M.; Hanson, K.; Bart, S. C. Conversion of Trivalent Uranium Anilido to Tetravalent Uranium Imido Species via Oxidative Deprotonation. *Inorg. Chem.* **2020**, *59*, 11910–11914.
- (25) Brennan, J. G.; Andersen, R. A. Electron-transfer reactions of trivalent uranium. Preparation and structure of the uranium metallocene compounds (MeC<sub>5</sub>H<sub>4</sub>)<sub>3</sub>U = NPh and [(MeC<sub>5</sub>H<sub>4</sub>)<sub>3</sub>U]<sub>2</sub>[μ-η<sup>1</sup>,η<sup>2</sup>-PhNCO]. *J. Am. Chem. Soc.* **1985**, *107*, 514–16.
- (26) Matson, E. M.; Crestani, M. G.; Fanwick, P. E.; Bart, S. C. Synthesis of U(IV) imidos from Tp\*<sub>2</sub>U(CH<sub>2</sub>Ph) (Tp\* = hydrotris(3,5-dimethylpyrazolyl)borate) by extrusion of dibenzyl. *Dalton Trans.* **2012**, *41*, 7952–7958.
- (27) Graves, C. R.; Yang, P.; Kozimor, S. A.; Vaughn, A. E.; Clark, D. L.; Conradson, S. D.; Schelter, E. J.; Scott, B. L.; Thompson, J. D.; Hay, P. J.; Morris, D. E.; Kiplinger, J. L. Organometallic uranium(V) imido halide complexes: from synthesis to electronic structure and bonding. *J. Am. Chem. Soc.* **2008**, *130*, 5272–5285.
- (28) Castro-Rodriguez, L.; Meyer, K. Small molecule activation at uranium coordination complexes: control of reactivity via molecular architecture. *Chem. Commun.* **2006**, 1353–1368.
- (29) Graves, C. R.; Kiplinger, J. L. Pentavalent uranium chemistry: synthetic pursuit of a rare oxidation state. *Chem. Commun.* **2009**, 3831–3853.
- (30) Bell, N. L.; Maron, L.; Arnold, P. L. Thorium Mono- and Bis(imido) Complexes Made by Reprotonation of cyclo-Metalated Amides. *J. Am. Chem. Soc.* **2015**, *137*, 10492–10495.
- (31) Gillespie, R. J. Fifty years of the VSEPR model. *Coord. Chem. Rev.* **2008**, *252*, 1315–1327.
- (32) King, D. M.; McMaster, J.; Tuna, F.; McInnes, E. J. L.; Lewis, W.; Blake, A. J.; Liddle, S. T. Synthesis and Characterization of an f-Block Terminal Parent Imido [U = NH] Complex: A Masked Uranium(IV) Nitride. *J. Am. Chem. Soc.* **2014**, *136*, 5619–5622.
- (33) Neidig, M. L.; Clark, D. L.; Martin, R. L. Covalency in f-element complexes. *Coord. Chem. Rev.* **2013**, *257*, 394–406.
- (34) Keridge, A. Quantification of f-element covalency through analysis of the electron density: insights from simulation. *Chem. Commun.* **2017**, *53*, 6685–6695.
- (35) Anderson, N. H. *Controlling Electronics for the Formation of High Valent Uranium Imido Complexes*; Purdue University: West Lafayette, IN, 2016.
- (36) Pangborn, A. B.; Giardello, M. A.; Grubbs, R. H.; Rosen, R. K.; Timmers, F. J. Safe and Convenient Procedure for Solvent Purification. *Organometallics* **1996**, *15*, 1518–1520.
- (37) Chakraborty, S.; Chattopadhyay, J.; Guo, W.; Billups, W. E. *Angew. Chem., Int. Ed.* **2007**, *46*, 4486–4488.
- (38) ADF 2019.3, SCM; Theoretical Chemistry, Vrije Universiteit: Amsterdam, The Netherlands, 2019; <http://www.scm.com>.
- (39) te Velde, G.; Bickelhaupt, F. M.; Baerends, E. J.; Fonseca Guerra, C.; van Gisbergen, S. J. A.; Snijders, J. G.; Ziegler, T. Chemistry with ADF. *J. Comput. Chem.* **2001**, *22*, 931–967.
- (40) van Lenthe, E.; Snijders, J. G.; Baerends, E. J. The zero-order regular approximation for relativistic effects: The effect of spin–orbit coupling in closed shell molecules. *J. Chem. Phys.* **1996**, *105*, 6505–6516.
- (41) Adamo, C.; Barone, V. Toward reliable density functional methods without adjustable parameters: The PBE0 model. *J. Chem. Phys.* **1999**, *110*, 6158–6170.
- (42) Weigend, F.; Ahlrichs, R. Balanced basis sets of split valence, triple zeta valence and quadruple zeta valence quality for H to Rn: Design and assessment of accuracy. *Phys. Chem. Chem. Phys.* **2005**, *7*, 3297.
- (43) Pantazis, D. A.; Neese, F. All-Electron Scalar Relativistic Basis Sets for the Actinides. *J. Chem. Theory Comput.* **2011**, *7*, 677–684.
- (44) Hess, B. A. Relativistic electronic-structure calculations employing a two-component no-pair formalism with external-field projection operators. *Phys. Rev. A: At., Mol., Opt. Phys.* **1986**, *33*, 3742–3748.
- (45) Roos, B. O.; Taylor, P. R.; Sigbahn, P. E. M. A complete active space SCF method (CASSCF) using a density matrix formulated super-CI approach. *Chem. Phys.* **1980**, *48*, 157–173.
- (46) Angeli, C.; Cimiraglia, R.; Malrieu, J.-P. n-electron valence state perturbation theory: A spinless formulation and an efficient implementation of the strongly contracted and of the partially contracted variants. *J. Chem. Phys.* **2002**, *117*, 9138–9153.
- (47) Neese, F. Software update: the ORCA program system, version 4.0. *Wiley Interdiscip. Rev.: Comput. Mol. Sci.* **2018**, *8*, 1327.
- (48) Fdez. Galván, I.; Vacher, M.; Alavi, A.; Angeli, C.; Aquilante, F.; Autschbach, J.; Bao, J. J.; Bokarev, S. L.; Bogdanov, N. A.; Carlson, R. K.; Chibotaru, L. F.; Creutzberg, J.; Dattani, N.; Delcey, M. G.; Dong, S. S.; Dreuw, A.; Freitag, L.; Frutos, L. M.; Gagliardi, L.; Gendron, F.; Giussani, A.; González, L.; Grell, G.; Guo, M.; Hoyer, C. E.; Johansson, M.; Keller, S.; Knecht, S.; Kovačević, G.; Kállman, E.; Li Manni, G.; Lundberg, M.; Ma, Y.; Mai, S.; Malhado, J. P.; Malmqvist, P. Å.; Marquetand, P.; Mewes, S. A.; Norell, J.; Olivucci, M.; Oppel, M.; Phung, Q. M.; Pierloot, K.; Plasser, F.; Reiher, M.; Sand, A. M.; Schapiro, I.; Sharma, P.; Stein, C. J.; Sørensen, L. K.; Truhlar, D. G.; Ugandi, M.; Ungur, L.; Valentini, A.; Vancoillie, S.; Veryazov, V.; Weser, O.; Wesolowski, T. A.; Widmark, P.-O.; Wouters, S.; Zech, A.; Zobel, J. P.; Lindh, R. OpenMolcas: From Source Code to Insight. *J. Chem. Theory Comput.* **2019**, *15*, 5925–5964.
- (49) Roos, B. O.; Lindh, R.; Malmqvist, P.-Å.; Veryazov, V.; Widmark, P.-O. Main Group Atoms and Dimers Studied with a New Relativistic ANO Basis Set. *J. Phys. Chem. A* **2004**, *108*, 2851–2858.
- (50) Roos, B. O.; Lindh, R.; Malmqvist, P.-Å.; Veryazov, V.; Widmark, P.-O.; Borin, A. C. New Relativistic Atomic Natural Orbital Basis Sets for Lanthanide Atoms with Applications to the Ce Diatom and LuF<sub>3</sub>. *J. Phys. Chem. A* **2008**, *112*, 11431–11435.
- (51) Malmqvist, P. Å.; Roos, B. O.; Schimmelpennig, B. The restricted active space (RAS) state interaction approach with spin–orbit coupling. *Chem. Phys. Lett.* **2002**, *357*, 230–240.
- (52) Heß, B. A.; Marian, C. M.; Wahlgren, U.; Gropen, O. A mean-field spin-orbit method applicable to correlated wavefunctions. *Chem. Phys. Lett.* **1996**, *251*, 365–371.
- (53) Glendening, E. D.; Badenhop, J. K.; Reed, A. E.; Carpenter, J. E.; Bohmann, J. A.; Morales, C. M.; Karafiloglou, P.; Landis, C. R.; Weinhold, F. *NBO 7.0*; Theoretical Chemistry Institute, University of Wisconsin: Madison, WI, 2018.
- (54) Keith, T. A. *AIMAll*, version 19.10.12; TK Gristmill Software: Overland Park, KS, 2019; [aim.tkgristmill.com](http://aim.tkgristmill.com).
- (55) Mitoraj, M. P.; Michalak, A.; Ziegler, T. A Combined Charge and Energy Decomposition Scheme for Bond Analysis. *J. Chem. Theory Comput.* **2009**, *5*, 962–975.